

Application of phenotyping and therapeutic drug monitoring in personalised drug treatment

Inauguraldissertation

zur

Erlangung der Würde eines Doktors der Philosophie

vorgelegt der

Philosophisch-Naturwissenschaftlichen Fakultät

der Universität Basel

von

Peter Benjamin Berger

aus Basel, Basel-Stadt

Basel, 2016

Originaldokument gespeichert auf dem Dokumentenserver der Universität Basel
edoc.unibas.ch



Dieses Werk ist unter dem Vertrag "Creative Commons Namensnennung - Keine kommerzielle Nutzung - Keine Bearbeitung 3.0 Schweiz" (CC BY-NC-ND 3.0 CH) lizenziert. Die vollständige Lizenz kann unter <https://creativecommons.org/licenses/by-nc-nd/3.0/ch> eingesehen werden.

Genehmigt von der Philosophisch-Naturwissenschaftlichen Fakultät

auf Antrag von

Prof. Dr. Stephan Krähenbühl

Prof. Dr. Jörg Huwyler

Basel, den 19. April 2016

Prof. Dr. Jörg Schibler

Dekan der Philosophisch-

Naturwissenschaftlichen Fakultät

This body of work is dedicated
to my Mother, Jane Ann Berger,
and
to my Grandfather, Brian Sidney Kellett.



Acknowledgments

The work that went into this project would have taken even more detours or ‘short-cuts leading to long delays’ without all the guidance, support, and encouragement I received from so many people. It has been a period of intense learning, not only in the scientific arena, but also on a personal level. It is therefore my humble pleasure to thank all those individuals on this most important section of my doctoral thesis.

First and foremost I would like to thank PD Dr. Manuel Haschke and Prof. Stephan Krähenbühl for supervising my PhD, and giving me the opportunity of working in the analytical laboratory of the Clinical Pharmacology Department of the University Hospital Basel. They both helped me achieve the scientific objectives set out for this PhD thesis: their advice, their insight, and their stupendously vast knowledge were invaluable whenever a stumbling block was encountered.

Additionally, I am very grateful to Manuel for *de-Tolkien-ifying* my written work.

Besides my advisors, I would like to thank Prof. Jörg Huwyler, who kindly agreed to act as co-referee of my thesis, and Prof. Christoph Meier, for taking up the position of chairman of the faculty.

Many thanks are also due to Massimiliano Donzelli, my mentor, who had previously agreed to be my supervisor during my master’s thesis. He provided me with a great learning experience, through which I gained a valuable insight into the field of analytical chemistry and pharmacology. This set me on my way to commencing my PhD two years later, when he was fortunately still around, helping and guiding me wherever he could, before finishing his own dissertation.


Enter Urs “the gentle bear giant” Duthaler, filling the void left by the afore mentioned Sir Max: words cannot possibly express how much I appreciated working with him during the final two years of my PhD. He took it upon himself to further aid me wherever he could and through his contagious enthusiasm, his patience, his vast knowledge, and experience, helped me buckle down and finish this dissertation. Little did I know, that by working ‘hand-in-hand’ on a number of projects, while having far too much fön and laughing way more than I deemed it to be possible in a working environment, it led us to develop a fierce friendship that has allowed me to consider Urs to be my bear brother.

I would also like to convey a heartfelt ‘Dankeschön’ to Beatrice Vetter. It has been an absolute pleasure to work alongside such a kind, helpful, and genuinely nice person.

She was the one person that made the lab tick and I appreciated that she was paramount in helping to create an incredibly pleasant atmosphere in the lab. I will be eternally grateful to her for always looking out for me. Also, thank you for your artistic contribution to this thesis.

Thank you to Franziska Boess, Nathalie Schaub, and Evelyne Durr at Roche, for the opportunities I was given to conduct my research, while providing me with the tools that I needed to successfully complete my work there.

Finally, there are my dear friends, past and present, in the lab and thereabout: Riccardo, Jamal, François, Patrizia, Rejane, Pete, Swarna, Annalisa, David, Dino, Gerda, Andrea, Cedric, Anna, Cristian “el fuego” Setz, Fabio, Soledad, Evelyne, Felix, Anne, and Eva. We were not only able to support each other by occasionally deliberating over our problems and findings, but more importantly by talking about other critical topics such as the origin of the importance of “42,” the possible whereabouts of Benjen Stark, PSG surprisingly not winning a football match, British cuisine, and of course my distinguished taste in music.

I would of course also like to thank my mother, Jane, for always having a sympathetic ear, and my dear brother Michael for reminding me to use the force. Furthermore, I am much obliged to another family member, Michelle Witen , for proof reading this thesis.

It is also of the upmost importance to convey my sincere gratitude to the love of my life, Nerina Vischer, for always being there for me and for putting up with my mood swings, while supporting and encouraging me by enforcing her belief that this thesis is not the end of the world, but simply a doctoral thesis that has an end.

And speaking of endings, last but not least, I would like to thank the eternal greats that are Ian Curtis, David Bowie, Noel & Liam Gallagher, Brett Anderson, Paul Weller, Steven Morrissey, Johnny Marr, Paul Smith, Nicky Wire, James D. Bradfield, Damon Albarn, Graham Coxon, John Lennon, Paul McCartney, George Harrison, and Ringo Star, for keeping me sane through the auditory bliss they created.

Thank you.



Table of contents

1.	Summary	5
2.	Abbreviations	7
3.	General Introduction	11
4.	<i>Project 1</i> - Comparison of liver cell models using the Basel phenotyping cocktail	19
5.	<i>Project 2</i> - Assessment of cytochrome p450 2D6 activity with metoprolol α -hydroxylation <i>in vivo</i> and <i>in vitro</i>	45
6.	<i>Project 3</i> - <i>In vitro</i> evaluation of replacing losartan by flurbiprofen as a probe substrate for cytochrome p450 2C9 in the Basel phenotyping cocktail	67
7.	<i>Project 4</i> - Cytochrome p450 3A4 and 1A2 phenotyping for the individualisation of treatment with erlotinib (or sunitinib) in cancer patients	83
8.	<i>Project 5</i> - Therapeutic drug monitoring of antiretroviral drugs using a fully automated dried blood spot extraction method to measure samples from a clinical study in rural Tanzania	123
9.	General conclusions and outlook	155
10.	General references	159

Reference lists for each of the five projects (chapters 4, 5, 6, 7, and 8) are presented at the end of the relevant chapters. A reference list covering the summary, the general introduction, and the general conclusions and outlook, can be found at the end of the thesis.

1. Summary

As every individual is a product of his/her genes and environment, which can be regarded as a paraphrase of an individual's phenotypic characteristic, it becomes apparent as to why the concept of personalised medicine, i.e. tailoring a treatment regimen to an individual's needs, remains an ever-prevalent topic in the medical community. Human cytochrome P450 enzymes (CYPs) are accountable for the oxidative metabolism of approximately 50% of commonly used drugs as well as endogenous compounds. However, CYP activity is exceedingly variable amongst individuals.

Over the course of my PhD project, I worked on five different projects that implicated the utility of two valuable tools in personalised medicine: namely, phenotyping and therapeutic drug monitoring. The determination of a person's enzymatic activity through phenotyping can help guide a GP's effort to personalise drug therapy by administering the applicable dose, thereby improving efficacy and reducing side effects at the start of therapy. Therapeutic drug monitoring (TDM) on the other hand, enables the continued observation of a patient's drug concentration, predominantly in plasma, thus allowing patients that are at risk of either over-/ or underdosing to be identified.

In the past two decades, many different *in vivo* phenotyping cocktails, enabling the simultaneous assessment of multiple CYP isoforms, e.g. Cooperstown- [1], Inje- [2], Quebec- [3], Karolinska- [4], and the Pittsburgh-cocktail [5], as well as a great number of *in vitro* cocktails [6-14] were developed. Metabolism studies performed *in vitro* are useful to the extent of acquiring anticipatory information of *in vivo* predictions of CYP- inhibition/ -induction in an efficient time and cost saving manner. It is, however, uncommon to use established *in vivo* cocktails for *in vitro* studies [7]. Nevertheless, using probe substrates previously unaccustomed to *in vitro* cocktail studies, e.g. efavirenz (CYP2B6), losartan (CYP2C9), and metoprolol (CYP2D6), we were able to show the potential of the Basel cocktail [15, 16] to characterise a variety of different liver cell models. Of particular interest to our study was the characterisation of 3D primary human hepatocytes (PHH), co-cultured with 3T3-mouse fibroblasts [17]. By using the same batch of PHH in 2D and 3D-culture, we were able to show the functional benefits of a co-culture system, enabling hepatocytes to reside in a 3D environment, and leading to improved CYP activity and mRNA expression. In subsequent studies, we were able to provide explanations for

pending *in vivo* observations [15], through combining knowledge of freshly acquired *in vitro* and *in vivo* characterisation data of the Basel cocktail.

In the second study, we demonstrated that the α -hydroxymetoprolol formation is not mediated solely by CYP2D6, since under induced conditions and through experiments in isoform specific supersomes, the involvement of CYP3A4 also became apparent. This does not, however, impede the continued applicability of metoprolol as probe substrate of CYP2D6 since the involvement of CYP3A4 only becomes apparent when induction is evaluated, which is commonly not done for CYP2D6.

In the third study, we were able to show, through an *in vitro* interactions study, that flurbiprofen can be used to replace losartan as a phenotyping drug for CYP2C9. Subsequently, a pilot study (n=2) showed the prospect of simplifying the cocktail administration through the use of a combi-capsule containing all six probe drugs of the modified Basel cocktail.

After having previously tested the phenotyping capacities of the Basel cocktail in two studies involving young, healthy, male volunteers [15, 16], the fourth study of this thesis demonstrates that we successfully used caffeine (CYP1A2) and midazolam (CYP3A4) to phenotype elderly, patients of both sexes that were being treated for non-small cell lung cancer (NSCLC) with erlotinib (Tarceva[®]). In so doing, we were able to show that subjects with a slow CYP3A4 metabolism had a higher likelihood of developing cutaneous toxicity than patients with an extensive metabolism.

While the fourth study touched upon the possible usefulness of collecting DBS with which to perform TDM, as opposed to conventional plasma samples, the fifth and final study was devoted entirely to this topic. Here, we demonstrate the development, validation, and application of an automated DBS extraction method, while incorporating an evaluation of an antiretroviral adherence/ therapeutic drug monitoring study. Our study was able to show that concentrations of two antiretroviral drugs, nevirapine and efavirenz, could reliably be determined by automated extraction in DBS samples that had been obtained in a challenging setting in rural Tanzania.

2. Abbreviations

3-MC	3-methylcholanthrene
ABCB1	ATP binding cassette subfamily B member 1; P-glycoprotein (P-gp); multidrug resistance protein 1 (MDR1)
ABCG2	ATP-binding cassette sub-family G member 2; breast cancer resistance protein (BCRP)
AE	Adverse event
AhR	Aryl hydrocarbon receptor
ALAT	Alanine aminotransferase
ASAT	Aspartate aminotransferase
ATP	Adenosine triphosphate
AUC	Area under the curve
bp	base pair
CAR	Constitutive androstane receptor
cART	combined antiretroviral treatment
CYP450	Cytochrome p450
C_{\max}	Peak plasma concentration
CPS	Counts per second
C_{ss}	Steady-state plasma concentration
$C_{ss/dose}$	Dose normalised steady-state plasma concentration
C_{trough}	Trough plasma concentration
CTCAE	Common Terminology Criteria for Adverse Events
CV%	coefficient of variation
DBS	Dried Blood Spot
DMEM	Dulbecco's modified Eagle's medium
DMSO	Dimethyl sulfoxide
E-3174	Losartan carboxylic acid, main metabolite of losartan
EDTA	Ethylenediaminetetraacetic acid

EFA	Efavirenz
EGFR	Epidermal growth factor receptor
EM	Extensive metaboliser
ESI	Electrospray ionisation
FCS	Foetal calf serum
FDA	Food and Drug Administration
G6PDH	Glucose-6-phosphate dehydrogenase
GAPDH	Glyceraldehyde 3-phosphate dehydrogenase
GIST	Gastrointestinal stromal tumour
GP	General practitioner
HBV	Hepatitis B virus
HIV	Human immunodeficiency virus
HPLC	High Performance Liquid Chromatography
HPRT1	Hypoxanthine phosphoribosyltransferase 1
HCT	Haematocrit
IM	Intermediate metaboliser
IS	Internal standard
i.v.	Intravenous
LC-MS/MS	Liquid Chromatography-Triple quadrupole Mass Spectrometry
LLOQ	Lowest limit of quantification
LPV	Lopinavir
mAbs	Monoclonal antibodies
MeOH	Methanol
MR	Metabolic ratio
MRM	Multiple reaction monitoring
m/z	mass-to-charge ratio
NONMEM	Nonlinear-mixed-effects modelling
NSCLC	Non-small cell lung cancer

NVP	Nevirapine
OSI-420	Desmethyl erlotinib, main active metabolite of erlotinib
PDGFR	Platelet derived growth factor receptor
PHH	Primary human hepatocytes
PPI	Proton pump inhibitor
PK	Pharmacokinetic
PM	poor metaboliser
pmol	picomol
PXR	Pregnane X receptor
RCC	Renal-cell cancer
SCFR	Stem cell factor receptor
SD	Standard deviation
SEM	Standard error of the mean
Su-12662	N-desethyl sunitinib, main active metabolite of sunitinib
T_{\max}	Time corresponding to peak plasma concentration
$t_{1/2}$	Half-time
TDM	Therapeutic Drug Monitoring
TK	Tyrosine Kinase
TKI	Tyrosine Kinase Inhibitor
TSH	Thyroid stimulating hormone
ULN	Upper limit of normal
VEGFR	Vascular endothelial growth factor receptor
v/v	percentage volume of a substance of the total volume
WHO	World Health Organisation

3. General Introduction

The concept of addressing each patient according to his or her individuality was introduced as early as Ancient Greece, through Hippocrates, the ‘father of western medicine’ [18]. He is reputed to have said, *“It is far more important to know what sort of person has a disease, than to know what sort of disease a person has,”* long before the concept of personalised medicine was coined [19]. Personalised medicine challenges the age-old “one dose fits all” therapy strategy, favouring instead a treatment tailored to the individual (Figure 1). Following the rule of the 5Rs – to be able to give “the right dose of the right drug for the right indication for the right patient at the right time” – personalised medicine is intent on maximising the likelihood of therapeutic efficacy, whilst minimising the risk of toxicity for an individual patient [20].

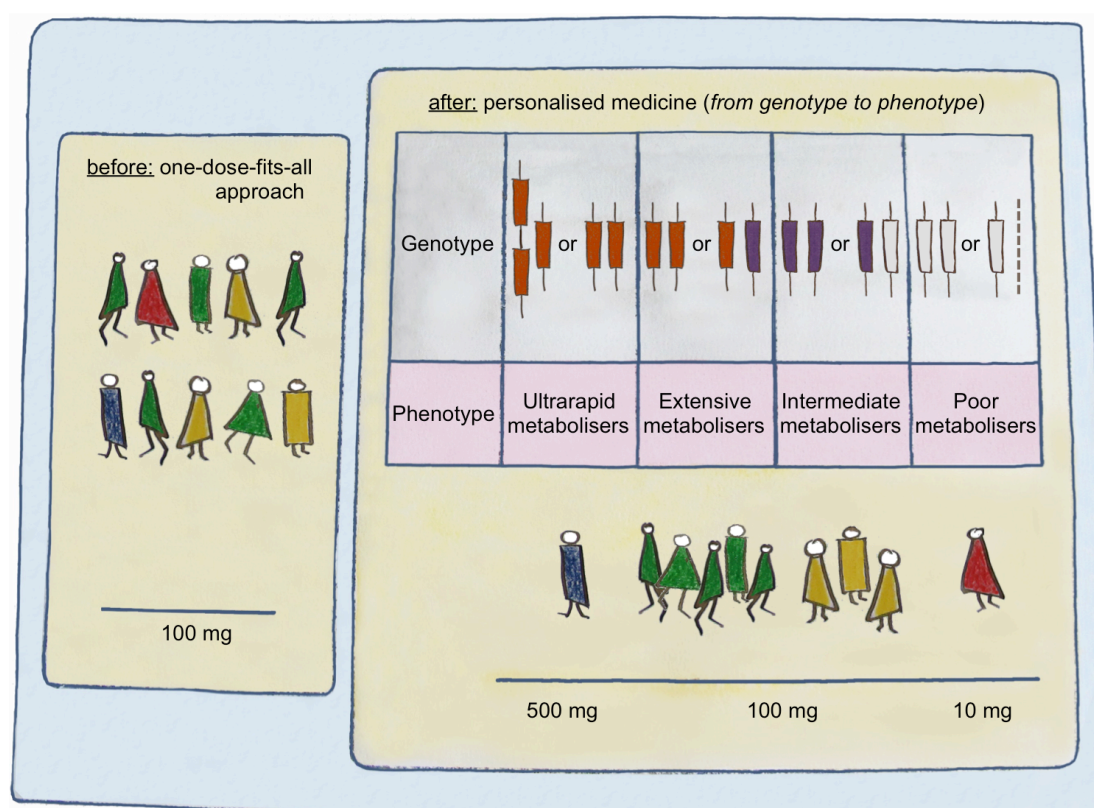


Figure 1. Differences in prescribing the same drug (e.g. nortryptiline, metabolised by CYP2D6) with the ‘one-dose-fits-all’ approach (left panel) and through personalised medicine (right panel). In the right panel, fully functional alleles of the CYP2D6 gene are illustrated by orange boxes, functional but impaired alleles by purple boxes, non-functional alleles by white boxes, and deletion of the whole CYP2D6 gene by a dashed line. The phenotype is predicted for each individual patient. To achieve the same plasma drug level dose adjustments are required. Adapted from [20, 21].

Further long-term benefits of personalised medicine, a term that has been used interchangeably with precision medicine, stratified medicine, and p4 (**p**redictive, **p**reventive, **p**ersonalised, **p**articipatory) medicine, include personalised prescriptions, improved patient compliance, and a reduction in the costs of disease management [22].

The extent to which a person responds to any given drug is determined by the set of an individual's genes (genotype) and the influence of a variety of different environmental and non-genetic factors that make up the expression of an individual's characteristic phenotype (Figure 2). Through phenotype-guided dosing, an individual's ability to metabolise drugs according to the activity of their respective cytochrome P450 (CYP450) enzymes (or ABC-transporters) can be investigated. Phenotyping of CYP450 is performed by administering a selective substrate for a specific CYP enzyme, e.g. midazolam for the CYP450 isoform 3A4.

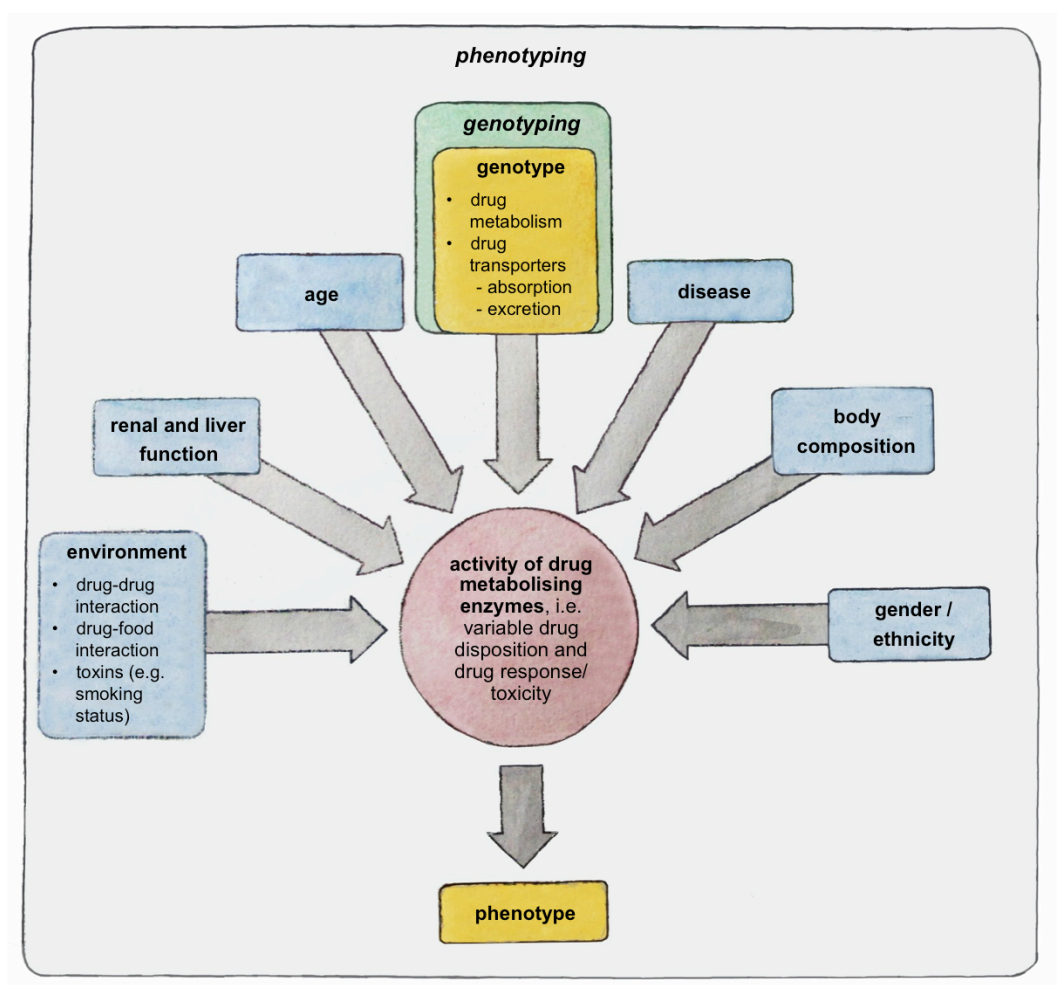


Figure 2. The phenotype, i.e. the variability of drug disposition and drug response, is determined by an interplay of the genotype and a variety of non-genetic factors, adapted from [23].

Subsequently either pharmacokinetic parameters or the measurement of single concentration ratios at selected time points of the parent drug (e.g. midazolam) and its respective metabolite (e.g. 1'-hydroxymidazolam) can be used to assess the metabolic activity of the CYP450 enzyme in question [23]. The cocktail approach makes use of a number of selective probe substrates that do not interact amongst themselves and can be applied when two or more CYP450 isoforms are to be assessed simultaneously [24].

Pharmacogenomics, the study of how genes affect a person's response to drugs, has progressed in leaps and bounds since the completion of the human genome project [25, 26], opening up new possibilities for personalised medicine. For instance, a number of drugs, such as the tyrosine kinase inhibitor Tarceva® (erlotinib) or the monoclonal antibody Herceptin® (trastuzumab), are only effective in sub-populations. Early identification of responders through screening for pharmacogenomic biomarkers, e.g. EGFR activating mutations or Her2/neu overexpression respectively, enables the effective treatment of that sub-population. On the other hand, non-responders are not being subjected to the unnecessary risk of adverse events through a drug treatment with no benefit.

Another form of personalised treatment is therapeutic drug monitoring (TDM), through which plasma concentrations are most commonly measured at designated intervals in order to achieve and uphold target blood concentration. It can furthermore be used to design individualised dosage regimens. Quantitation of plasma levels is routinely performed through liquid-chromatography tandem mass spectrometry (LC-MS/MS) analysis. A rationale to perform TDM includes the assessment of AEs, the diagnosis of dietary or drug-drug interactions, dose adjustments, the monitoring of high-risk patients (children, elderly, patients with impaired organ function), minimising underdosing of patients, and the monitoring of adherence [27]. TDM is most commonly used during treatments in which a drug has a narrow therapeutic range, marked pharmacokinetic variability, and where a direct relationship between drug concentration and efficacy/ toxicity has been established. TDM is widely applied to antibiotic, anticonvulsant, antipsychotic, and antineoplastic treatment [28].

The overall goal of this doctoral thesis was to investigate phenotyping and TDM as two important tools of personalised medicine. In the first three projects, the recently developed *in vivo* Basel phenotyping cocktail was investigated *in vitro* using different

liver cell models. In the fourth study, patients that were being treated with tyrosine kinase inhibitors were phenotyped using two probe drugs of the Basel cocktail. In the fifth and final project, the use of dried blood spots for the TDM of antiretroviral drugs from a clinical study conducted in a resource-limited setting was investigated. For the reliable analysis of samples from all sub-projects, liquid chromatography tandem mass-spectrometry (LC-MS/MS) was utilised as a key bioanalytical method.

Previously, the Basel cocktail – an *in vivo* phenotyping tool that contains caffeine (CYP1A2), efavirenz (CYP2B6), losartan (CYP2C9), omeprazole (CYP2C19), metoprolol (CYP2D6), and midazolam (CYP3A4) – was characterised in healthy male volunteers after being treated with a combination of different CYP450 inhibitors and a broad CYP inducer [15, 16]. After this detailed *in vivo* characterisation, it was relevant to also evaluate the utilised probe drugs *in vitro*. In the first study, we, therefore, assessed the performance and usability of the Basel cocktail *in vitro* by comparing *in vitro* and *in vivo* results. Furthermore, we wanted to evaluate the suitability of a variety of different liver cell models, i.e. the hepatoma cell lines HepG2 and HepaRG, and primary hepatocytes in 2-Dimensional (2D) culture and in 3D co-culture as hepatocyte-spheroids [17], to investigate drug metabolism and CYP induction.

The metabolism of metoprolol, a cardio-selective beta-blocker currently used mainly in the treatment of heart failure [29], myocardial infarction [30], and arterial hypertension [31], to its α -hydroxy-metabolite is considered to be exclusively mediated by CYP2D6 [32, 33]. On that account, it has been used as a probe substrate for CYP2D6 [3, 34-36], including in the Basel phenotyping cocktail [15, 16]. After induction treatment with rifampicin, we surprisingly observed a change not only in the metabolic ratios for CYP1A2, CYP2B6, CYP2C9, CYP2C19 and CYP3A4, but also for CYP2D6 [15]. Since CYP2D6 is considered to be a non-inducible CYP isoform [37-42], these results were difficult to interpret. We thus decided to first confirm these findings *in vitro* using two different hepatocyte systems, and subsequently to find out the mechanism leading to this observation.

Another *in vivo* observation that warranted closer inspection was the inclusion of losartan as a probe substrate of CYP2C9. Unlike other cytochrome P450 isoforms readily inducible by rifampicin, i.e. CYP2B6, CYP2C19, and CYP3A4, the use of losartan metabolic ratios did not reflect induction of CYP2C9 [15, 16]. Thus, in the third study, we assessed whether flurbiprofen, a non-steroidal anti-inflammatory drug (NSAIDs) [43, 44] previously used in cocktail studies [5, 45], could replace losartan

as a selective substrate for CYP2C9 in the Basel cocktail. Instead of performing another time-consuming and cost-intensive clinical trial, this was evaluated *in vitro* using the previously characterised primary human hepatocytes in 3D-co culture. Furthermore, to streamline the administration of the phenotyping cocktail, we evaluated a newly developed combination-capsule, containing all six low dosed drugs in place of separate commercially available formulations, in a pilot study, which was necessary to design the formal evaluation process in a future clinical trial.

Tyrosine kinase inhibitors (TKIs) are antineoplastic agents given orally at a fixed dose, despite their large pharmacokinetic variability. Due to the relationship between drug exposure and treatment outcome, the “one-dose-fits-all” approach can unintentionally lead either to under- or overexposure [46]. After having previously characterised the Basel phenotyping cocktail in healthy, male subjects [15, 16], this fourth study represents the first time we used two of its substrates, namely midazolam and caffeine, to gather phenotyping information in elderly patients of both sexes, being treated with erlotinib (Tarceva®) for non-small cell lung cancer (NSCLC). The primary aim of the study was to evaluate the relationship between individual CYP3A4 and CYP1A2 phenotype with erlotinib exposure. A secondary aim was to assess the correlation of individual CYP-phenotype with treatment-related toxicity. Furthermore, we were also interested in determining the feasibility of using dried blood spots (DBS), a microsampling technique whereby capillary blood is spotted onto a filter paper after a simple fingerprick, to perform bio-analysis of erlotinib.

The aim of the last study was to develop and validate an automated extraction method for the analysis of three antiretroviral agents in TDM DBS samples. On the one hand, adherence to antiretroviral therapy has been strongly correlated with viral suppression, an increase in survival, and improved quality of life [47, 48]. On the other hand, patients with suboptimal adherence are at risk of HIV progression and the development of drug resistance, which consequently narrows options for future treatment [47, 49, 50]. However, adherence assessment by health care providers, particularly in developing countries, is performed infrequently [47, 49, 51]. Within the framework of an adherence assessment study in rural Tanzania (Ifakara) DBS and plasma samples of patients treated with combined antiretroviral therapy (cART) were collected [52]. For TDM in remote settings, obtaining dried blood spots (DBS) is particularly advantageous, as DBS samples do not yield a further biohazardous risk and are generally stable at room temperature, making the maintenance of cold chains unnecessary [53, 54]. Treatments with two non-nucleoside reverse

transcriptase inhibitors, efavirenz and nevirapine, and a protease inhibitor, lopinavir, were monitored in this study. Unlike previous studies dealing with the measurement and validation of the respective cART compounds through manual DBS extraction [55-59], in this study, DBS were extracted in a fully automated manner using a CAMAG DBS-MS-500 autosampler [60]. Here, the objective was to test whether automated extraction would help to overcome drawbacks of conventional DBS methodology. Additionally, to show the utility of DBS collection in rural settings, we compared concentrations measured in plasma with corresponding concentrations found in DBS.

Below, the five sub-projects of this thesis are listed and will be presented in detail in the following chapters:

- Comparison of liver cell models using the Basel phenotyping cocktail (**Chapter 4**)
- Assessment of cytochrome p450 2D6 activity with metoprolol α -hydroxylation *in vivo* and *in vitro* (**Chapter 5**)
- *In vitro* evaluation of replacing losartan by flurbiprofen as a probe substrate for cytochrome p450 2C9 in the Basel phenotyping cocktail (**Chapter 6**)
- Cytochrome p450 3A4 and 1A2 phenotyping for the individualisation of treatment with erlotinib (or sunitinib) in cancer patients (**Chapter 7**)
- Therapeutic drug monitoring of antiretroviral drugs using a fully automated dried blood spot extraction method to measure samples from a clinical study in rural Tanzania (**Chapter 8**)

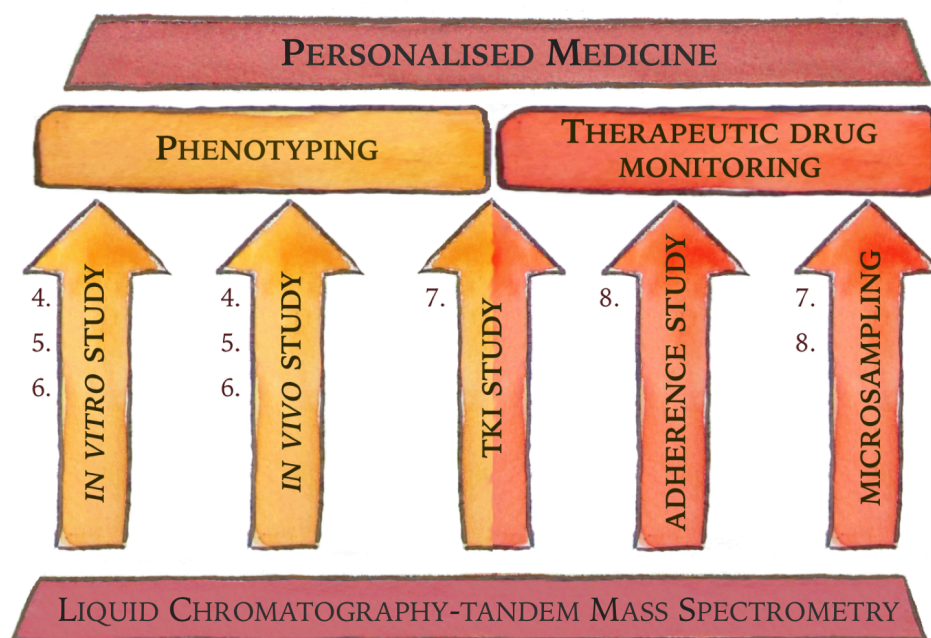


Figure 3. Interplay of the five sub-projects making up this thesis. Numbers match the respective chapter mentioned above.

4. Comparison of liver cell models using the Basel phenotyping Cocktail

Benjamin Berger¹, Massimiliano Donzelli¹, Swarna Maseneni¹, Franziska Boess²,
Adrian Roth², Stephan Krähenbühl^{1,3}, Manuel Haschke¹

¹Division of Clinical Pharmacology & Toxicology, University Hospital Basel and Department of Biomedicine, University of Basel, Switzerland

²Non-Clinical Safety, Hoffmann-La Roche Ltd, Basel, Switzerland

³Swiss Center for Applied Human Research (SCAHT)

Published in
Frontiers in Pharmacology, 2016, 7:443 (*doi: 10.3389*)

Abstract

Currently used hepatocyte cell systems for in vitro assessment of drug metabolism include hepatoma cell lines and primary human hepatocyte (PHH) cultures. We investigated the suitability of the validated in vivo Basel phenotyping cocktail (caffeine [CYP1A2], efavirenz [CYP2B6], losartan [CYP2C9], omeprazole [CYP2C19], metoprolol [CYP2D6], midazolam [CYP3A4]) in vitro and characterised four hepatocyte cell systems (HepG2 cells, HepaRG cells, and primary cryopreserved human hepatocytes in 2-dimensional [2D] culture or in 3D-spheroid co-culture) regarding basal metabolism and CYP inducibility. Under non-induced conditions, all CYP activities could be determined in 3D-PHH, CYP2B6, CYP2C19, CYP2D6 and CYP3A4 in 2D-PHH and HepaRG, and CYP2C19 and CYP3A4 in HepG2 cells. The highest non-induced CYP activities were observed in 3D-PHH and HepaRG cells. mRNA expression was at least 4-fold higher for all CYPs in 3D-PHH compared to the other cell systems. After treatment with 20µM rifampicin, mRNA increased 3 to 50-fold for all CYPs except CYP1A2 and 2D6 for HepaRG and 3D-PHH, 4-fold (CYP2B6) and 17-fold (CYP3A4) for 2D-PHH and 4-fold (CYP3A4) for HepG2. In 3D-PHH at least a 2-fold increase in CYP activity was observed for all inducible CYP isoforms while CYP1A2 and CYP2C9 activity did not increase in 2D-PHH and HepaRG. CYP inducibility assessed in vivo using the same phenotyping probes was also best reflected by the 3D-PHH model.

Our studies show that 3D-PHH and (with some limitations) HepaRG are suitable cell systems for assessing drug metabolism and CYP induction in vitro. HepG2 cells are less suited to assess CYP induction of the 2C and 3A family. The Basel phenotyping cocktail is suitable for the assessment of CYP activity and induction also in vitro.

Key words: *cytochrome P450 (CYP), Basel cocktail, 3-dimensional spheroid primary human hepatocyte culture, CYP induction, liquid chromatography tandem mass spectrometry*

1. Introduction

Cytochrome P450 enzymes (CYPs) are involved in the oxidative metabolism of the majority of the commonly used low molecular weight drugs, thereby influencing the pharmacokinetics of these drugs and having an important role in drug-drug interactions [1]. Genetic variants and exogenous factors such as diet, smoking habits, and concomitant medication can affect the activity of CYPs. All of these factors are responsible for wide interindividual variations in CYP activity and drug plasma concentrations, which can be associated with either increased toxicity or an insufficient pharmacological effect.

Simultaneous determination of the activity of different CYPs in an individual patient can be performed by administering a combination (“cocktail”) of specific probe drugs [2]. Several cocktails have been characterised in clinical studies and are used in individual patients, including the Karolinska cocktail [3], the Cooperstown 5+1 cocktail [4], the Geneva cocktail [5] and the Basel Cocktail [6]. These cocktails have also been shown to be valuable tools to assess the capacity of drugs to induce or inhibit CYPs [5, 7]. Drug cocktails have also been used to perform *in vitro* studies, in particular when assessing the CYP inhibition and induction potential of chemical compounds [8-10].

Suitable *in vitro* systems to assess drug metabolism are mainly liver microsomes, hepatocarcinoma cell cultures (e.g. HepG2 and HepaRG cells) and primary human hepatocytes. Monolayer-grown primary human hepatocytes or hepatocarcinoma cell-lines are currently the gold standard for *in vitro* drug-drug interaction and hepatotoxicity studies. However, monolayer hepatocyte culture systems have major drawbacks. Primary human hepatocyte cultures suffer from a rapid loss of cell polarity and of specific hepatic functions, which limits their applicability for drug metabolism experiments to a few days. Furthermore, they exhibit a large variation in cell functions, especially in CYP activities, as well as a variable response to CYP inducers [11, 12]. In comparison, hepatocarcinoma cell line cultures can be used over extended periods of time, but their metabolic activity and response to CYP inducers are generally limited [13]. As an alternative to 2D cultures of primary human hepatocytes or hepatocarcinoma cell lines, a variety of different 3D liver models are being explored, as they are thought to approximate the *in vivo* tissue structure and cell behaviour more closely [12, 14].

Limited availability of phenotyping probe drugs is a frequent limitation of published *in vivo* phenotyping cocktails. To facilitate clinical application of phenotyping, we there-

fore developed a new low-dose cocktail, which is based on probe drugs that are widely used in clinical practice [6]. In a subsequent study, we characterised this cocktail in healthy male subjects treated with a combination of different CYP inhibitors and a CYP inducer [7]. Since we now have a detailed *in vivo* characterisation of this cocktail, it was of interest to also test the cocktail *in vitro*. The two principle aims of our investigation were therefore i) to assess the performance and usability of the Basel cocktail *in vitro* by comparing *in vitro* with *in vivo* results and ii) to assess the suitability of different hepatocyte cell models for the investigation of drug metabolism and CYP induction.

In order to accomplish these aims, we tested the metabolism of the Basel cocktail (containing caffeine, metoprolol, omeprazole, losartan, efavirenz and midazolam) in HepG2 cells, HepaRG cells, and primary cryopreserved human hepatocytes grown in 2D and in 3D culture under basal conditions and after CYP induction with rifampicin. CYP induction achieved by rifampicin *in vitro* could then be compared with the extent of *in vivo* CYP induction.

2. Materials and methods

2.1. Chemicals and reagents

8'-hydroxyefavirenz, efavirenz-d4, losartan, losartan-carboxylic acid (E3174), losartan-d4, omeprazole, 5'-hydroxyomeprazole, omeprazole-d3, metoprolol, α -hydroxymetoprolol, and metoprolol-d7 were purchased from TRC (Toronto, Canada). 1'-hydroxymidazolam and midazolam-d6 were acquired from Lipomed (Arlesheim, Switzerland), whereas rifampicin and β -glucuronidase (type HP-2 from *Helix pomatia*) were obtained from Sigma-Aldrich (Sigma- Aldrich Chemie GmbH, Buchs, Switzerland). Midazolam (F. Hoffmann-La Roche, Basel, Switzerland) and efavirenz (Merck, NJ, USA) were kindly provided by the respective manufacturers. The chemical structures of the probe drugs and their phase I metabolites are provided in Supplementary Figure 2. Formic acid, HPLC grade methanol, and HPLC grade water were purchased from Merck (Darmstadt, Germany). Media used were purchased from GIBCO (Lucerne, Switzerland).

Stock solutions, calibration and quality control spiking solutions were prepared in DMSO. Calibration standards and quality controls were prepared by enriching the

respective medium with the corresponding spiking solutions. Internal standard solutions containing the deuterated cocktail probe drugs were prepared in methanol.

2.2. Cell cultures

The human hepatoma cell line HepG2 was obtained from ATCC (Manassas, VA, USA). HepG2 cells were cultured in Dulbecco's modified Eagle's medium (DMEM; with 2 mM GlutaMAX®, 1.0 g/l glucose and sodium bicarbonate) supplemented with 10% (v/v) heat-inactivated foetal calf serum (FCS), and 10 mM HEPES buffer, pH 7.2. In general, all cells were kept at 37°C in a humidified 5% CO₂ cell culture incubator and passaged using trypsin, while the cell number was determined using a Neubauer hemacytometer. Viability was checked using the trypan blue exclusion method. For the experiments, HepG2 cells were seeded at 10'000 cells/ well in 96-well plates or 150'000 cells/ well in 12-well plates.

HepaRG cells were purchased from Biopredic International (Rennes, France) as undifferentiated cryopreserved cells with the associated medium. Freshly split HepaRG cells were seeded at 9000 cells/ well in 96-well plates and treated over the course of the next four weeks as previously described (Aninat *et al.*, 2006).

Primary cryopreserved human hepatocytes (Life Technologies, Lot Hu8119, female donor) were plated at 50'000 cells/ well in collagen type-1 precoated 96 well plates in William's E medium supplemented with 10% FBS (v/v), 1% L-Glutamine 200 mM (v/v), 1% Pen Strep (v/v), 0.1% dexamethasone 100 µM (v/v), and 0.1% insulin 100 µM (v/v) and left to incubate at 37°C, 95% humidity, 5% CO₂.

For the 3D-hepatocyte co-culture model originally described by Ohkura *et al.* [15], 3T3 fibroblast cells from Swiss albino mouse embryo tissue (3T3 Balb/clone A31, ATCC product number CCL 163) were seeded at a density of 8000 cells/well in 96-well plates or at 40'000 cells/ well in 24-well plates into micro-patterned plates (Cellable™, Cosmo Bio USA Inc., CA, USA) in Dulbecco's Modified Eagle's medium (DMEM; with 2mM GlutaMAX®,) supplemented with 10% FBS. The cells were cultured in a 5% CO₂, 95% air humidified environment at 37°C. After 2 days, cryopreserved human hepatocytes (Life Technologies Lot Hu8119) were seeded at a density of 25'000 cells/well in the same 96 well plates containing the 3T3 cells (or 125'000 cells/ well in 24-well plates). The 3T3-cryopreserved human hepatocyte co-culture was maintained for a minimum of two days to allow for spheroid formation,

using the same medium as for the conventional two-dimensional (2D) cryopreserved hepatocyte culture.

Cryopreserved human hepatocyte preparations were only used for experiments if their morphological characteristics and viability (>85%) were acceptable.

2.3. Markers of CYP450 activity

CYP activity was assessed by the addition of a CYP probe drug cocktail consisting of caffeine (CYP1A2, 80 μ M), efavirenz (CYP2B6, 10 μ M), losartan (CYP2C9, 14 μ M), omeprazole (CYP2C19, 17 μ M), metoprolol (CYP2D6, 23 μ M), and midazolam (CYP3A4, 5 μ M). The substrates were used at concentrations close to their K_m values previously published.

A previously developed liquid chromatography tandem mass spectrometry (LC-MS/MS) method [6] was used to analyse the phase I metabolites of the probe drugs. Chromatographic separation was performed on a Shimadzu HPLC system (Shimadzu AG, Reinach, Switzerland) coupled to a triple quadrupole tandem mass spectrometer (API4000, AB/MDS Sciex, Concord, Canada) operating in positive electrospray ionisation mode, except for 8'-hydroxyefavirenz, which was detected in negative mode. Total run time was 2.9 minutes. Inter-assay accuracy (determined as the % bias) ranged from -10.7 to 9.8 and inter-assay precision (determined as the CV%) was lower than 11.3 for all analytes. The lower limit of quantification (LLOQ) was 0.25 ng/ml for hydroxymetoprolol, 8-hydroxyefavirenz, 1'-hydroxymidazolam, 5-hydroxyomeprazole, E-3174, and 0.5 ng/ml for paraxanthine.

2.4. CYP450 induction experiments

2.4.1. Evaluation of mRNA expression

HepG2 cells, HepaRG cells, 2D-cultured human hepatocytes and 3D-cultured human hepatocytes were seeded in 24 well plates and treated for 48 h with rifampicin 20 μ M. 350 μ L of RLT buffer (Qiagen, Hombrechtikon, Switzerland) was used to lyse the respective hepatocytes, after which the lysate was transferred to Qiasredder columns and centrifuged for 2 min at 13'000 rpm. From the eluate, total RNA was extracted and purified according to the manufacturer's instructions (Qiagen, RNeasy mini extraction kit). The concentration of the extracted RNA was measured spectrophotometrically at 260 nm on a NanoDrop 2000 (Thermo Fisher Scientific, Wohlen,

Switzerland). cDNA was reverse-transcribed from the isolated RNA using the Qiagen omniscrypt system. For quantitative RT-PCR 10 ng cDNA was used. Forward and reverse primers for all CYPs tested and endogenous references, hypoxanthine phosphoribosyltransferase 1 (HPRT1) and Glyceraldehyde 3-phosphate dehydrogenase (GAPDH), were purchased from Microsynth (Balgach, Switzerland; listed in Table 1). rt-PCR was performed using SYBR green (Roche Diagnostics, Rotkreuz, Switzerland) on an ABI PRISM 7700 sequence detector (PE Biosystems, Rotkreuz, Switzerland). Quantification of mRNA expression levels was performed using the comparative-threshold cycle method [16].

Table 1. Gene-specific primers used for rt-PCR.

Target Gene	Organism		Primer Sequence (5'- 3')	Length (bp)
CYP1A2	human	Fw	GGACAGCACTTCCCTGAGAG	20
		Rev	GCTCCTGGACTGTTTTCTGC	20
CYP2B6	human	Fw	CAGTGAATTCAGCCACCAGA	20
		Rev	ATTTTGGCTCGGTCATGAAG	20
CYP2C9	human	Fw	AGGAAAACGGATTTGTGTGG	20
		Rev	GGCCATCTGCTCTTCTTCAG	20
CYP2C19	human	Fw	GGATTGTAAGCACCCCCTG	19
		Rev	TAAAGTCCCGAGGGTTGTTG	20
CYP2D6	human	Fw	TGTGCCCATCACCCAGAT	18
		Rev	AAGGTGGAGACGGAGAAGC	19
CYP3A4	human	Fw	TACACAAAAGCACCGAGTGG	20
		Rev	TGCAGTTTCTGCTGGACATC	20
HPRT1	human	Fw	GGTCCTTTTCACCAGCAAGCT	21
		Rev	TGACACTGGCAAAACAATGCA	21
GAPDH	human	Fw	AGCCACATCGCTCAGACAC	19
		Rev	GCCCAATACGACCAAATCC	19

2.4.2. Functional assessment of CYP induction

HepG2 cells, HepaRG cells, cryopreserved human hepatocytes, as well as three-dimensionally seeded co-cultured cryopreserved human hepatocyte spheroids, were cultured in a 5% CO₂ and 95% air humidified atmosphere at 37°C. Induction treatment (rifampicin 20 µM) lasted for 72 h, with the medium being changed every 24 h. Rifampicin stock solution was prepared in DMSO and further diluted in the appropriate culture medium to achieve a final DMSO concentration of 0.1% (v/v). Experimental control culture wells were treated with solvent (DMSO, 0.1% (v/v)) alone. Following induction treatment, CYP activity was assessed by the addition of fresh medium containing the cocktail probe drugs to the control and pre-treated cells. Substrates were dissolved and serially diluted in DMSO to the required concentrations. The final concentration of DMSO during the cocktail incubation was 0.2% (v/v). At selected time points (0, 15, 30, 45, 60, 90, and 120 min) the incubation was stopped by the addition of a threefold volume of ice-cold methanol containing the respective internal standards. The bottom of the wells was scraped using a pipette tip, after which the contents were transferred to an autosampler vial. After vigorous shaking (10 minutes) and centrifugation (3220 g, 30 min, 10°C) the supernatants were stored at -20°C until quantification by LC-MS/MS.

To determine the velocity of midazolam 1'-hydroxylation and efavirenz 8'-hydroxylation, the entire content of the autosampler vials were evaporated using a minivap microplate evaporator (Porvair Sciences Ltd., King's Lynn, Norfolk, UK). The analytes were then resuspended in 45 µl of the respective culture medium to which 5 µl (500 units) of β-glucuronidase was added. Following a 12 h incubation at 37°C, the reaction was terminated by the addition of methanol, after which the samples were treated as described above.

2.5. *In vivo* assessment of CYP induction

The *in vivo* characterisation of the Basel cocktail has been described in previous publications [6, 7]. Fifteen healthy volunteers were treated with 600 mg rifampicin per day for 7 days to induce CYP activity [7]. Genotyping identified one subject as a CYP2D6 intermediate metaboliser (CYP2D6*4/*41) and another subject as a CYP2C19 poor metaboliser (CYP2C19*2/*2). Data from these two subjects were not included in the analysis for CYP2C19 (n=14) and CYP2D6 (n=14), respectively.

Clearance ratios of the probe drugs (induced vs non-induced) were used to assess the extent of CYP induction.

2.6. Data analysis

CYP activities were determined as the respective metabolite formation rates corresponding to the slope in the metabolite concentration versus time graphs. Metabolite concentrations were quantified using standard curves of pure compounds as previously described [6].

For induction experiments, formation rates were determined and the fold change versus the basal conditions was calculated as the ratio of the metabolite formation rate in wells exposed to an inducer and control wells.

Means were compared with the two-tailed Student's *t*-test using GraphPad Prism 6.0 (GraphPad Software, San Diego, CA, USA). Data are presented as mean \pm SEM unless stated otherwise.

3. Results

CYP mRNA expression and CYP activities were investigated using four different liver cell cultures: HepG2 cells, HepaRG cells, primary human hepatocytes seeded two-dimensionally (2D) and primary hepatocytes from the same donor in three-dimensional (3D) spheroid co-culture.

3.1. Basal mRNA expression of CYPs in the different liver cell models

Basal CYP mRNA expression relative to GAPDH was detectable in all cell systems investigated and was highest in 3D-cultured primary human hepatocytes (Figure 1). For HepG2 cells, the CYP mRNA expression was lower than for every other cell system investigated. In comparison to 3D-cultured primary human hepatocytes, HepaRG cells showed a 4 times lower mRNA expression of CYP3A4 and 2C19, whereas the mRNA expression of the other CYPs investigated was more than 10 times lower. In 2D-cultured primary human hepatocytes, CYP2C19 mRNA expression was approximately 4 times lower than in 3D-cultured hepatocytes, whereas the mRNA expression of the other CYPs was more than 10 times lower.

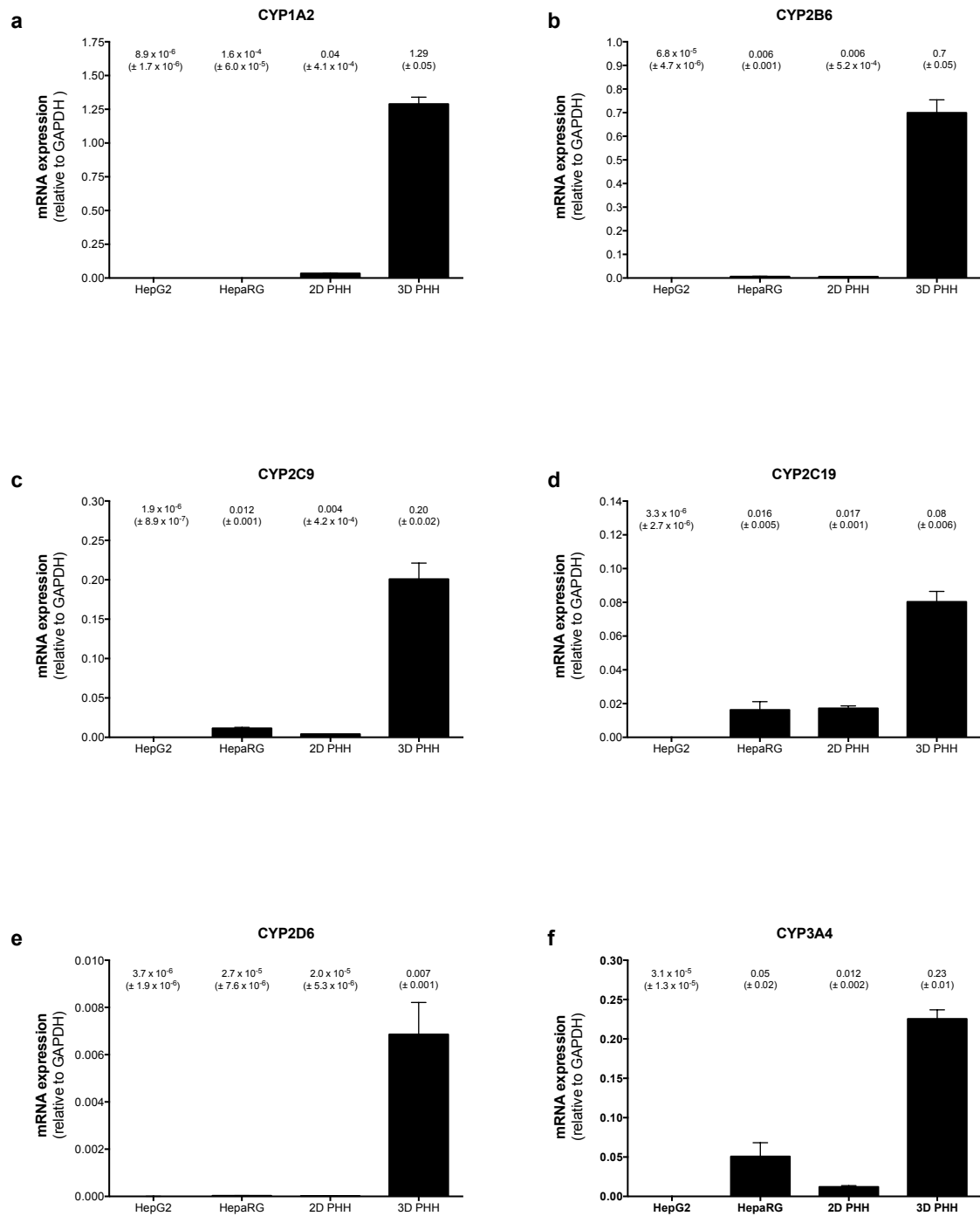


Figure 1. Basal mRNA expression of CYP1A2 (a), 2B6 (b), 2C9 (c), 2C19 (d), 2D6 (e), and 3A4 (f) in HepG2, HepaRG, 2D-, and 3D-cultured primary cryopreserved human hepatocytes. mRNA expression was determined by rt-PCR as described in the methods section. Results are expressed as mean \pm SEM relative to GAPDH of at least 3 independent experiments. PHH = primary human hepatocytes.

3.2. Basal metabolic activity of the liver cell models used

Experiments using single substrates instead of the entire cocktail showed no mutual interactions between the probe drugs, except for 10 μ M efavirenz, which was associated with a 30% decrease in CYP2C9 and a 20% decrease in CYP2C19 activity (results not shown). For HepaRG and conventional hepatocyte incubations, the use of 10 μ M efavirenz was necessary, as lower efavirenz concentrations did not yield quantifiable concentrations of 8'-hydroxyefavirenz. All experiments were performed with the entire cocktail, hence the slight inhibitory effect of efavirenz was present in both conditions (basal and induced). In the *in vivo* cocktail, this interaction had been avoided by using efavirenz at a very low dose [7].

Basal activities for all substrates investigated could be determined in HepaRG cells, 2D- and 3D-cultured primary human hepatocytes, but not in HepG2 cells (Table 2).

Table 2. Basal CYP activity in HepG2, HepaRG, 2D-, and 3D-cultured primary cryopreserved human hepatocytes (PHH). Primary human hepatocytes used for 2D- and 3D-cultures were from the same batch of cryopreserved cells. Values presented are the metabolite formation rates (see Figure 2) and the corresponding regression coefficients (r^2) of the metabolite-time curves. Metabolite concentrations were determined by LC-MS/MS. Data are presented as mean \pm SEM of at least 3 independent experiments. Values in brackets are based on measurements of the last experimental time-point only, concentrations of all earlier time-points were below LLOQ. nd = not determinable (i.e. lacking basal activity).

Basal CYP activities (pmol/ h / 50'000 cells)				
	HepG2 cells	HepaRG cells	2D-cultured PHH	3D-cultured PHH
CYP1A2	nd	(0.46 \pm 0.02)	(0.09 \pm 0.01)	0.22 \pm 0.02 0.932
CYP2B6	nd	0.33 \pm 0.02 0.999	0.54 \pm 0.04 0.905	2.11 \pm 0.07 0.985
CYP2C9	nd	(0.11 \pm 0.01)	(0.016 \pm 0.002)	0.16 \pm 0.01 0.854
CYP2C19	0.16 \pm 0.01 0.976	18.5 \pm 1.0 0.939	0.47 \pm 0.04 0.815	3.7 \pm 0.1 0.978
CYP2D6	nd	0.69 \pm 0.06 0.823	0.25 \pm 0.01 0.950	6.2 \pm 0.3 0.935
CYP3A4	0.64 \pm 0.04 0.645	85.6 \pm 4.5 0.991	27.4 \pm 1.5 0.903	60.4 \pm 1.5 0.993

The highest activities were observed for CYP3A4, CYP2C19 and CYP2D6 in 3D-cultured primary human hepatocytes and in HepaRG cells. In HepG2 cells, only activities of CYP3A4 and CYP2C19 could reliably be determined; metabolite formation remained below the limit of detection for the other CYPs.

Figure 2 shows the metabolite formation rates for the two CYP isoforms (CYP2C19 and CYP3A4) with activity in all four cell models using omeprazole and midazolam as probe drugs. Metabolite accumulation was linear with time up to 45 minutes for CYP3A4 and up to 1 hour for CYP2C19, respectively. The metabolite formation rates were highest for HepaRG cells and lowest for HepG2 cells. Formation rates in 3D-cultured primary hepatocytes were higher than in 2D-cultures, illustrating a benefit of the 3D spheroid co-culture.

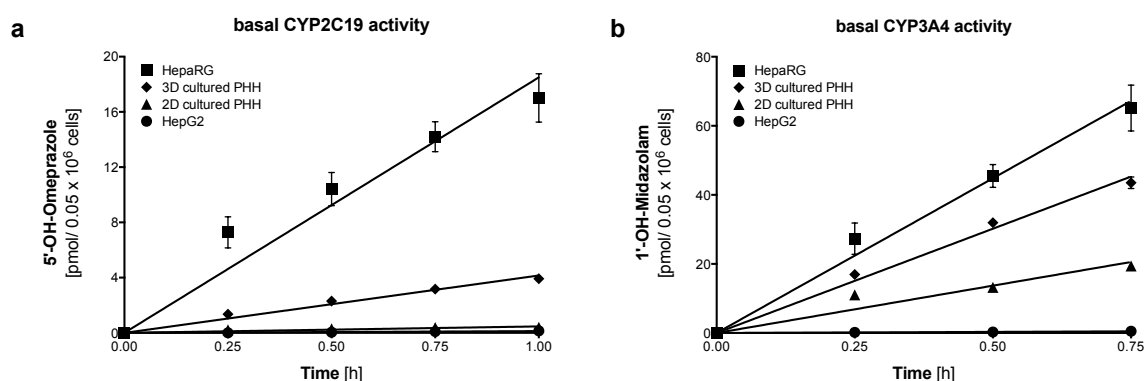


Figure 2. Basal activity of CYP2C19 and CYP3A4 assessed using formation rates of 5-hydroxyomeprazole (a) and 1'-hydroxymidazolam (b) in HepG2, HepaRG, 2D-, and 3D-cultured primary cryopreserved human hepatocytes. Primary hepatocytes were from the same batch of cryopreserved cells. Metabolite concentrations were determined by LC-MS/MS. The corresponding velocities and regressions are given in Table 2. Data are presented as mean \pm SEM of at least 3 independent experiments. PHH = primary human hepatocytes.

3.3. Induced mRNA expression of CYPs in liver cell models exposed to rifampicin

Liver cell models were exposed to 20 μ M rifampicin for 48 h and mRNA expression of the 6 CYPs isoforms was determined. In HepG2 cells, mRNA expression increased only for CYP3A4 (Figure 3). In HepaRG cells, mRNA expression increased for CYP2B6, 2C9, 2C19 and 3A4, but not for CYP1A2 and 2D6. A similar pattern of CYP induction was obtained for 3D-cultured primary human hepatocytes, showing

induction for CYP2B6, 2C9, 2C19 and 3A4, but not for CYP2D6 and 1A2. In comparison, when primary hepatocytes from the same batch were cultured conventionally (2D), induced mRNA expression could only be found for CYP3A4 and CYP2B6.

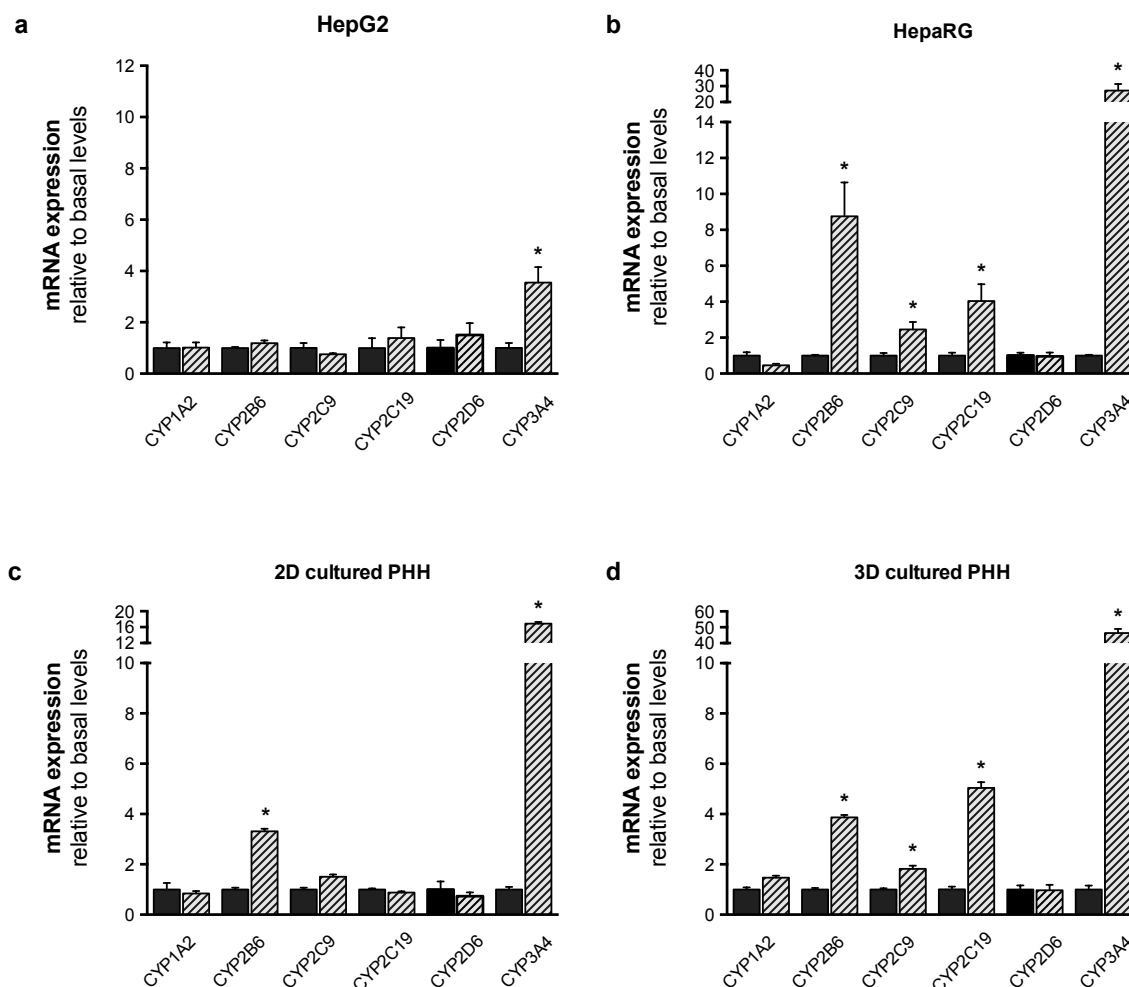


Figure 3. mRNA expression of CYP1A2, 2B6, 2C9, 2C19, 2D6, and 3A4 in HepG2 (a), HepaRG (b), 2D- (c), and 3D-cultured primary cryopreserved human hepatocytes (d) after treatment with 20 μ M rifampicin for 48 h. mRNA expression was determined by rt-PCR as described in the methods section. Values were normalized to GAPDH expression. Results are expressed as the mean \pm SEM fold increase after treatment with rifampicin relative to levels observed in control cultures. PHH = primary human hepatocytes. * p <0.05 vs. control culture.

Since rifampicin is only a weak inducer of CYP1A2, we exposed 3D-cultured primary human hepatocytes also to 3-methylcholanthrene, which is a well-established in vitro CYP1A2 inducer [17, 18]. As shown in Supplementary Figure 1 (S1), in 3D-cultured primary human hepatocytes CYP1A2 mRNA was induced approximately 13 times by

3-methylcholathrene, which was also reflected in an approximately six times higher production of paraxanthine from caffeine.

3.4. CYP activity after treatment of liver cell models with rifampicin

Metabolite formation was assessed after treatment of liver cells with 20 μ M rifampicin for 72 h. As shown in Figure 4, treatment of 3D-cultured primary human hepatocytes was associated with increased metabolite formation by all tested CYP isoforms. The metabolite production rates were linear for at least 45 min (midazolam) and up to 120 min (caffeine and efavirenz).

In agreement with the mRNA expression data after induction with rifampicin and basal CYP activity, metabolite formation could be determined for all substrates in HepaRG cells, and in 2D- and 3D-cultured primary human hepatocytes, but not in HepG2 cells (Table 3). The highest activities were detected for CYP3A4 and CYP2C19 in 3D-cultured primary human hepatocytes and in HepaRG cells. In HepG2 cells, only activities of CYP3A4 and 2C19 could be detected.

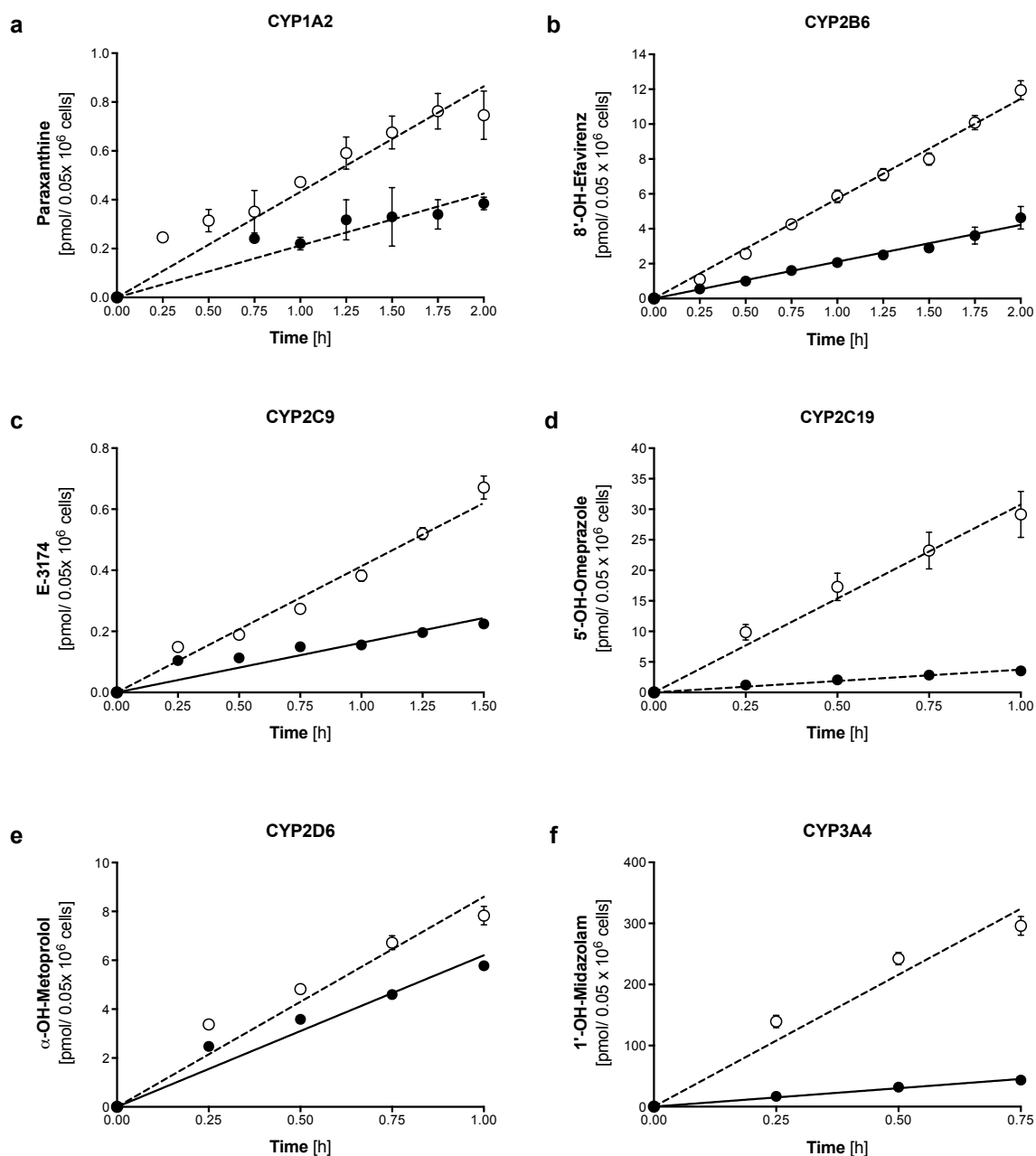


Figure 4. Formation of paraxanthine (a), 8'-OH-efavirenz (b), E-3174 (c), 5'-OH-omeprazole (d), α-OH-metoprolol (e), and 1'-hydroxymidazolam (f) by 3D-cultured primary human hepatocytes after treatment with 20 μM rifampicin for 72 h (open symbols) compared to control cultures (closed symbols). Metabolite concentrations were determined by LC-MS/MS. The corresponding formation rates and regression coefficients in control cultures and after treatment with 20 μM rifampicin are given in Tables 2 and 3. Data are presented as mean ± SEM of at least 3 independent experiments.

Table 3. CYP activity in HepG2, HepaRG, 2D-, and 3D-cultured primary cryopreserved human hepatocytes (PHH) after treatment with 20 μ M rifampicin for 72 h. Primary human hepatocytes used for 2D- and 3D-cultures were from the same batch of cryopreserved cells. Values presented are the metabolite formation rates and the regression coefficients (r^2) of the metabolite-time curves after pre-treatment with rifampicin. Metabolite concentrations were determined by LC/MS. Data are presented as mean \pm SEM of at least 3 independent experiments. Values in brackets are based on measurements of the last experimental time-point only, concentrations of all earlier time-points were below LLOQ. nd = not determinable (lacking basal activity).

Induced CYP activities [20μM rifampicin]				
(pmol/ h / 50'000 cells)				
	HepG2 cells	HepaRG cells	2D-cultured PHH	3D-cultured PHH
CYP1A2	nd	(0.51 \pm 0.04)	(0.09 \pm 0.01)	0.46 \pm 0.02 0.956
CYP2B6	nd	1.31 \pm 0.04 0.998	1.7 \pm 0.1 0.975	5.7 \pm 0.1 0.994
CYP2C9	nd	(0.12 \pm 0.02)	(0.022 \pm 0.002)	0.41 \pm 0.01 0.985
CYP2C19	0.21 \pm 0.01 0.979	75.9 \pm 1.8 0.996	1.96 \pm 0.11 0.978	30.7 \pm 1.7 0.980
CYP2D6	nd	3.9 \pm 0.2 0.992	0.35 \pm 0.01 0.928	8.6 \pm 0.4 0.952
CYP3A4	1.1 \pm 0.1 0.999	675 \pm 20 0.999	129 \pm 8 0.943	432 \pm 17 0.952

3.5. Comparison rifampicin-induced CYP activity in vitro and in vivo

Compared to baseline, CYP2C9 and CYP3A4 activities were increased 1.5 to 2 times in HepG2 cells without reaching statistical significance (Figure 5). In HepaRG cells, activities of CYP3A4, CYP2D6, 2C19 and 2B6 were increased significantly, with the exception of CYP2D6 matching well with the mRNA induction data. An almost identical result was obtained for 2D-cultured primary human hepatocytes. In 3D-cultured primary human hepatocytes, CYP activities of all inducible CYP isoforms were increased at least 2-fold after rifampicin induction.

Treatment of healthy volunteers with rifampicin [7] was associated with an approximately 7-fold induction of CYP3A4, a 14-fold induction of CYP2C19, a doubling of

CYP2C9 activity and an approximately 1.7-fold increase in CYP2B6 activity. When compared to the liver cell models investigated, this pattern was reflected best by the 3D-cultured primary human hepatocytes.

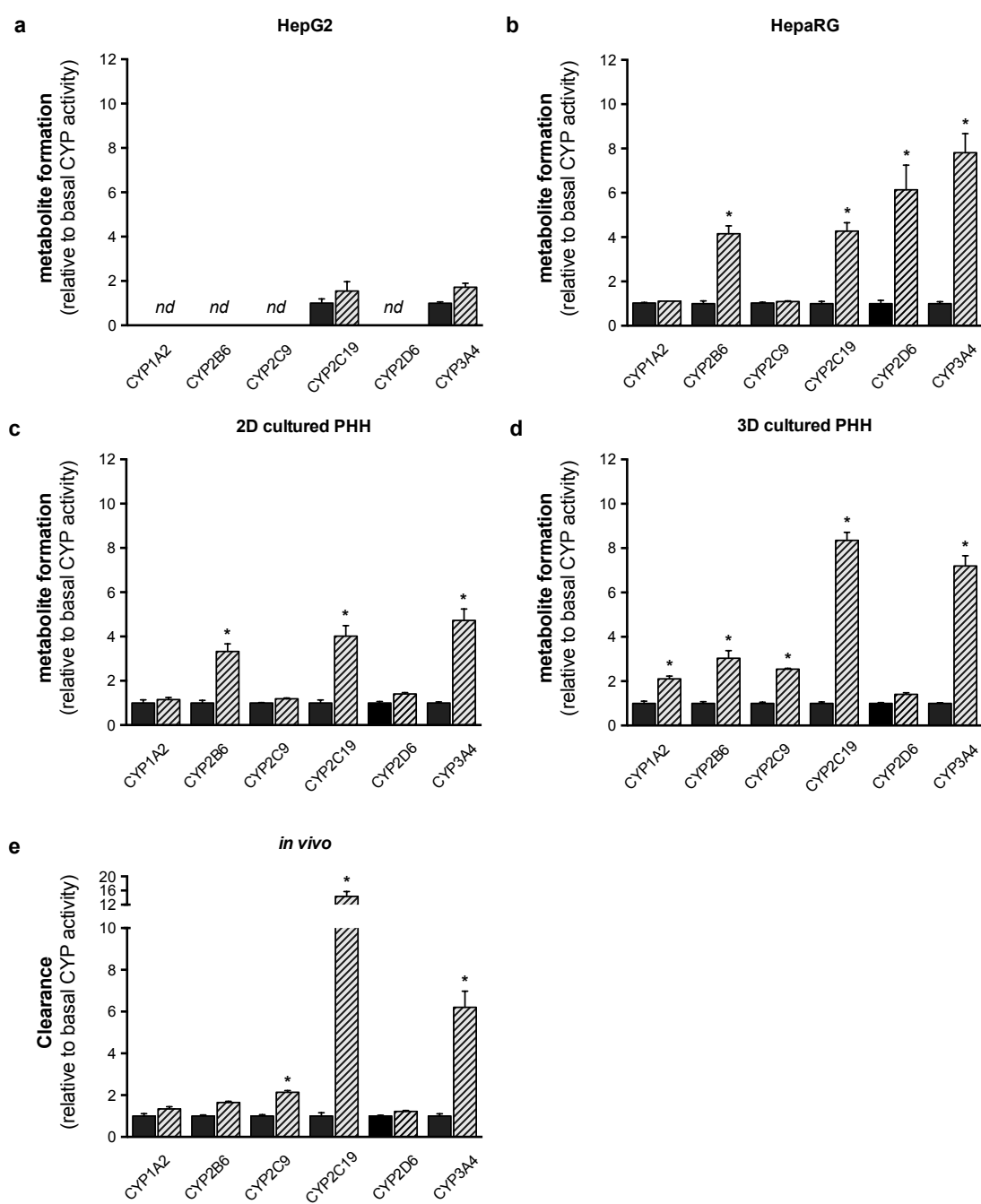


Figure 5. Fold increase (relative to non-induced control) of CYP activity *in vitro* in HepG2 (A), HepaRG (B), 2D-, and 3D-cultured primary human hepatocytes (C and D), and *in vivo* in healthy male subjects (E, n=14 for CYP2C19 and CYP2D6; n=15 for all other CYP isoforms) after treatment with rifampicin. Hepatocyte cell lines were treated with 20 μ M rifampicin for 72 h and healthy volunteers with 600 mg rifampicin per day for 7 days as described in the methods section. Metabolite and parent drug concentrations were determined by LC-MS/MS. Results are expressed as mean \pm SEM. PHH = primary human hepatocytes. * p <0.05 vs. control.

4. Discussion

This study confirms that basal mRNA expression and CYP activity as well as CYP inducibility show large differences between *in vitro* used hepatocyte cell models and, depending on the hepatocyte model used, that the *in vivo* characterised Basel phenotyping cocktail is suitable for CYP induction experiments *in vitro*.

HepG2 cells represent a hepatoma cell line, which is used extensively for toxicological studies but less frequently for studies of drug metabolism [19-21]. Drug metabolism is difficult to assess with this cell line since CYPs show weak mRNA expression and activity [13, 22, 23]. In this point, the results of the current investigation are in agreement with these previous studies. In the basal state, mRNA expression was clearly lower than in the other cell types for every CYP investigated and the activity could reliably be determined only for CYP3A4 and CYP2C19. CYP induction with rifampicin resulted in a significant 4-fold increase in the CYP3A4 mRNA, which was only partially reflected in a corresponding increase in CYP3A4 activity. A limited inducibility of the CYP3A and CYP2C families in HepG2 cells has also been shown in other studies [13, 22] and has been attributed to a low expression of the nuclear receptors CAR and PXR [24, 25], which are mediating the induction of the CYP2C and 3A families [26]. In contrast, inducibility of CYP1A2 (which we did not determine in our studies) has been shown to be maintained in HepG2 cells [27]. CYP1A2 induction is mediated by the aryl hydrocarbon receptor [26], which is highly expressed in HepG2 cells [24]. In contrast to phase I enzyme activities, conjugation reactions appear to be maintained quite well in HepG2 cells [28]. HepG2 cells can therefore only be used to answer very specific questions regarding drug metabolism.

HepaRG cells represent a hepatoma cell line, which has first been described in 2002 as a cell model suitable for HBV infection and propagation [29]. Soon after their first description, HepaRG cells were characterised and proposed for their use as a model for drug metabolism studies [24]. The gene expression profile shows profound differences compared to HepG2 cells, explaining the observed differences in their drug metabolism phenotype [30]. HepaRG cells have also been used in drug toxicity studies, particularly, when active metabolites are suspected [22, 25]. Considering the current study, HepaRG cells were clearly a more suitable hepatocyte model for studying drug metabolism than HepG2 cells. mRNA expression could be detected for all CYPs investigated and was inducible except for CYP1A2 and 2D6. Lack of CYP1A2 induction is not a problem of the cell line, but of rifampicin, which was used as a CYP inducer. As shown *in vitro* [22, 27] and *in vivo* [7], rifampicin is a good inducer for the

CYP2C and 3A families, but not for CYP1A2. With specific CYP1A2 inducers such as 3-methylcholanthrene CYP1A2 can be induced in HepaRG cells on both the mRNA and the activity level [24, 25]. CYP2D6 has a low activity in HepaRG cells, possibly because the cell line originates from a slow CYP2D6 metaboliser [25], and it cannot be induced with rifampicin [22].

Interestingly, the activity for CYP3A4 and 2C19 were higher in HepaRG cells as compared to 3D-cultured primary human hepatocytes, whereas the corresponding mRNA expressions (relative to GAPDH) were lower. This could be a problem of standardisation to GAPDH (different GAPDH expression in HepaRG cells and primary hepatocytes) or a bad correlation between mRNA levels and protein expression and/or activity. In the study of Choi et al. [27], GAPDH mRNA expression was quite stable among different hepatocyte cell lines, arguing against the first possibility. On the other hand, it is well established that posttranslational modifications such as acetylation, glycosylation and phosphorylation can have a large impact on protein activity [31], favouring the second possibility. In our study, the CYP activity profile and inducibility of HepaRG cells were more closely related to primary hepatocytes than to HepG2 cells.

Primary hepatocytes are currently considered to be the gold standard for drug metabolism studies. By using the same batch of human cryopreserved hepatocytes in the 2D- and 3D-cultures, we were able to estimate whether the 3D environment would lead to differences in CYP activity and/or expression compared to the 2D-cultures. Indeed, in comparison to 2D-cultures, 3D-cultured primary human hepatocytes exhibited a higher CYP mRNA expression, a higher basal CYP activity and a better inducibility. In comparison to the *in vivo* results regarding CYP induction, 3D-cultured primary human hepatocytes showed a better agreement than the other cell lines tested, suggesting that they could be usable to predict the induction potential of new drugs. Hepatocyte 3D-cultures are currently being developed and characterise as an alternative to 2D-cultures in order to overcome well-known drawbacks of 2D-cultures such as varying expression of CYP activities, varying CYP inducibility and loss of differentiation over time [24, 32]. Assuming that 3D-cultures of primary human hepatocytes may offer advantages compared to the corresponding 2D-cultures, many 3D-hepatocyte models have been and are currently being explored for drug metabolism and drug toxicity studies [12, 14, 33, 34].

We performed our studies with a co-culture system using 3T3-Swiss albino mouse fibroblasts as feeder cells for human cryopreserved primary hepatocytes. This sys-

tem has originally been described in detail by Ohkura et al. [15] who characterised it regarding the mRNA expression of phase I and phase II drug metabolism enzymes and demonstrated its capacity to produce metabolites from different drugs. The model uses special plates coated with a block co-polymer that allows the fibroblasts and hepatocytes to only adhere to certain areas of the wells. In time, the mouse fibroblasts and human cryopreserved hepatocytes are able to form 3D structures described as spheroids. Spheroids can be regarded as a cell aggregation with an energy- and surface-minimised structure that, according to van Zijl et al. [35] mimic the *in vivo* situation quite efficiently regarding cell shape and cellular environment. The results of our study support this assumption.

After having been characterised *in vivo* [6, 7], the substrate cocktail showed a satisfactory performance also *in vitro*. Critical substrates were losartan (CYP2C9) and caffeine (CYP1A2), which were metabolised at a low rate even in 3D-cultured primary human hepatocytes and showed no significant metabolism in HepG2 cells. On the other hand, they correctly reflected CYP2C9 induction by rifampicin and CYP1A2 induction by 3-methylcholanthrene. Depending on the question to be answered and on the cell system used, they could be replaced by phenacetin (CYP1A2) and diclofenac (CYP2C9), which have been shown to be suitable substrates *in vitro* [8, 10, 32].

In conclusion, our studies demonstrate that the 3D-primary human hepatocyte spheroid culture system is suitable for the assessment of drug metabolism and CYP induction *in vitro*. Among the four tested cell systems, 3D-cultured primary human hepatocytes best reflect CYP inducibility *in vivo*. HepaRG cells are close to 3D-cultured primary human hepatocytes but induced CYP activities correlate less well with CYP induction *in vivo*. HepG2 cells are known to predict CYP1A2 induction but are less suitable for CYPs of the 2C and 3A family. The substrates of the Basel phenotyping cocktail only show minimal interactions *in vitro* and the cocktail is thus suitable for the assessment of CYP induction *in vitro*.

Acknowledgements

We would like to thank Nathalie Schaub², Evelyne Durr², François Singh¹, Annalisa Bonifacio¹, Beatrice Vetter¹, and Urs Duthaler¹ for their valuable advice and technical support.

Financial support

SK was supported by a grant of the Swiss National Science Foundation (SNF 31003A_156270).

Conflict of interest

None of the authors reports any conflict of interest regarding this study.

5. References

1. Wilkinson, G.R., *Drug metabolism and variability among patients in drug response*. N Engl J Med, 2005. **352**(21): p. 2211-21.
2. Fuhr, U., A. Jetter, and J. Kirchheiner, *Appropriate phenotyping procedures for drug metabolizing enzymes and transporters in humans and their simultaneous use in the "cocktail" approach*. Clin Pharmacol Ther, 2007. **81**(2): p. 270-83.
3. Christensen, M., et al., *The Karolinska cocktail for phenotyping of five human cytochrome P450 enzymes*. Clin Pharmacol Ther, 2003. **73**(6): p. 517-28.
4. Chainuvati, S., et al., *Combined phenotypic assessment of cytochrome p450 1A2, 2C9, 2C19, 2D6, and 3A, N-acetyltransferase-2, and xanthine oxidase activities with the "Cooperstown 5+1 cocktail"*. Clin Pharmacol Ther, 2003. **74**(5): p. 437-47.
5. Bosilkovska, M., et al., *Geneva cocktail for cytochrome p450 and P-glycoprotein activity assessment using dried blood spots*. Clin Pharmacol Ther, 2014. **96**(3): p. 349-59.
6. Donzelli, M., et al., *The basel cocktail for simultaneous phenotyping of human cytochrome P450 isoforms in plasma, saliva and dried blood spots*. Clin Pharmacokinet, 2014. **53**(3): p. 271-82.
7. Derungs, A., et al., *Effects of Cytochrome P450 Inhibition and Induction on the Phenotyping Metrics of the Basel Cocktail: A Randomized Crossover Study*. Clin Pharmacokinet, 2016. **55**(1): p. 79-91.
8. Mori, K., et al., *Cocktail-substrate assay system for mechanism-based inhibition of CYP2C9, CYP2D6, and CYP3A using human liver microsomes at an early stage of drug development*. Xenobiotica, 2009. **39**(6): p. 415-22.
9. Spaggiari, D., et al., *A cocktail approach for assessing the in vitro activity of human cytochrome P450s: an overview of current methodologies*. J Pharm Biomed Anal, 2014. **101**: p. 221-37.
10. Youdim, K.A., et al., *Induction of cytochrome P450: assessment in an immortalized human hepatocyte cell line (Fa2N4) using a novel higher throughput cocktail assay*. Drug Metab Dispos, 2007. **35**(2): p. 275-82.
11. Abadie-Viollon, C., et al., *Follow-up to the pre-validation of a harmonised protocol for assessment of CYP induction responses in freshly isolated and cryopreserved human hepatocytes with respect to culture format, treatment, positive reference inducers and incubation conditions*. Toxicol In Vitro, 2010. **24**(1): p. 346-56.
12. Godoy, P., et al., *Recent advances in 2D and 3D in vitro systems using primary hepatocytes, alternative hepatocyte sources and non-parenchymal liver cells and their use in investigating mechanisms of hepatotoxicity, cell signaling and ADME*. Arch Toxicol, 2013. **87**(8): p. 1315-530.

13. Donato, M.T. and J.V. Castell, *Strategies and molecular probes to investigate the role of cytochrome P450 in drug metabolism: focus on in vitro studies*. Clin Pharmacokinet, 2003. **42**(2): p. 153-78.
14. Roth, A. and T. Singer, *The application of 3D cell models to support drug safety assessment: opportunities & challenges*. Adv Drug Deliv Rev, 2014. **69-70**: p. 179-89.
15. Ohkura, T., et al., *Evaluation of human hepatocytes cultured by three-dimensional spheroid systems for drug metabolism*. Drug Metab Pharmacokinet, 2014. **29**(5): p. 373-8.
16. Livak, K.J. and T.D. Schmittgen, *Analysis of relative gene expression data using real-time quantitative PCR and the 2(-Delta Delta C(T)) Method*. Methods, 2001. **25**(4): p. 402-8.
17. Morel, F., et al., *Effects of various inducers on the expression of cytochromes P-450 IIC8, 9, 10 and IIIA in cultured adult human hepatocytes*. Toxicol In Vitro, 1990. **4**(4-5): p. 458-60.
18. Rodriguez-Antona, C., et al., *Quantitative RT-PCR measurement of human cytochrome P-450s: application to drug induction studies*. Arch Biochem Biophys, 2000. **376**(1): p. 109-16.
19. Xu, J.J., D. Diaz, and P.J. O'Brien, *Applications of cytotoxicity assays and pre-lethal mechanistic assays for assessment of human hepatotoxicity potential*. Chem Biol Interact, 2004. **150**(1): p. 115-28.
20. Yoshitomi, S., et al., *Establishment of the transformants expressing human cytochrome P450 subtypes in HepG2, and their applications on drug metabolism and toxicology*. Toxicol In Vitro, 2001. **15**(3): p. 245-56.
21. Zahno, A., et al., *The role of CYP3A4 in amiodarone-associated toxicity on HepG2 cells*. Biochem Pharmacol, 2011. **81**(3): p. 432-41.
22. Gerets, H.H., et al., *Characterization of primary human hepatocytes, HepG2 cells, and HepaRG cells at the mRNA level and CYP activity in response to inducers and their predictivity for the detection of human hepatotoxins*. Cell Biol Toxicol, 2012. **28**(2): p. 69-87.
23. Westerink, W.M. and W.G. Schoonen, *Cytochrome P450 enzyme levels in HepG2 cells and cryopreserved primary human hepatocytes and their induction in HepG2 cells*. Toxicol In Vitro, 2007. **21**(8): p. 1581-91.
24. Aninat, C., et al., *Expression of cytochromes P450, conjugating enzymes and nuclear receptors in human hepatoma HepaRG cells*. Drug Metab Dispos, 2006. **34**(1): p. 75-83.
25. Guillouzo, A., et al., *The human hepatoma HepaRG cells: a highly differentiated model for studies of liver metabolism and toxicity of xenobiotics*. Chem Biol Interact, 2007. **168**(1): p. 66-73.

26. Xu, C., C.Y. Li, and A.N. Kong, *Induction of phase I, II and III drug metabolism/transport by xenobiotics*. Arch Pharm Res, 2005. **28**(3): p. 249-68.
27. Choi, J.M., et al., *HepG2 cells as an in vitro model for evaluation of cytochrome P450 induction by xenobiotics*. Arch Pharm Res, 2015. **38**(5): p. 691-704.
28. Westerink, W.M. and W.G. Schoonen, *Phase II enzyme levels in HepG2 cells and cryopreserved primary human hepatocytes and their induction in HepG2 cells*. Toxicol In Vitro, 2007. **21**(8): p. 1592-602.
29. Gripon, P., et al., *Infection of a human hepatoma cell line by hepatitis B virus*. Proc Natl Acad Sci U S A, 2002. **99**(24): p. 15655-60.
30. Jennen, D.G., et al., *Comparison of HepG2 and HepaRG by whole-genome gene expression analysis for the purpose of chemical hazard identification*. Toxicol Sci, 2010. **115**(1): p. 66-79.
31. Glanemann, C., et al., *Disparity between changes in mRNA abundance and enzyme activity in Corynebacterium glutamicum: implications for DNA microarray analysis*. Appl Microbiol Biotechnol, 2003. **61**(1): p. 61-8.
32. Halladay, J.S., et al., *An 'all-inclusive' 96-well cytochrome P450 induction method: measuring enzyme activity, mRNA levels, protein levels, and cytotoxicity from one well using cryopreserved human hepatocytes*. J Pharmacol Toxicol Methods, 2012. **66**(3): p. 270-5.
33. Astashkina, A. and D.W. Grainger, *Critical analysis of 3-D organoid in vitro cell culture models for high-throughput drug candidate toxicity assessments*. Adv Drug Deliv Rev, 2014. **69-70**: p. 1-18.
34. Schyschka, L., et al., *Hepatic 3D cultures but not 2D cultures preserve specific transporter activity for acetaminophen-induced hepatotoxicity*. Arch Toxicol, 2013. **87**(8): p. 1581-93.
35. van Zijl, F. and W. Mikulits, *Hepatospheres: Three dimensional cell cultures resemble physiological conditions of the liver*. World J Hepatol, 2010. **2**(1): p. 1-7.

Supplementary Files

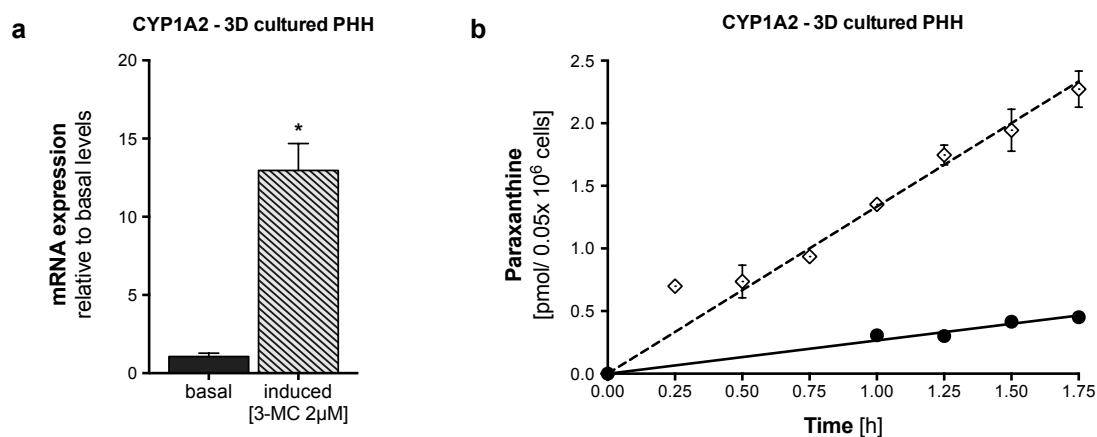


Figure S1. (a) Fold increase (relative to non-induced control) of CYP1A2 mRNA levels after treatment of 3D-cultured primary human hepatocytes with 3-methylcholanthrene [2 μ M] for 72 h. mRNA levels were determined using rt-PCR as described in the methods section. mRNA expression in control cultures and after treatment with 3-methylcholanthrene was first normalized to the respective GAPDH expression. Data are given as mean \pm SEM of at least 3 independent experiments **(b)** Activity of CYP1A2 assessed using caffeine-N₃-demethylation in 3D-cultured primary cryopreserved human hepatocytes after treatment with 3-methylcholanthrene [2 μ M] (open symbols) for 72 h compared to control cultures (closed symbols). * = $p < 0.05$ vs. corresponding basal value.

**5. Assessment of cytochrome p450 2D6 activity with
metoprolol α -hydroxylation *in vivo* and *in vitro***

Benjamin Berger¹, Urs Duthaler¹, Franziska Boess², Adrian Roth²,
Stephan Krähenbühl^{1,3}, Manuel Haschke¹

¹Division of Clinical Pharmacology & Toxicology, University Hospital Basel and Department of Biomedicine, University of Basel, Switzerland

²Non-Clinical Safety, Hoffmann-La Roche Ltd, Basel, Switzerland

³Swiss Center for Applied Human Research (SCAHT)

Abstract

Metoprolol α -hydroxylation has been described as exclusively catalysed by CYP2D6, a CYP450 isoform that is considered to be not inducible through the use of typical inducers of the CYP2C and CYP3A families, such as rifampicin, phenobarbital, and hypericum extract. While assessing CYP2D6 activity under basal conditions and after pretreatment with rifampicin *in vivo*, we observed a surprising, slight change in metoprolol AUC ratio as well as in the metabolic ratio. We investigated these findings *in vitro* using HepaRG cells and primary human hepatocytes, studied before and after treatment with 20 μ M rifampicin. While mRNA expression levels of CYP3A4 showed a 15- to 30-fold increase in both cell models, mRNA of CYP2D6 was not affected by rifampicin. 1'-hydroxymidazolam formation (a marker of CYP3A4 activity) increased by a factor of 5 to 8 in both cell models, while the formation of α -hydroxymetoprolol increased by a factor of 6 in HepaRG cells and by a factor of 1.4 in primary cryo-preserved human hepatocytes. In order to test whether CYP3A4 was contributing to metoprolol α -hydroxylation, we studied midazolam and metoprolol metabolism in supersomes expressing CYP3A4. Midazolam was rapidly converted to 1'-hydroxymidazolam in CYP3A4 supersomes, a reaction strongly inhibited by the CYP3A4 inhibitor ketoconazole. However, metoprolol was also α -hydroxylated by CYP3A4 supersomes. This reaction was inhibited with ketoconazole, but not with the CYP2D6-specific inhibitor quinidine. Therefore, we can conclude that α -hydroxylation of metoprolol is not exclusively metabolised by CYP2D6 and that CYP3A4 is also involved to some extent. This contribution is larger when CYP3A4 is induced but is too small to compromise the usability of metoprolol α -hydroxylation for phenotyping.

Keywords: *CYP2D6, α -hydroxymetoprolol, metoprolol, phenotyping, CYP induction, rifampicin*

1. Introduction

Metoprolol is a cardioselective beta blocker, that is currently mainly used in the treatment of heart failure [1], myocardial infarction [2], and arterial hypertension [3]. Intestinal absorption of metoprolol is rapid and almost complete; however, due to an extensive first pass metabolism [4], the bioavailability of metoprolol is approximately 50%. The half-life is in the range of 3 to 4 hours in young adults and between 7 to 9 hours in elderly patients [5]. Due to its short half-life, sustained release preparations have been developed and are currently prescribed for patients with heart failure and/or hypertension. Metoprolol is thoroughly biotransformed with less than 5% of an oral dose being excreted in non-metabolised form by the kidneys [4-7]. Approximately 70% of orally administered metoprolol is metabolized by CYP2D6 [8]. Major oxidative pathways are: O-demethylation to O-desmethylmetoprolol and its further oxidation to the corresponding metoprolol acid (65% of the oral dose recovered in urine); N-dealkylation to form N-desisopropylmetoprolol (10%); and α -hydroxylation to form α -hydroxymetoprolol (10%) [9] (Figure 1).

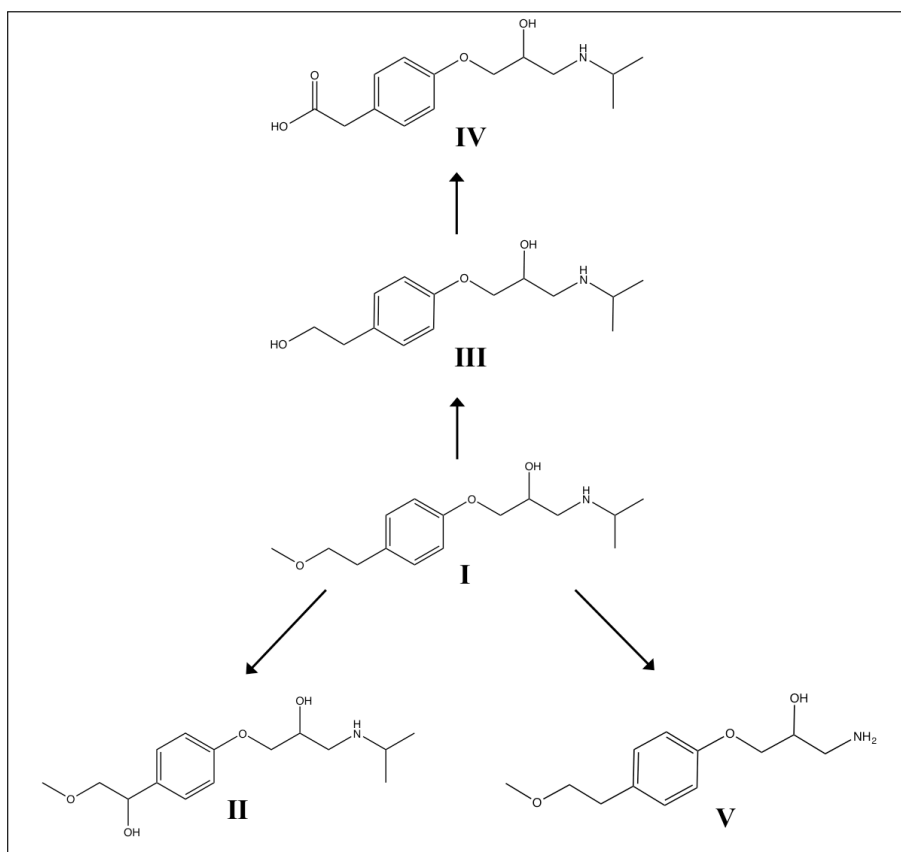


Figure 1. Major metabolic pathway of metoprolol in man. Metoprolol (I), α -hydroxymetoprolol (II), O-desmethylmetoprolol (III), metoprolol acid (IV), and N-desisopropylmetoprolol (V), adapted from [6, 7].

Whereas the carboxylic acid metabolites have no pharmacological activity, the α -hydroxymetabolite on the other hand is active, but only contributes to approximately 10% of the total beta-blocking activity of metoprolol [10]. Crucially, in contrast to the formation of the carboxylic acid metabolites, the α -hydroxylation of metoprolol only involves one enzymatic step, which is considered to be exclusively mediated by CYP2D6 [6, 11]. Furthermore, the metabolism of metoprolol is stereoselective; in extensive CYP2D6 metabolisers (CYP2D6 EM), R-metoprolol has a 40% higher clearance than S-metoprolol [12].

Due to the exclusive nature by which CYP2D6 is responsible for the metabolism of metoprolol, this step in the metabolic pathway of metoprolol has previously been used for the assessment of CYP2D6 activity *in vivo* [13-17] and *in vitro* [18]. We have recently published a clinical study in healthy volunteers investigating the effect of CYP inhibitors and inducers on the Basel phenotyping cocktail, which contains six low-dosed commercially available drugs (caffeine, efavirenz, losartan, omeprazole, metoprolol, and midazolam) [13]. After CYP induction with rifampicin, we not only observed a change in the phenotyping metric for CYP1A2, CYP2B6, CYP2C9, CYP2C19, and CYP3A4, but also surprisingly for CYP2D6, which was evaluated through use of the metabolic ratio of metoprolol and its α -hydroxy-metabolite, as well as the corresponding AUC_{0-24h} ratio. As CYP2D6 is considered to be non-inducible [19-24], this result was difficult to interpret.

Since it has been shown in a clinical study that the metabolism of metoprolol cannot be completely inhibited by quinidine [8], an efficient and specific CYP2D6 inhibitor [25, 26], it is likely that apart from CYP2D6, other CYP isoforms are also involved in the oxidative degradation of this drug, possibly even in its α -hydroxylation. Taking the results obtained from our *in vivo* study into account [13], we set out to confirm these findings *in vitro* using two different hepatocyte systems. We then attempted to figure out the mechanism behind this observation.

2. Materials and methods

2.1. Chemicals and reagents

Metoprolol, α -hydroxymetoprolol, O-desmethylnmetoprolol, metoprolol acid, and metoprolol-d7 were purchased from TRC (Toronto, Canada). 1'-hydroxymidazolam and midazolam-d6 were acquired from Lipomed (Arlesheim, Switzerland), while ri-

fampicin, ketoconazole, quinidine, and β -glucuronidase (type HP-2 from *Helix pomatia*) were obtained from Sigma-Aldrich (Sigma-Aldrich Chemie GmbH, Buchs, Switzerland). Midazolam was provided by Roche (Hoffmann-La Roche, Basel, Switzerland). Formic acid, HPLC grade methanol, and HPLC grade water were purchased from Merck (Darmstadt, Germany). The media used were purchased from GIBCO (Lucerne, Switzerland).

Stock solutions, calibration spiking solutions, and quality controls were prepared in DMSO. Calibration standards and quality controls were prepared by enriching the respective medium with the corresponding spiking solutions. Internal standard solutions containing the deuterated cocktail probe drugs were prepared in methanol.

2.2. Cell culture

Recombinant human CYP3A4 supersomes (rhCYP3A4, + P450 reductase + cytochrome b₅, Lot #4070007) and NADPH regenerating solutions A and B (A, contains NADP⁺, glucose-6-phosphate, and MgCl₂; B, contains glucose-6-phosphate dehydrogenase) were purchased from Corning Life science (Woburn, MA, USA). HLM samples were stored at -80°C until used.

HepaRG cells were purchased from Biopredic International (Rennes, France) as undifferentiated cryopreserved cells with the associated medium. Freshly split HepaRG cells were seeded at 9000 cells/well in 96-well plates (or 0.05x10⁶ cells/well in 24-well plates) and treated over the course of the next four weeks as previously described [27].

Primary cryopreserved human hepatocytes (Life Technologies, Lot #Hu8119 and Lot #Hu8124) were plated at 0.05x10⁶ cells/well in collagen type-1 precoated 96-well plates (or 0.25x10⁶ cells/well in 24-well plates) in William's E medium supplemented with 10% FCS (v/v), 1% L-Glutamine 200 mM (v/v), 1% Pen Strep (v/v), 0.1% dexamethasone 100 μ M (v/v), and 0.1% insulin 100 μ M (v/v), and then left to incubate at 37°C, 95% humidity, 5% CO₂.

2.3. Markers of CYP450 activity

CYP activity was assessed by the addition of metoprolol (CYP2D6, 23 μ M) and midazolam (CYP3A4, 5 μ M). The substrates were used at concentrations close to their previously published K_m values.

A previously developed liquid chromatography-tandem mass spectrometry (LC-MS/MS) method [14] was used to analyse the phase I metabolites of the probe substrates. Chromatographic separation was performed on a Shimadzu HPLC system (Shimadzu AG, Reinach, Switzerland), coupled to a triple quadrupole tandem mass spectrometer (API4000 or API5500, AB/MDS Sciex, Concord, Canada), operating in positive electrospray ionisation mode. The total run time was 2.9 minutes. Inter-assay accuracy (determined as the % bias) ranged from -8.6 to 8.9 and inter-assay precision (determined as the CV%) was lower than 8.3 for all analytes. The lower limit of quantification (LLOQ) utilising the API 4000 was 0.25 ng/mL for α -hydroxymetoprolol and 1'-hydroxymidazolam, whereas on the API5500 the LLOQ for α -hydroxymetoprolol, O-desmethylnetoprolol, and metoprolol acid was 0.025 ng/mL.

2.4. *In vivo* assessment of CYP induction

The *in vivo* characterisation of the Basel cocktail has been described in prior publications [13, 14]. Here, CYP induction had been achieved by treating 15 healthy volunteers with 600 mg rifampicin per day for 7 days [13]. Genotyping identified one subject as a CYP2D6 intermediate metabolizer (IM, CYP2D6*4/*41). As such, data from this subject was included in the analysis for CYP2D6. We used the ratio between the induced and the basal state of the clearance of the parent drug as a marker of CYP induction.

2.5. CYP2D6 and CYP3A4 induction experiments

2.5.1. Gene expression evaluation

HepaRG cells and primary cryopreserved human hepatocytes were seeded in 24 well plates and treated for 48h with rifampicin 20 μ M. 350 μ L of RLT buffer (Qiagen, Hombrechtikon, Switzerland) was used to lyse the respective liver cell models, after which the lysate was transferred to Qiashredder columns and centrifuged for 2 minutes at 13'000 rpm. From the eluate, total RNA was extracted and purified according to the manufacturer's instructions (Qiagen, RNeasy mini extraction kit). The concentration of the extracted RNA was measured spectrophotometrically at 260 nm on a NanoDrop 2000 (Thermo Scientific, Wohlen, Switzerland). cDNA was reverse transcribed from the isolated RNA using the Qiagen omniscript system. For quantitative rt-PCR, 10 ng cDNA was used. Forward and reverse primers for all CYPs tested, and endogenous references, Hypoxanthine phosphoribosyltransferase 1 (HPRT1)

and GAPDH, were purchased from Microsynth (Balgach, Switzerland; listed in Table 1). rt-PCR was performed using SYBR green (Roche Diagnostics, Rotkreuz, Switzerland) on an ABI PRISM 7700 sequence detector (PE Biosystems, Rotkreuz, Switzerland). Quantification of mRNA expression levels was performed using the comparative-threshold cycle method [28].

Table 1. Gene-specific primers for rt-PCR.

Target Gene	Organism		Primer Sequence (5'→3')	Length (bp)
CYP2D6	human	Fw	TGTGCCCATCACCCAGAT	18
		Rev	AAGGTGGAGACGGAGAAGC	19
CYP3A4	human	Fw	TACACAAAAGCACCGAGTGG	20
		Rev	TGCAGTTTCTGCTGGACATC	20
HPRT1	human	Fw	GGTCCTTTTCACCAGCAAGCT	21
		Rev	TGACACTGGCAAAACAATGCA	21
GAPDH	human	Fw	AGCCACATCGCTCAGACAC	19
		Rev	GCCCAATACGACCAAATCC	19

2.5.2. Functional assessment of CYP induction

HepaRG cells and primary cryopreserved human hepatocytes were cultured in a 5% CO₂ and 95% air-humidified atmosphere at 37°C. Induction treatment (rifampicin 20µM) lasted for 72h, with the medium being changed every 24h. Rifampicin stock solution was prepared in DMSO and further diluted in the appropriate culture medium, to achieve a final DMSO concentration of 0.1% (v/v). Experimental control culture wells were treated with solvent (DMSO, 0.1% (v/v)) alone. Following induction treatment, CYP activity was assessed by the addition of fresh medium, containing the probe drugs, to the control and pre-treated cells. Substrates were dissolved and serially diluted to the required concentrations with DMSO. The final concentration of DMSO during the incubation was 0.2% (v/v). At selected time points (0, 15, 30, 45, 60, 90, 105, and 120 min), the incubation was stopped by the addition of a threefold volume of ice-cold methanol containing the respective internal standards. The bottoms of the wells were scraped using a pipette tip, after which the contents were transferred to an autosampler vial. After vigorous shaking (10 min) and centrifugation (3220 g; 30 min; 10°C), the supernatants were stored at -20°C until analysis by LC-MS/MS.

To determine 1'-hydroxymidazolam, the entire content of the autosampler vials were evaporated using a minivap microplate evaporator (Porvair Sciences Ltd., King's Lynn, Norfolk, UK). The analytes were then re-suspended in 45 μ l of the respective culture medium, to which 5 μ l (500 units) of β -glucuronidase was added. Following a 12 h incubation at 37°C, the reaction was terminated by the addition of methanol, after which the samples were treated in the same manner as above.

2.6. Metabolism of metoprolol and midazolam by rHCYP3A4 supersomes

The reaction mixture (final volume of 500 μ L) contained test compounds, incubation buffer (0.1 M potassium phosphate buffered saline, pH 7.4), rhCYP3A4 (20 pmol P450/mL) and an NADPH-generating system. For inhibition studies, the reaction mixture was pre-incubated with either 0.5 μ M ketoconazole or 1 μ M quinidine for 10 minutes prior to addition of test compounds and NADPH. The suspensions were incubated at 37°C in a thermomixer (compact 5350, Eppendorf, Hamburg, Germany). Following the incubation in the absence (control) and presence of inhibitors at selected time-points (0, 1, 2, 4, 8, 15, 30, and 60 min), the reactions were terminated by transferring 50 μ L of the incubation mixture into a matrix autosampler vial, to which a threefold volume of ice-cold methanol, containing the internal standards, was added. After vigorous shaking (10 min) and centrifugation (3220 g; 30 min; 10°C) the samples were stored at -20°C until analysis by LC-MS/MS. The remaining percentage formation rate (pmol/ min/ pmol P450) after inhibition relative to control (without inhibitors) was calculated.

2.7. Data analysis

CYP activities were determined as the respective metabolite formation rates corresponding to the slope in the metabolite concentration versus time graphs. Metabolite concentrations were quantified using standard curves of pure compounds as previously described [14].

For induction experiments, formation rates were determined, and the fold change versus the basal conditions was calculated as the ratio of the metabolite formation rate in wells exposed to an inducer and control wells.

Means were compared with the two-tailed Student's *t*-test using GraphPad Prism 6.0 (GraphPad Software, San Diego, CA, USA). Data are presented as mean \pm SD unless otherwise stated. Induction levels above 2-fold with statistically significant differences ($p < 0.05$) were considered relevant. Areas under the curve (AUC), from times

0 to 24h after dosing (AUC_{0-24h}), were estimated with non-compartmental methods using Phoenix WinNonlin software (Certara, Princeton, NJ, USA).

3. Results

3.1. *In vivo* clearance of metoprolol before and after treatment with rifampicin

We have performed a clinical study using 15 healthy volunteers, where we investigated the effect of pretreatment with rifampicin on the Basel phenotyping cocktail, which contains caffeine, efavirenz, losartan, omeprazole, metoprolol and midazolam as probe drugs [13]. As expected, we observed an increase in midazolam clearance (Figure 2a) and a decrease in midazolam AUC_{0-24h} (supplemental material, Figure S1a) in all subjects tested, which is used as a marker of CYP3A4 activity. Surprisingly, we also observed a considerable change in metoprolol concentrations between basal and induced conditions, leading to a significant increase in metoprolol clearance (Figure 2b) and a decrease in metoprolol AUC_{0-24h} (supplemental material, Figure S1b) through rifampicin treatment. A slight change in the formation of α -hydroxymetoprolol was also observed after treatment with rifampicin. However, unlike with metoprolol, the difference between basal and induced concentrations did not lead to a significant change in AUC_{0-24h} of α -hydroxymetoprolol (supplemental material, Figure S1c). In order to study this question in more detail, we performed *in vitro* investigations in primary human hepatocytes and in HepaRG cells.

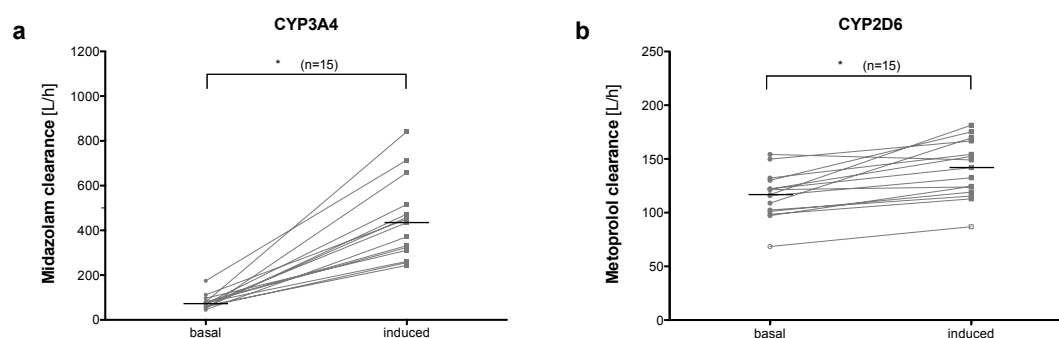


Figure 2. Effect of rifampicin on (a) midazolam and (b) metoprolol clearance in human subjects. Subjects were treated orally with 12.5 mg metoprolol and 2 mg midazolam before (basal, grey circles) and after pre-treatment with rifampicin, 600 mg once daily for 7 days (induced, grey squares). Metoprolol and Midazolam was determined using LC/MS-MS. Clearance was calculated by dividing the dose by the respective AUCs (trapezoidal rule) of the subjects. Closed symbols represent CYP2D6 EMs; open symbol represents the CYP2D6 IM. The black horizontal lines signify the median. The p-value (* = $p < 0.05$) for midazolam clearance (a) is from a paired t-test, while for metoprolol clearance (b), it is from a Wilcoxon matched-pairs signed ranks test.

3.2. mRNA expression of CYP2D6 and CYP3A4, metoprolol and midazolam metabolism before and after rifampicin in HepaRG cells

HepaRG cells represent a hepatoma cell line with inducible CYPs [20, 27, 29]. In HepaRG cells, mRNA of CYP3A4 (determined as a control) increased approximately 30-fold after treatment with rifampicin (20 μ M for 48h) compared to basal conditions (Figure 3a). In contrast, mRNA of CYP2D6 was not induced by pre-treatment with rifampicin (Figure 3a).

In agreement with the mRNA data, pre-treatment with rifampicin was associated with a significant increase in the formation of 1'-hydroxymidazolam (Figure 3b), reflecting induction of CYP3A4 by rifampicin. In contrast to the results obtained for CYP2D6 mRNA, pre-treatment with rifampicin was associated with a significant increase in α -hydroxymetoprolol formation (Figure 3c). Since α -hydroxylation of metoprolol is considered to be specific for CYP2D6 [6, 11], this would, at first sight, suggest induction of CYP2D6 in HepaRG cells.

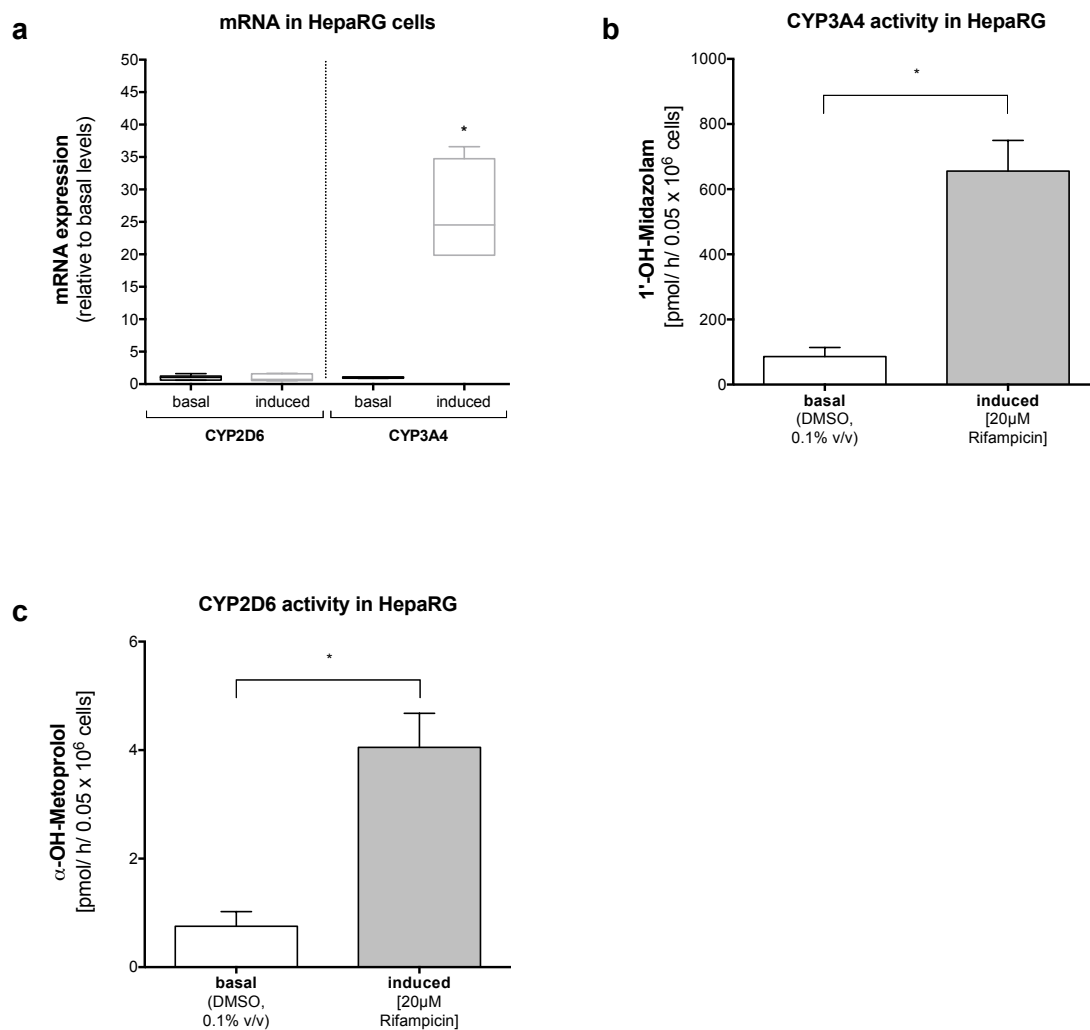


Figure 3. Effect of rifampicin pretreatment on mRNA expression (a), and CYP activity of CYP3A4 (b), and CYP2D6 (c) in HepaRG cells. HepaRG cells were studied for either 48h or 72h under basal activity (0.1% DMSO, v/v; either white box plot [a] or white bars [b, c]) and compared to treatment with rifampicin (20 μM; either dark grey box plot [a] or dark grey bars [b, c]). mRNA was quantified using rt-PCR, while metabolite formation was determined using LC/MS-MS, both as described in Methods section. Data are presented as mean ± SEM of at least 3 independent experiments. The p-values (* = $p < 0.05$) for 1'-hydroxymidazolam and α-hydroxymetoprolol formation are from paired t-tests.

3.3. mRNA expression of CYP2D6 and CYP3A4, metoprolol and midazolam metabolism before and after rifampicin in 2D primary hepatocytes

In order to confirm the results obtained in HepaRG cells, we performed the same experiments using primary human hepatocytes. Identical to our findings in HepaRG cells, pre-treatment with rifampicin was associated with a 16-fold increase in CYP3A4 mRNA expression, whereas no increase in mRNA expression levels could be observed for CYP2D6 (Figure 4a).

Pre-treatment with rifampicin led to a five-fold increase in production of 1'-hydroxymidazolam (Figure 4b). Similar to the findings in HepaRG cells, rifampicin increased α -hydroxylation of metoprolol in primary human hepatocytes (Figure 4c), but to a much lesser extent than in HepaRG cells. These findings confirmed the results obtained with HepaRG cells, while at the same time excluding an artifact due to modified regulation of CYP expression in the HepaRG hepatoma cell line.

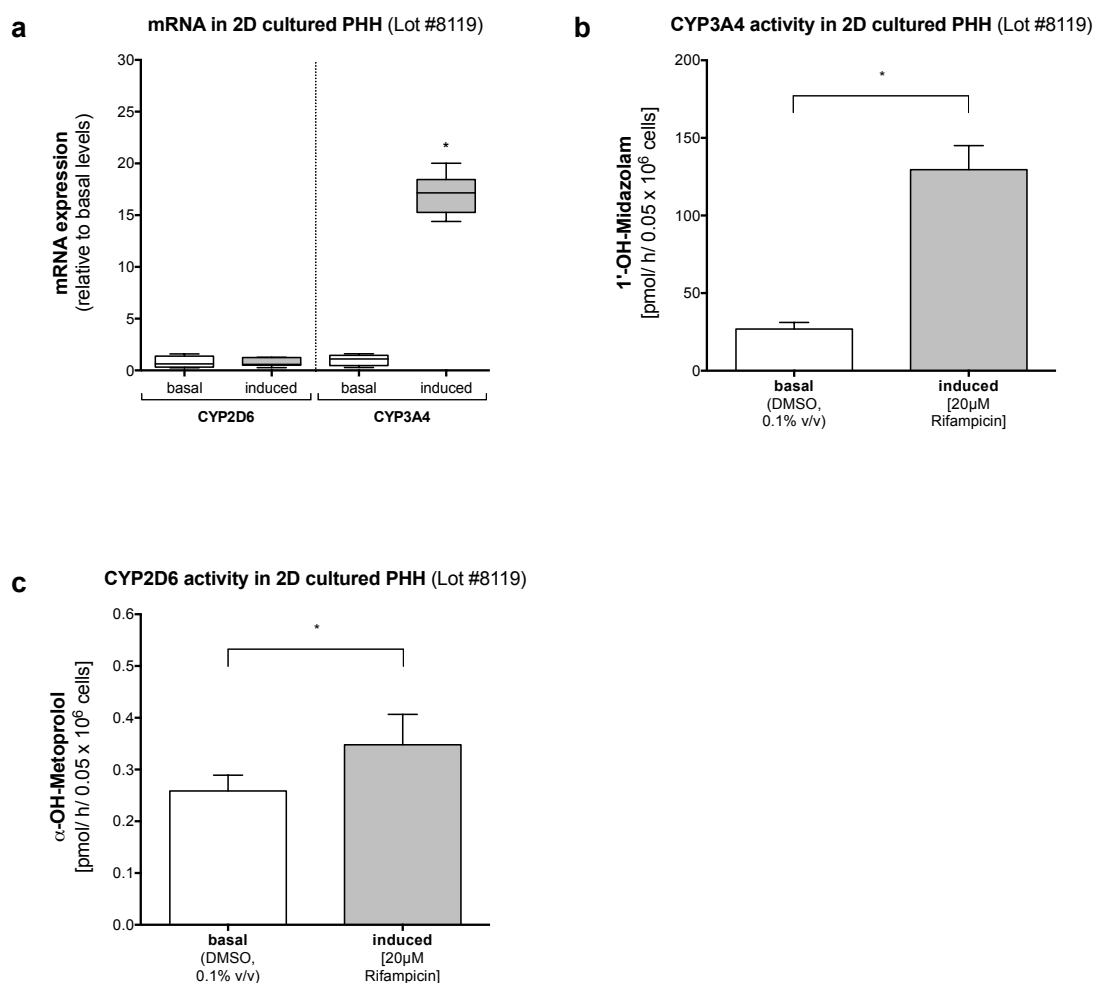


Figure 4. Effect of rifampicin pretreatment on (a) mRNA expression, and CYP activity of (b) CYP3A4, and (c) CYP2D6, in primary human hepatocytes cultured in 2D. Primary human cryopreserved hepatocytes (Lot #8119) were studied for either 48h or 72h under basal activity (0.1% DMSO, v/v; either white box plot [a] or white bars [b, c]) and compared to treatment with rifampicin (20 μ M; either dark grey box plot [a] or dark grey bars [b, c]). mRNA was quantified using rt-PCR, while metabolite formation was determined using LC/MS-MS, both as described in methods. Data are presented as mean \pm SEM of at least 3 independent experiments. The p-values (* = $p < 0.05$) for 1'-hydroxymidazolam and α -hydroxymetoprolol formation are from paired t-tests.

Using a different batch of primary cryopreserved human hepatocytes we additionally investigated whether O-desmethylnetoprolol and metoprolol acid, which make up the

main metabolic pathway of metoprolol, would also be susceptible to induction by rifampicin. Our findings show, that similar to the increase of α -hydroxymetoprolol (Figure 5b), the O-demethylation of metoprolol (Figure 5c) and its subsequent oxidation to metoprolol acid (Figure 5d) increased 1.4-fold through treatment with rifampicin.

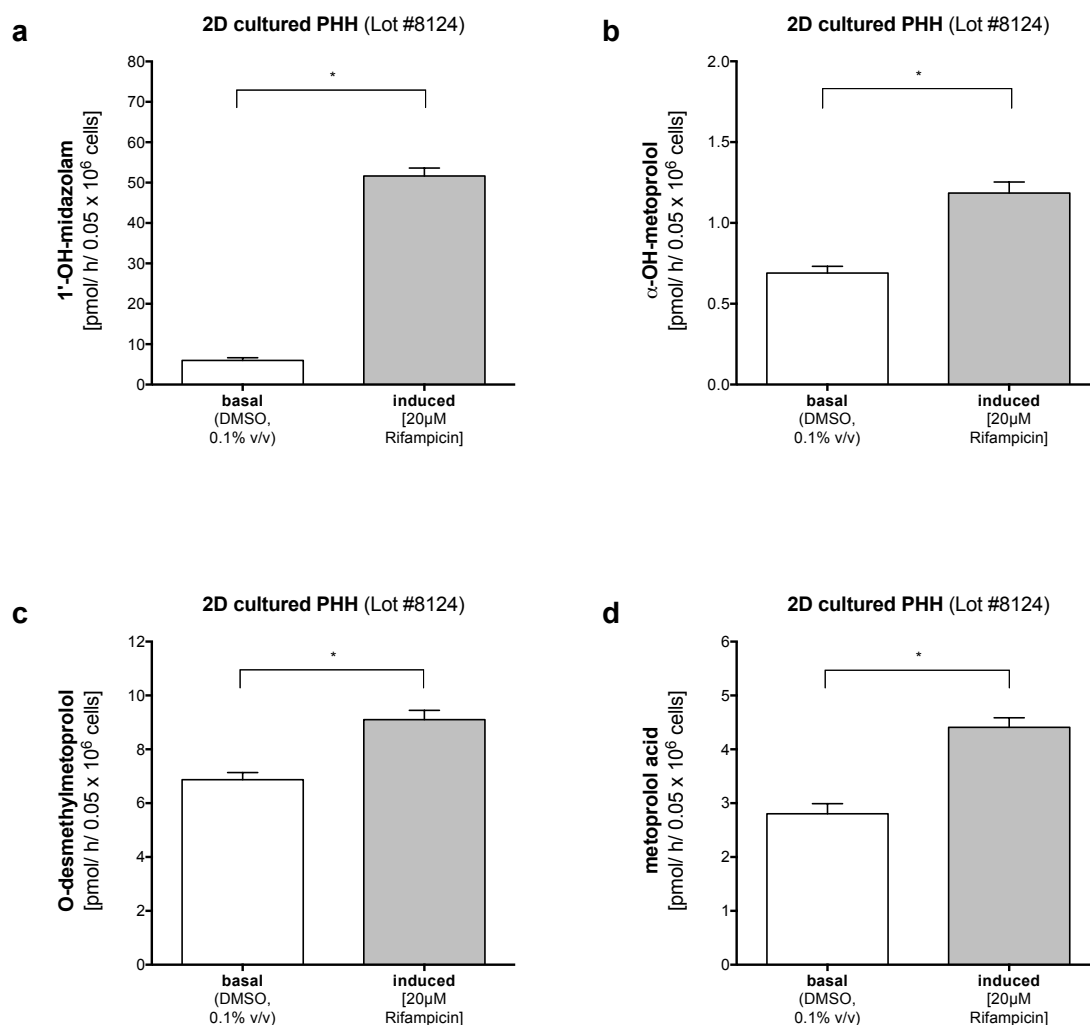


Figure 5. Effect of rifampicin pretreatment on the formation of 1'-hydroxymidazolam (**a**), α -hydroxymetoprolol (**b**), O-desmethylmetoprolol (**c**), and metoprolol acid (**d**) in primary cryopreserved human hepatocytes. Primary human cryopreserved hepatocytes (Lot #8124) were studied for either 48h or 72h under basal activity (0.1% DMSO, v/v; either white box plot [a] or white bars [b, c, d]) and compared to treatment with rifampicin (20 μ M; either dark grey box plot [a] or dark grey bars [b, c]). Data are presented as mean \pm SEM of at least 3 independent experiments. The p-values (* = $p < 0.05$) for the respective metabolites of metoprolol and midazolam are from paired t-tests.

3.4. Experiments with rHCYP3A4 supersomes

Other than CYP2D6 induction, an alternative explanation for the observed increase in α -hydroxymetoprolol formation through rifampicin treatment could be the involvement

through induction of an altogether different CYP isoform. Since CYP3A4 can perform hydroxylation reactions and is the CYP involved in most phase I reactions [30], we investigated the possible involvement of CYP3A4 in the metabolism of metoprolol by using recombinant human CYP3A4 supersomes (rHCYP3A4). To ensure that these supersomes do not contain CYP2D6 activity, we exposed the supersomes to dextromethorphan, a typical CYP2D6 substrate [15]. The conversion to dextrophan was not quantifiable, excluding a significant CYP2D6 activity (data not shown).

As shown in Figure 6a, the formation of 1'-hydroxymidazolam from midazolam was rapid, showing non-linearity after 4 minutes of incubation due to substrate depletion. Midazolam 1'-hydroxylation could be almost completely inhibited by ketoconazole, a CYP3A4 inhibitor. Crucially, metoprolol was also α -hydroxylated by CYP3A4 supersomes, but at a much slower rate, compared to midazolam.

As shown in Figure 6b, α -hydroxylation of metoprolol could be inhibited by ketoconazole, but not by quinidine, which is a specific CYP2D6 inhibitor [8, 11]. This proves that α -hydroxylation of metoprolol cannot only be catalysed by CYP2D6, but also by CYP3A4.

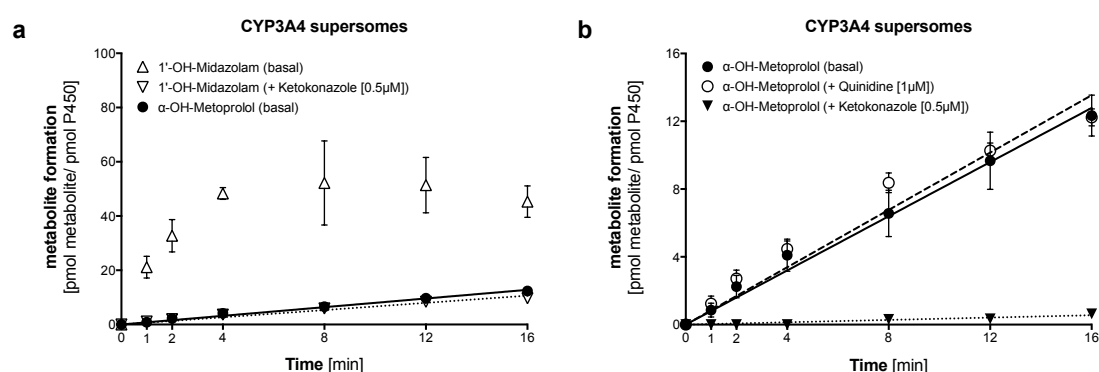


Figure 6. Formation of 1'-hydroxymidazolam and α -OH-metoprolol by CYP3A4 expressing supersomes **(a)** 1'-hydroxymidazolam formation before (open triangles) and after (open upside down triangles) treatment with inhibitors (0.5 μ M ketoconazole); and **(b)** α -OH-metoprolol formation before (closed circles) and after treatment with inhibitors, 1 μ M quinidine (open circles) and 0.5 μ M ketoconazole (closed upside down triangles). Metabolite concentrations were determined by LC-MS/MS. Data are presented as mean \pm SEM of at least 3 independent experiments.

4. Discussion

In two hepatocyte models, we could show that treatment with rifampicin induced CYP3A4, but not CYP2D6 mRNA expression. In comparison, in the same hepatocyte models, treatment with rifampicin was associated with increased activity of midazolam 1'-hydroxylation (reflecting CYP3A4 activity) and also of metoprolol α -hydroxylation, which is considered to reflect CYP2D6 activity [6, 11]. Our *in vitro* data are in agreement with *in vivo* data showing that rifampicin treatment lead to a considerable increase of midazolam clearance (decrease in midazolam AUC_{0-24h}, Figure 2a in the current publication; also [13]) compared to basal activity, while also indicating that CYP2D6 can be either induced to a small extent by rifampicin or that another inducible CYP isoform contributes to metoprolol degradation.

In our studies, we found metoprolol clearance significantly increased (AUC_{0-24h} decreased) in patients being treated with rifampicin for 1 week. This is consistent with previous findings, which showed a decrease of metoprolol AUC after induction treatment [31, 32]. However, the slightly higher concentrations of α -hydroxymetoprolol under induced condition did not yield a relevant change in clearance. This would support the hypothesis that treatment with rifampicin leads to an increased metabolic activity of an alternative CYP isoforms involved in the degradation of metoprolol. By demonstrating that rifampicin treatment leads to an increase in the formation of O-desmethylemetoprolol (and metoprolol acid) *in vitro*, which make up the main metabolic pathway of metoprolol [9], we would consider this to be the most likely explanation for the significant increase in metoprolol clearance found *in vivo*. Alternatively, the lack of a significant increase in α -hydroxymetoprolol found in plasma could be due to induced excretion into the urine. Increased phase II metabolism of α -hydroxymetoprolol, i.e. glucuronidation, would be another possibility [33]; however, this was ruled out by treating samples with β -glucuronidase, which did not result in a significant change of α -hydroxymetoprolol concentrations (results not shown). A previous study supported this finding by showing that the glucuronide of α -hydroxymetoprolol is only formed in significant amounts in horses, not, however, in humans (nor in rats and dogs), therefore, making the aforementioned assumption all the more unlikely [34].

The mRNA expression data of CYP2D6, which showed no increase after pretreatment with rifampicin, agree with other studies in primary human hepatocytes [20, 23]. An increase in mRNA transcription of CYP2D6 appears therefore not to be the cause

of our observations. In human subjects treated with 600 mg rifampicin for 10 days, the CYP2D6 protein content in enterocytes increased by a factor of 1.6, but with a large variability without reaching statistical significance [21]. Post-transcriptional mechanisms can therefore not be ruled out with complete certainty. Sparteine metabolic clearance, an *in vivo* marker of CYP2D6 activity [6], increased by a factor of 1.3 in subjects treated with rifampicin compared to the basal state, without reaching statistical significance [19]. Similarly, in primary human hepatocytes, the activity of dextromethorphan O-demethylation increased by a factor of 1.3, without reaching statistical significance [22]. In the same publication, phenobarbital had an almost identical effect on dextromethorphan O-demethylation as rifampicin [22]. Similarly, hypericum extract did not significantly affect the metabolic ratio of dextromethorphan/ dextromethorphan, suggesting that CYP2D6 is not induced by this treatment [24].

These data show that CYP2D6 is not induced by the classical inducers of the CYP2C and CYP3A family. Our findings in HepaRG cells and primary hepatocytes were, therefore, surprising and suggested that α -hydroxylation of metoprolol is not mediated exclusively by CYP2D6, but also by at least one other inducible CYP-isoform. Since CYP3A4 was strongly induced by rifampicin in both evaluated cell systems, and as CYP3A4 is the most important CYP involved in oxidative reactions, such as hydroxylation reactions [30], we decided to study metoprolol α -hydroxylation in supersomes exclusively expressing CYP3A4. Using this system, we could demonstrate that metoprolol can be α -hydroxylated by CYP3A4, since the supersomes used had no CYP2D6 activity, and ketoconazole (but not quinidine) could block this reaction almost completely. Based on our experiments, we cannot, however, exclude with certainty that other CYPs are also involved in this reaction.

The study of McGourty et al. [6] showed that debrisoquine EM excreted 7.4% of an oral dose of metoprolol as α -hydroxy metabolite in the urine, whereas this was only 0.06% in debrisoquine PM. Furthermore, urinary excretion of α -hydroxymetoprolol showed a bimodal distribution and correlated with the debrisoquine phenotype, indicating that metoprolol α -hydroxylation is a function of CYP2D6. Similarly, Otton et al. [11] demonstrated that liver microsomes from a liver of a debrisoquine poor metaboliser (PM) did not produce α -hydroxymetoprolol and that α -hydroxymetoprolol production by microsomes from debrisoquine EM could be inhibited completely by quinidine. These studies suggest that α -hydroxylation of metoprolol is mediated only by CYP2D6, but a small contribution from other CYPs in both investigations could not be

excluded. In the case of CYP induction, this contribution can increase, since, as discussed above, CYP2D6 cannot be induced, while CYP3A4 is highly inducible.

The question now arises whether metoprolol can be recommended as a substrate for CYP2D6 phenotyping, taking into account the contribution of CYP3A4 to metoprolol α -hydroxylation. The problem could be that CYP2D6 PM might not be recognised due to the contribution of CYP3A4, which is not affected by this polymorphism. In the study of McGourty et al. [6] there was a clear separation in renal excretion of α -hydroxymetoprolol into debrisoquine EM and PM. Also in the study of Tamminga et al. [17] and of Derungs et al. [13], CYP2D6 EM and PM could clearly be distinguished using α -hydroxymetoprolol plasma concentrations. A further potential problem could be the distinction between CYP2D6 EM and PM in patients with CYP3A4 induction. However, also in this situation, it was possible to classify patients using their respective α -hydroxymetoprolol plasma concentrations [13].

In conclusion, CYP3A4 contributes to metoprolol α -hydroxylation. This contribution explains a very slight increase in α -hydroxymetoprolol formation *in vivo* and the more pronounced increase *in vitro* through induction of CYP3A4. However, the contribution of CYP3A4 is low and does not impair the usability of α -hydroxymetoprolol formation for CYP2D6 phenotyping, especially as the involvement of CYP3A4 only becomes apparent when induction is evaluated, which is not commonly done for CYP2D6 [19-24].

Acknowledgements

We would like to thank Nathalie Schaub², Evelyne Durr², François Singh¹, Annalisa Bonifacio¹, Beatrice Vetter¹, Massimiliano Donzelli¹, and Sebastian Fürer for their valuable advice and technical support.

Financial support

SK was supported by a grant from the Swiss National Science Foundation (SNF 31003A_156270).

Conflict of interest

None of the authors report any conflict of interest regarding this study.

5. References

1. Group, M.-H.S., Effect of metoprolol CR/XL in chronic heart failure: Metoprolol CR/XL Randomised Intervention Trial in Congestive Heart Failure (MERIT-HF). *Lancet*, 1999. **353**(9169): p. 2001-7.
2. Chen, Z.M., et al., Early intravenous then oral metoprolol in 45,852 patients with acute myocardial infarction: randomised placebo-controlled trial. *Lancet*, 2005. **366**(9497): p. 1622-32.
3. Hansson, L., et al., Randomised trial of old and new antihypertensive drugs in elderly patients: cardiovascular mortality and morbidity the Swedish Trial in Old Patients with Hypertension-2 study. *Lancet*, 1999. **354**(9192): p. 1751-6.
4. Regardh, C.G. and G. Johnsson, *Clinical pharmacokinetics of metoprolol*. *Clin Pharmacokinet*, 1980. **5**(6): p. 557-69.
5. Rigby, J.W., et al., A comparison of the pharmacokinetics of atenolol, metoprolol, oxprenolol and propranolol in elderly hypertensive and young healthy subjects. *Br J Clin Pharmacol*, 1985. **20**(4): p. 327-31.
6. McGourty, J.C., et al., Metoprolol metabolism and debrisoquine oxidation polymorphism--population and family studies. *Br J Clin Pharmacol*, 1985. **20**(6): p. 555-66.
7. Johansson, T., L. Weidolf, and U. Jurva, *Mimicry of phase I drug metabolism--novel methods for metabolite characterization and synthesis*. *Rapid Commun Mass Spectrom*, 2007. **21**(14): p. 2323-31.
8. Johnson, J.A. and B.S. Burlew, *Metoprolol metabolism via cytochrome P4502D6 in ethnic populations*. *Drug Metab Dispos*, 1996. **24**(3): p. 350-5.
9. Borg, K.O., et al., *Metabolism of metoprolol-(3-h) in man, the dog and the rat*. *Acta Pharmacol Toxicol (Copenh)*, 1975. **36**(Suppl 5): p. 125-35.
10. Regardh, C.G., et al., Pharmacokinetic studies on the selective beta1-receptor antagonist metoprolol in man. *J Pharmacokinet Biopharm*, 1974. **2**(4): p. 347-64.
11. Otton, S.V., et al., Use of quinidine inhibition to define the role of the sparteine/debrisoquine cytochrome P450 in metoprolol oxidation by human liver microsomes. *J Pharmacol Exp Ther*, 1988. **247**(1): p. 242-7.
12. Blake, C.M., et al., A meta-analysis of CYP2D6 metabolizer phenotype and metoprolol pharmacokinetics. *Clin Pharmacol Ther*, 2013. **94**(3): p. 394-9.
13. Derungs, A., et al., Effects of Cytochrome P450 Inhibition and Induction on the Phenotyping Metrics of the Basel Cocktail: A Randomized Crossover Study. *Clin Pharmacokinet*, 2016. **55**(1): p. 79-91.

14. Donzelli, M., et al., The basel cocktail for simultaneous phenotyping of human cytochrome P450 isoforms in plasma, saliva and dried blood spots. *Clin Pharmacokinet*, 2014. **53**(3): p. 271-82.
15. Frank, D., U. Jaehde, and U. Fuhr, *Evaluation of probe drugs and pharmacokinetic metrics for CYP2D6 phenotyping*. *Eur J Clin Pharmacol*, 2007. **63**(4): p. 321-33.
16. Sharma, A., et al., A convenient five-drug cocktail for the assessment of major drug metabolizing enzymes: a pilot study. *Br J Clin Pharmacol*, 2004. **58**(3): p. 288-97.
17. Tamminga, W.J., et al., An optimized methodology for combined phenotyping and genotyping on CYP2D6 and CYP2C19. *Eur J Clin Pharmacol*, 2001. **57**(2): p. 143-6.
18. Birkett, D.J., et al., *In vitro approaches can predict human drug metabolism*. *Trends Pharmacol Sci*, 1993. **14**(8): p. 292-4.
19. Eichelbaum, M., et al., *The influence of enzyme induction on polymorphic sparteine oxidation*. *Br J Clin Pharmacol*, 1986. **22**(1): p. 49-53.
20. Gerets, H.H., et al., Characterization of primary human hepatocytes, HepG2 cells, and HepaRG cells at the mRNA level and CYP activity in response to inducers and their predictivity for the detection of human hepatotoxins. *Cell Biol Toxicol*, 2012. **28**(2): p. 69-87.
21. Glaeser, H., et al., Influence of rifampicin on the expression and function of human intestinal cytochrome P450 enzymes. *Br J Clin Pharmacol*, 2005. **59**(2): p. 199-206.
22. Madan, A., et al., Effects of prototypical microsomal enzyme inducers on cytochrome P450 expression in cultured human hepatocytes. *Drug Metab Dispos*, 2003. **31**(4): p. 421-31.
23. Rae, J.M., et al., Rifampin is a selective, pleiotropic inducer of drug metabolism genes in human hepatocytes: studies with cDNA and oligonucleotide expression arrays. *J Pharmacol Exp Ther*, 2001. **299**(3): p. 849-57.
24. Wenk, M., L. Todesco, and S. Krahenbuhl, Effect of St John's wort on the activities of CYP1A2, CYP3A4, CYP2D6, N-acetyltransferase 2, and xanthine oxidase in healthy males and females. *Br J Clin Pharmacol*, 2004. **57**(4): p. 495-9.
25. Ai, C., et al., Insight into the effects of chiral isomers quinidine and quinine on CYP2D6 inhibition. *Bioorg Med Chem Lett*, 2009. **19**(3): p. 803-6.
26. Hutzler, J.M., G.S. Walker, and L.C. Wienkers, Inhibition of cytochrome P450 2D6: structure-activity studies using a series of quinidine and quinine analogues. *Chem Res Toxicol*, 2003. **16**(4): p. 450-9.

27. Aninat, C., et al., Expression of cytochromes P450, conjugating enzymes and nuclear receptors in human hepatoma HepaRG cells. *Drug Metab Dispos*, 2006. **34**(1): p. 75-83.
28. Livak, K.J. and T.D. Schmittgen, Analysis of relative gene expression data using real-time quantitative PCR and the 2(-Delta Delta C(T)) Method. *Methods*, 2001. **25**(4): p. 402-8.
29. Antherieu, S., et al., Stable expression, activity, and inducibility of cytochromes P450 in differentiated HepaRG cells. *Drug Metab Dispos*, 2010. **38**(3): p. 516-25.
30. Guengerich, F.P., *Cytochrome p450 and chemical toxicology*. *Chem Res Toxicol*, 2008. **21**(1): p. 70-83.
31. Bennett, P.N., V.A. John, and V.B. Whitmarsh, *Effect of rifampicin on metoprolol and antipyrine kinetics*. *Br J Clin Pharmacol*, 1982. **13**(3): p. 387-91.
32. Haglund, K., et al., *Influence of pentobarbital on metoprolol plasma levels*. *Clin Pharmacol Ther*, 1979. **26**(3): p. 326-9.
33. Bae, S.H., et al., Simultaneous determination of metoprolol and its metabolites, alpha-hydroxymetoprolol and O-desmethylemetoprolol, in human plasma by liquid chromatography with tandem mass spectrometry: Application to the pharmacokinetics of metoprolol associated with CYP2D6 genotypes. *J Sep Sci*, 2014. **37**(11): p. 1256-64.
34. Ma, B., et al., Biotransformation of metoprolol by the fungus *Cunninghamella blakesleeana*. *Acta Pharmacol Sin*, 2007. **28**(7): p. 1067-74.

Supplementary Figure

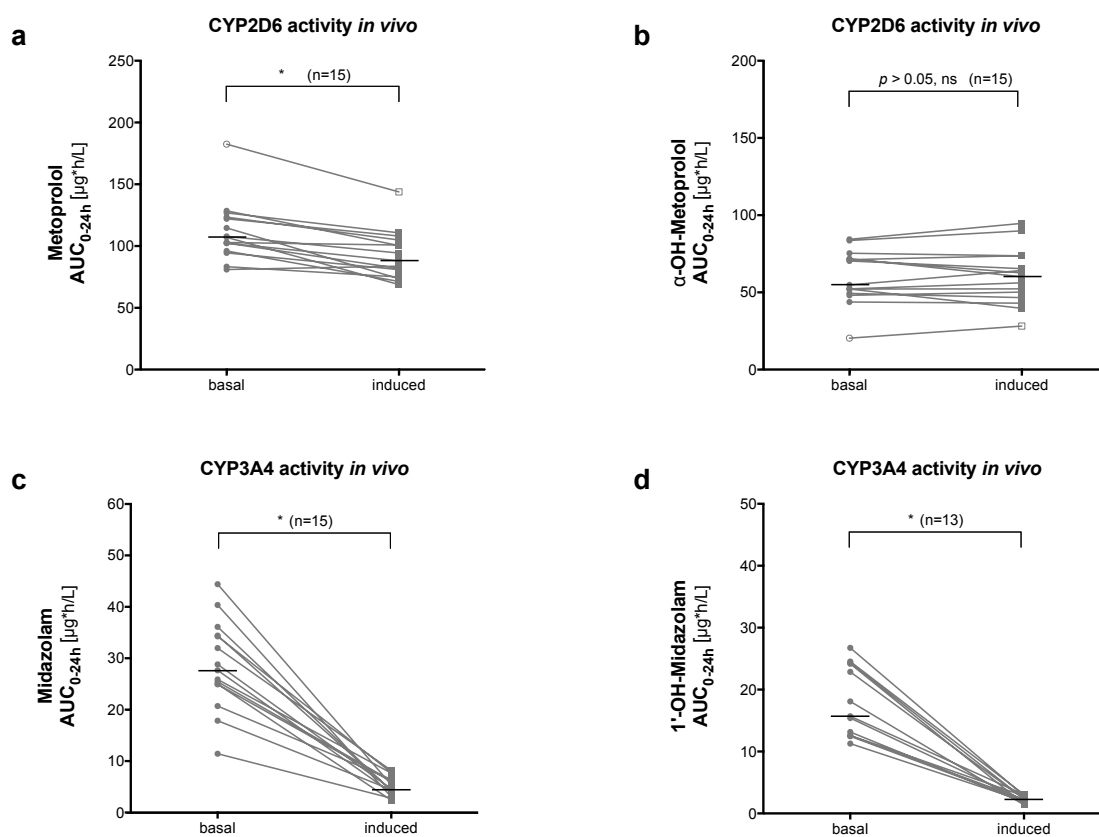


Figure S1. Effect of rifampicin on (a) metoprolol, (b) α -hydroxymetoprolol, (c) midazolam, and (d) 1'-hydroxymidazolam AUC_{0-24h} in human subjects. Subjects were treated orally with 12.5 mg metoprolol and 2 mg midazolam before (basal, grey circles) and after pre-treatment with rifampicin, 600 mg once daily for 7 days (induced, grey squares). Metoprolol, α -hydroxymetoprolol, midazolam, and 1'-hydroxymidazolam were determined using LC/MS-MS. AUCs were through the trapezoidal rule. Closed symbols represent CYP2D6 EMs, open symbols represent the CYP2D6 IM. The black horizontal lines signify the median. The p -value for midazolam and its metabolite (a, b) are from paired t -tests, while for metoprolol and its metabolite (c, d) they are from Wilcoxon matched-pairs signed ranks tests.

6. *In vitro* evaluation of replacing losartan by flurbiprofen as a probe substrate for cytochrome p450 2C9 in the Basel phenotyping cocktail

Benjamin Berger¹, Massimiliano Donzelli¹, Franziska Boess², Adrian Roth²,
Jörg Huwyler³, Marine Camblin³, Maxim Puchkov³,
Stephan Krähenbühl^{1,4}, Manuel Haschke¹

¹Division of Clinical Pharmacology & Toxicology, University Hospital Basel and Department of Biomedicine, University of Basel, Switzerland

²Non-Clinical Safety, Hoffmann-La Roche Ltd, Basel, Switzerland

³Department of Pharmaceutical Sciences, University of Basel, Switzerland

⁴Swiss Center for Applied Human Research (SCAHT)

Abstract

In an earlier *in vivo* study using the Basel *in vivo* phenotyping cocktail, losartan was used as a CYP2C9 probe drug. However, in plasma, the losartan/ losartan-carboxylic acid (E-3174) ratio did not reflect induction after pre-treatment with the inducer rifampicin (600 mg per day for 7 days). Therefore, losartan has to be replaced by a different CYP2C9 probe-drug to improve the performance of this cocktail. Flurbiprofen is primarily metabolised via the cytochrome P450 2C9 isoform to the 4'-hydroxy metabolite and has previously been evaluated as a phenotyping probe drug for CYP2C9 in urine, plasma, and DBS samples in two phenotyping cocktails. By incubating the five remaining probe substrates (caffeine [CYP1A2], efavirenz [CYP2B6], omeprazole [CYP2C19], metoprolol [CYP2D6], midazolam [CYP3A4]) of the Basel cocktail with and without flurbiprofen *in vitro*, using primary human hepatocytes in 3D co-culture, we were able to show that flurbiprofen did not cause a significant change in enzyme activity of any of the other five CYP450 isoforms, therefore enabling its inclusion into the cocktail.

Previously, the six probe drugs of the Basel cocktail were administered as individual commercially available formulations. However, for phenotyping to become more widely accepted as a routine tool in clinical practice, simplified administration of the probe drugs is of great importance. Therefore, as a secondary goal of this study, we were able to show in a pilot study (n=2), that the administration of a combination-capsule (combi-capsule) containing all six probe drugs of the modified Basel cocktail (including flurbiprofen instead of losartan) is feasible, which will consequently facilitate the intake of probe substrates.

Keywords: Cytochrome P450 (CYP), CYP2C9, Basel cocktail, Flurbiprofen, 3-dimensional spheroid primary human hepatocyte culture, phenotyping, LC-MS/MS

1. Introduction

In 2013 we first described and validated the Basel Cocktail which simultaneously measures the *in vivo* activity six specific cytochrome P450 (CYP450) enzymes using commercially available probe drugs, including caffeine [CYP1A2], efavirenz [CYP2B6], losartan [CYP2C9], omeprazole [CYP2C19], metoprolol [CYP2D6], and midazolam [CYP3A4]. Whilst further characterising the cocktail using known inhibitors and the inducer rifampicin in plasma, it became apparent that using the losartan/losartan carboxylic acid (E-3174) ratio did not reflect induction after pre-treatment with the inducer rifampicin (600 mg per day for 7 days). Therefore, losartan has to be replaced by a different CYP2C9 probe-drug to improve the performance of the cocktail. Flurbiprofen, a phenyl alkanoic acid derivative, is a non-steroidal anti-inflammatory drug (NSAID) used to treat rheumatoid arthritis or osteoarthritis, as well as serving as a pre-operative antimiotic ophthalmic solution [1, 2]. It is primarily metabolised via the cytochrome P450 2C9 isoform to the 4'-hydroxy metabolite [3, 4] and has previously been evaluated as a phenotyping probe drug for CYP2C9 in urine, plasma, and DBS samples [5, 6] in two phenotyping cocktails [7-9].

As we have previously found that certain *in vitro* cell systems, such as cryopreserved human hepatocytes in three-dimensional (3D) co-cultures (3D-PHH), provide comparable results to *in vivo* phenotyping [10], we decided to use this system to test whether losartan could be replaced by flurbiprofen without causing interference with the other probe drugs. This was implemented by incubating the five remaining probe substrates (caffeine, efavirenz, omeprazole, metoprolol, midazolam) with and without flurbiprofen *in vitro* using 3D-PHH.

A second aim of this study was to evaluate a newly developed combination-capsule (combi-capsule), containing all six probe drugs of the modified Basel phenotyping cocktail in the form of miniature tablets. As new drug formulations and lower doses of certain probe substrates are used in the combi-capsule, we assessed whether quantifiable concentrations of the probe drugs and their phase-I metabolites could be reached in plasma. Results of an *in vivo* pilot study involving three healthy volunteers are reported upon below.

2. Material and methods

2.1. Chemicals and reagents

The chemicals and reagents used for this project have previously been described [10]. Additionally, flurbiprofen, 4'-hydroxyflurbiprofen, and flurbiprofen-d3 (used as an internal standard) were purchased from TRC (Toronto, Canada).

2.2. Cell Culture

Preliminary *in vitro* experiments were performed using human liver microsomes, while the potential of flurbiprofen to impede metabolite production of Basel cocktail substrates was investigated using 3D-PHH.

Characterised human liver microsomes (HLM, pooled, n=35, Lot 4133007) and NADPH regenerating solutions A and B (A containing NADP⁺, glucose-6-phosphate, and MgCl₂; B containing glucose-6-phosphate dehydrogenase (G6PDH)) were purchased from Corning Life science (Woborn, MA, USA). HLM samples were stored at -80°C until used.

For microsomal experiments, the reaction mixture (final volume of 500 µL) contained either Losartan [14 µM] or flurbiprofen [5 µM], incubation buffer (0.1 M potassium phosphate buffered saline, pH 7.4), human liver microsomes (0.5 mg prot./mL), and a NADPH generating system. The suspensions were incubated at 37°C in a thermo-mixer (compact 5350, Eppendorf, Hamburg, Germany) for 5 minutes, after which the reaction was initiated through the addition of the NADPH generating system.

Experiments under basal conditions with primary human hepatocytes in 3D co-culture were performed as previously described in *chapter 4*. CYP activity was assessed by the addition of fresh medium, containing the cocktail with either n=5 (caffeine [80 µM], efavirenz [10 µM], omeprazole [17 µM], metoprolol [23 µM], and midazolam [5 µM]) or n=6 probe drugs (same composition as n=5, but with the addition of flurbiprofen).

Substrates were dissolved and serially diluted with DMSO to the required concentrations. Final concentration of DMSO during incubations was 0.2% (v/v). At selected time points - 0, 1, 2, 4, 8, 15, 30, 60 min in HLM, and 0, 15, 30, 45, 60, 75, 90, 105, 120 min in 3D-PHH - reactions were terminated by transferring 50 µL of the incubation mixture into a autosampler vial, to which a threefold volume of ice-cold methanol containing the internal standards was added. After vigorous shaking (10 min) and centrifugation (3220g; 30 min; 10°C), the samples were stored at -20°C until analysis by LC-MS/MS.

By comparing the metabolic production rate over time (pmol/ h/ 0.025×10^6 cells), with (n=6) or without (n=5) the inclusion of flurbiprofen, we could evaluate whether flurbiprofen influenced the CYP isoforms responsible for the production of the respective metabolites.

2.3. *In vivo* pilot study

To simplify simultaneous application of the cocktail probe drugs, a capsule containing the probe drugs of the modified Basel phenotyping cocktail in the form of miniature tablets (Figure 1), was developed by the Division of Pharmaceutical Technology, University of Basel (Prof. J. Huwyler). The novel composition of the combi-capsule content is given below (Table 1). Compared to the previous Basel cocktail [11, 12], the dose of caffeine was reduced from 100 mg to 7.5 mg (20 mini-tabs) to fit a size 0 capsule. Moreover, due to technical reasons, efavirenz was no longer used in a nano-milled form, but rather in a non-treated pure powder form, with an unknown impact on bioavailability of the active ingredient. Omeprazole was used as the racemate, containing both the (S)- and (R)-isomer of omeprazole (as found in Antramups®).



Figure 1. Mini-tabs (left) and mini-tabs in size 0 capsule (right).

Table 1. Composition of the combi-capsule (size 0).

Probe drug	Dose
Caffeine	7.5 mg
Efavirenz	49 mg
Flurbiprofen	11.7 mg
Omeprazole	10 mg
Metoprolol	9.3 mg
Midazolam	2 mg

The combi-pill was tested on three healthy male subjects in an *in vivo* pilot-study. Subjects were asked to adhere to a methylxanthine-free diet for 48 hours prior to the commencement of the pilot study. After an overnight fast, the combi-capsule was administered. Blood from an antecubital vein was collected into ethylenediaminetetraacetic acid (EDTA), containing vials before and 1, 2, 4, 6, and 8 hours after drug administration, according to the limited sampling strategy previously described [13]. Blood samples were centrifuged (1500 g; 10min; 4°C), and the ensuing plasma was stored at -20°C until analysis.

2.4. Bioanalytical analysis

A previously developed liquid chromatography tandem mass spectrometry (LC-MS/MS) method was used to analyse *in vitro* and plasma samples [11]. Flurbiprofen, 4'-hydroxyflurbiprofen, and the internal standard flurbiprofen-d3 were added to the existing method. Flurbiprofen (and its metabolite and IS) was detected using negative ESI (ion spray voltage -4500 eV).

Below, Table 2 outlines the additionally monitored MRM transitions, whereas Figure 2 shows a representative chromatogram of a calibration sample containing 250 ng/mL of each analyte in plasma.

Table 2. Additional multiple reaction monitoring (MRM) transitions monitored in the analytical method used to quantify the modified Basel cocktail.

Analyte	Precursor Ion (m/z)	Product Ion (m/z)	Ionisation mode
Flurbiprofen	243.0	199.0	ESI-
4'-OH-Flurbiprofen	259.1	212.9 / 214.9	ESI-
Flurbiprofen-d3	246.0	202.0	ESI-

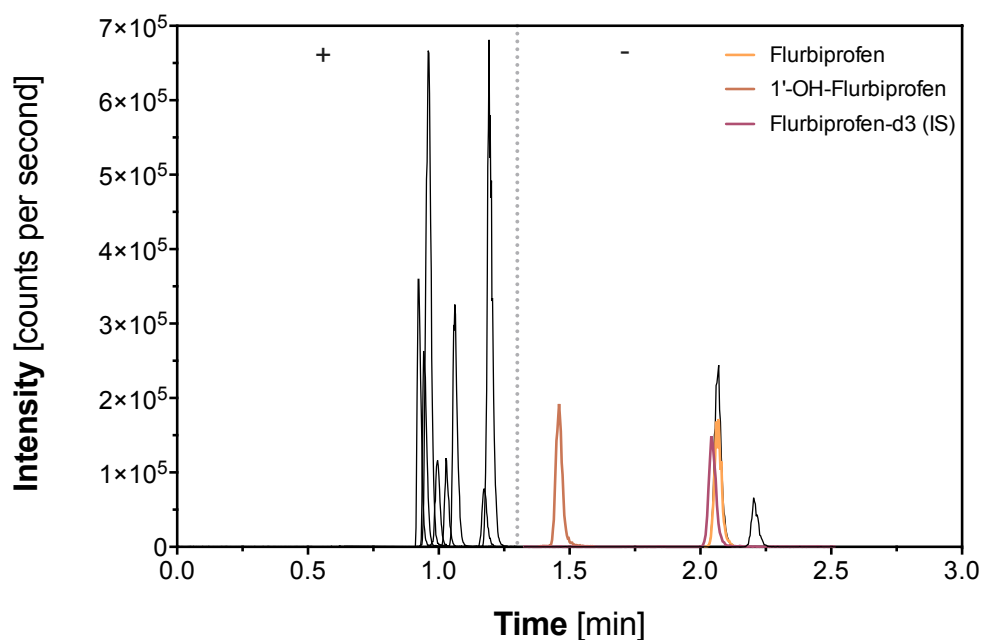


Figure 2. Chromatogram of the modified Basel cocktail LC-MS/MS method used in this study. The dotted line indicates the point at which the switch from positive ESI mode to negative ESI mode took place.

The total run time was 2.9 minutes. Inter-assay accuracy (determined as the % bias) ranged from -8.5 to 6.8 and inter-assay precision (determined as the CV,%) was lower than 13.9 for all analytes.

3. Results and discussion

Flurbiprofen was metabolised to 4'-hydroxyflurbiprofen in human liver microsomes, similar to the extent that losartan was metabolised to E-3174 (Figure 3).

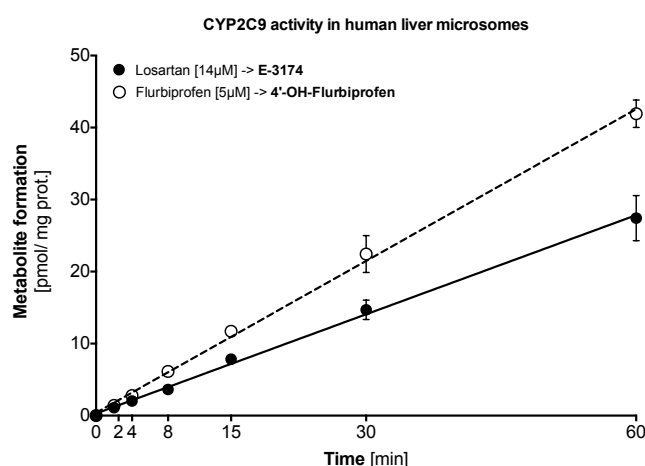


Figure 3. Metabolite formation of E-3174 (closed circles) and 4'-OH-Flurbiprofen (open circles) in HLM (0.5mg prot./mL) after a 1h incubation with either losartan [14µM] or flurbiprofen [5µM].

Previously, through incubations using cDNA-expressed microsomes for P450 CYP1A1, 1A2, 2A6, 2B6, 2C8, 2C19, 2D6, 2E1, and 3A4, two studies showed that flurbiprofen can be considered to be a highly specific probe substrate of CYP2C9, as none of the tested CYPs were involved in flurbiprofen hydroxylation at physiological concentrations [4, 14].

Furthermore, the Pittsburgh cocktail [9] and the Geneva cocktail [7, 8] have used some of the phenotyping drugs that are also contained in the Basel cocktail – i.e. caffeine (CYP1A2), omeprazole (CYP2C19), and midazolam (CYP3A4) – providing evidence that flurbiprofen does not interfere or inhibit the respective CYP isoforms. The other CYP isoforms characterised in the Basel cocktail were also evaluated by either the Pittsburgh or Geneva cocktail, making use of different probe substrates: i.e. bupropion (CYP2B6), debrisoquine, or dextromethorphan (CYP2D6). Thus, as could be expected, incubating the remaining five probe substrates of the Basel cocktail, with or without flurbiprofen, in cryopreserved human hepatocytes in 3D co-culture, did not lead to a significant change in the formation rates of their respective metabolites, as can be seen in Figure 4. Because linear curve fitting for paraxanthine formation (Fig-

ure 4a) was not ideal when using the time-point at 0.75h (saturation), it was excluded to be able to give a rough estimate of the slope.

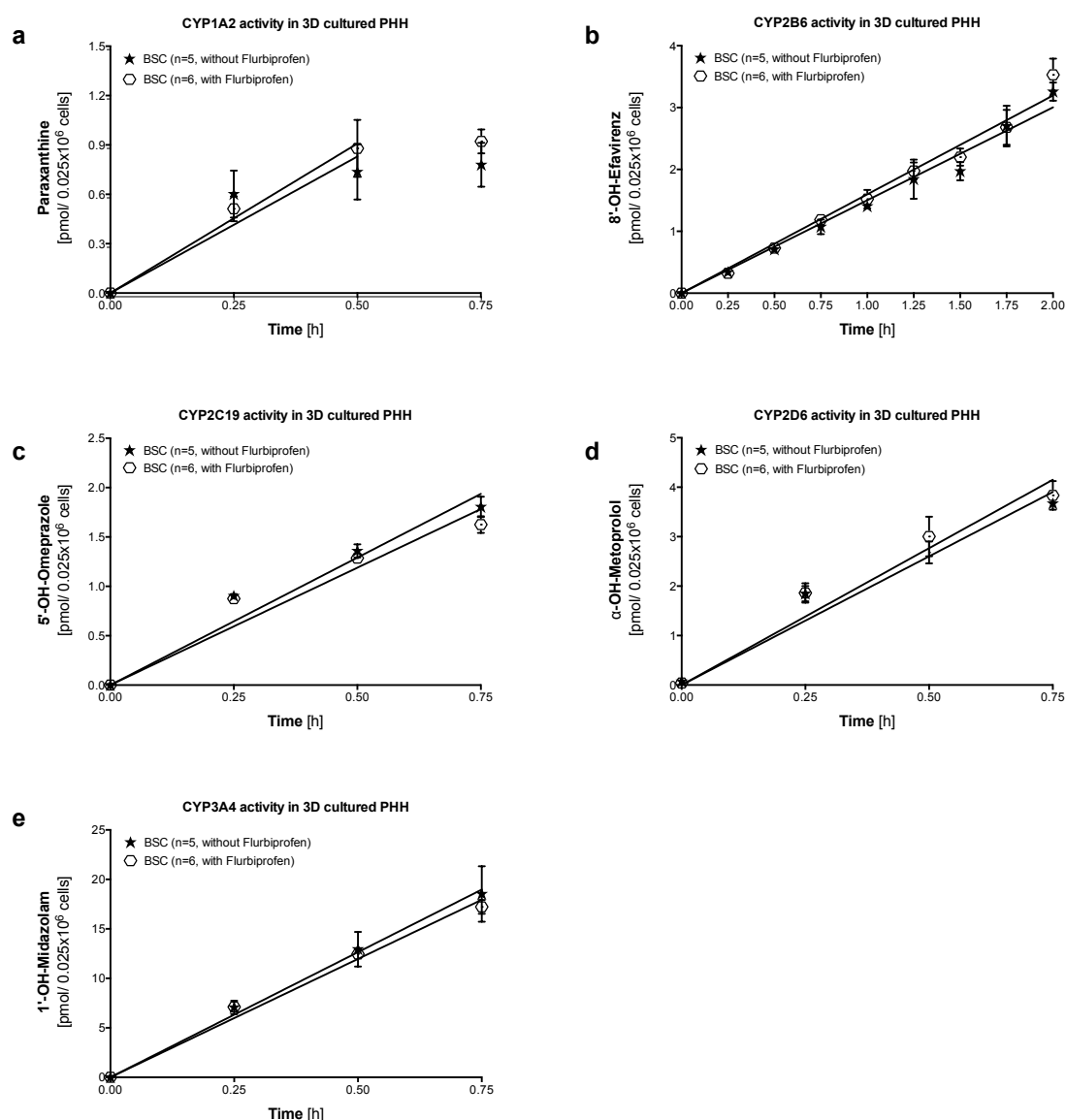


Figure 4. Metabolite formation of Phase-I metabolites of Basel cocktail probe substrates, **(a)** paraxanthine - CYP1A2, **(b)** 8'-hydroxyefavirenz - CYP2B6, **(c)** 5'-hydroxyomeprazole - CYP2C19, **(d)** α-hydroxymetoprolol - CYP2D6, and **(e)** 1'-hydroxymidazolam - CYP3A4, after incubation in primary human hepatocytes cultured in 3D, either cultured in the presence of flurbiprofen (hexagon, n=6 substrates incubated) or without flurbiprofen (5-pointed star, n=5 substrates incubated). PHH = primary human hepatocytes.

Although not directly comparable, due to shortened sampling time and aforementioned different dosages and formulations of probe substrates, the pharmacokinetic profiles and PK parameters measured after intake of the combi-capsule (Figure 4) seem to be in agreement with Basel cocktail studies [11, 12], and to a previous combi-pill prototype study. Metabolic single time-point ratios of parent/ metabolite (except for CYP1A2 and CYP2C9, metabolite/ parent ratio) calculated in this pilot-study were

all in the previously determined range [12], except for metoprolol (Table 3). This slight deviation encountered for metoprolol/ α -hydroxymetoprolol ratio is explained by the fact that, unlike in the combi-capsule, an extended release formulation (BelocZOK[®]) had been used in the initial Basel phenotyping cocktail.

In comparison to flurbiprofen ratios (4'-hydroxyflurbiprofen/ flurbiprofen) calculated through use of the Geneva cocktail in DBS [7], ratios found in the present study were around 50% lower.

Through use of the modified bioanalytical method used to determine parent and metabolites of the Basel cocktail, we were able to quantify all analytes. However, paraxanthine and 8'-hydroxyefavirenz concentrations were close to the respective LLOQs of the analytical method. For paraxanthine, this was due to the supposedly caffeine-free plasma used to create calibrators and QCs containing not entirely neglectable concentrations of paraxanthine.

Table 3. Comparison of probe drug metabolic ratios (MRs, i.e. concentration of metabolite/concentration of parent probe drug) determined in plasma after intake of either the combi-capsule or six separate commercially available formulations during the Basel cocktail study II [12] for **(a)** CYP1A2 - paraxanthine/ caffeine, **(b)** CYP2B6 - efavirenz/ 8'-hydroxyefavirenz, **(c)** CYP2C9 - 4'-hydroxyflurbiprofen/ flurbiprofen (compared to Geneva cocktail, concentrations measured in DBS [7]), **(d)** CYP2C19 - omeprazole/ 5'-hydroxymepirazole, **(e)** CYP2D6 - metoprolol/ α -hydroxymetoprolol, and **(f)** CYP3A4 - midazolam/1'-hydroxymidazolam.

a

metabolic ratio	Paraxanthine / Caffeine			Basel Cocktail II metabolic ratio (range - low to high)
	Subject 1	Subject 2	Subject 3	
2h	0.34	0.59	0.73	0.16 - 0.54
4h	0.45	0.81	0.73	0.24 - 0.92
6h	0.54	0.94	0.75	0.29 - 1.4
8h	0.58	0.98	0.74	0.38 - 1.64

b

metabolic ratio	Efavirenz / 8'-OH-Efavirenz			Basel Cocktail II metabolic ratio (range - low to high)
	Subject 1	Subject 2	Subject 3	
2h	n/a	21.4	51.5	13 - 46
4h	34.0	34.3	42.7	14 - 73
6h	49.6	46.4	68.8	29 - 78
8h	57.5	56.4	95.6	31 - 105

c

metabolic ratio	4'-OH-Flurbiprofen / Flurbiprofen			Geneva Cocktail (range - low to high)
	Subject 1	Subject 2	Subject 3	
2h	0.03	0.03	0.04	0.05 - 0.06
4h	0.04	0.04	0.05	0.05 - 0.07
6h	0.04	0.04	0.05	0.06 - 0.08
8h	0.04	0.03	0.04	0.05 - 0.08

d

metabolic ratio	Omeprazole / 5'-OH-Omeprazole			Basel Cocktail II metabolic ratio (range - low to high)
	Subject 1	Subject 2	Subject 3	
2h	1.08	0.71	n/a	0.6 - 3.1
4h	1.33	0.44	0.29	0.2 - 2
6h	0.72	0.35	0.11	0.16 - 1.16
8h	0.41	0.19	0.04	n/a

e

metabolic ratio	Metoprolol / α -OH-Metoprolol			Basel Cocktail II metabolic ratio (range - low to high)
	Subject 1	Subject 2	Subject 3	
2h	2.7	3.86	3.2	≈ 2 (not enough values)
4h	2.6	3.23	3.2	1.5 - 3.4
6h	1.8	2.75	2.5	1.4 - 3.7
8h	1.5	1.89	1.6	1.2 - 3.3

f

metabolic ratio	Midazolam / 1'-OH-Midazolam			Basel Cocktail II metabolic ratio (range - low to high)
	Subject 1	Subject 2	Subject 3	
2h	1.44	3.05	3.05	0.5 - 3.4
4h	1.97	3.26	3.34	0.5 - 3.9
6h	n/a	n/a	n/a	0.9 - 4.3
8h	n/a	n/a	n/a	n/a

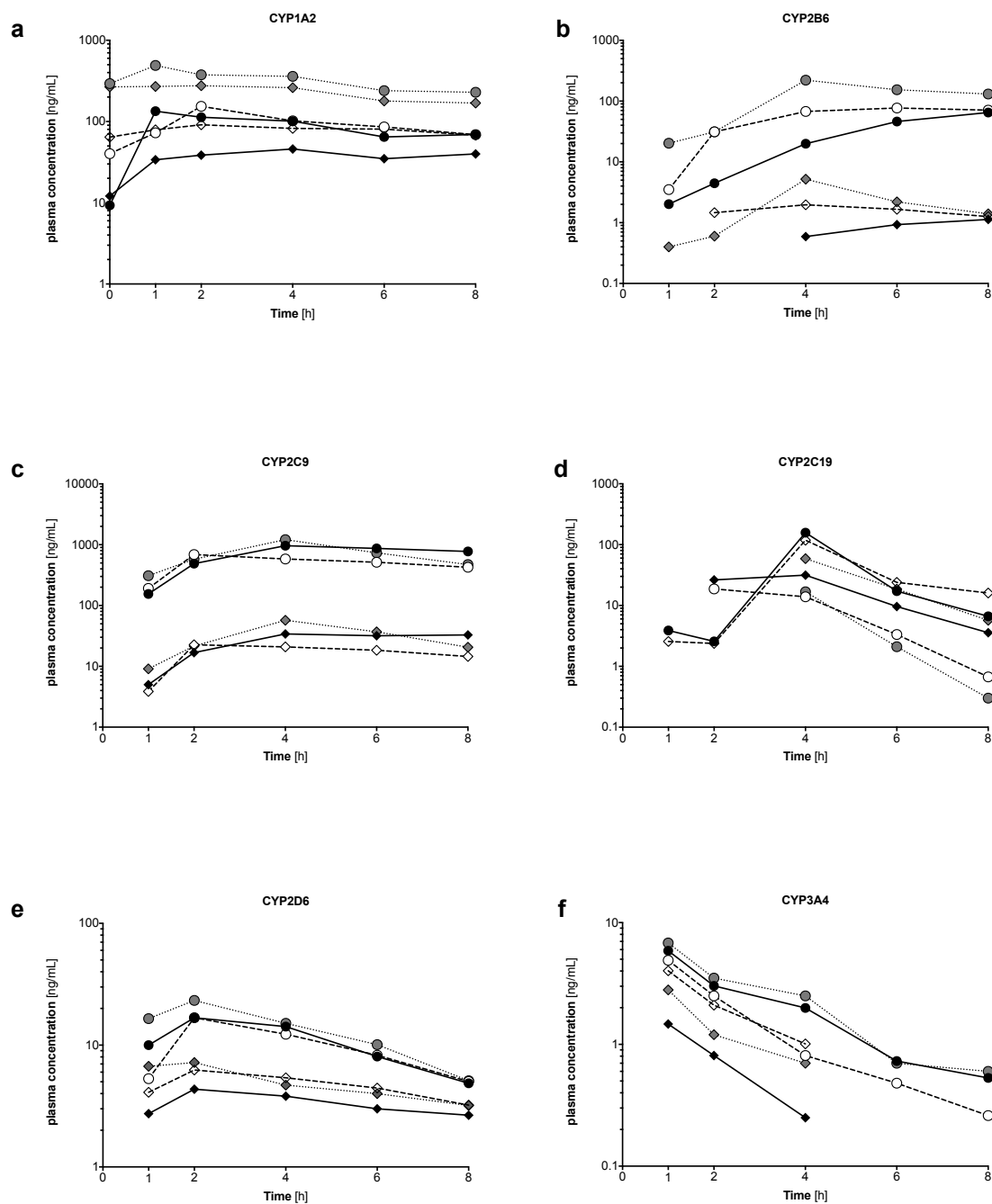


Figure 5. Plasma concentration time-profiles of the cocktail probe drugs (circle) and their metabolites (diamond) obtained after administration of the combi-capsule in three healthy subjects: black symbols correspond to subject 1, while white symbols correspond to subject 2, for (a) caffeine and paraxanthine (CYP1A2), (b) efavirenz and 8'-hydroxyefavirenz (CYP2B6), (c) flurbiprofen and 4'-hydroxyflurbiprofen (CYP2C9), (d) omeprazole and 5'-hydroxyomeprazole (CYP2C19), (e) metoprolol and α -hydroxymetoprolol (CYP2D6), and (f) midazolam and 1'-hydroxymidazolam (CYP3A4).

To facilitate and improve compliance, a number of drugs containing more than one active ingredient are already used in clinical practice, as is the case for certain anti-diabetic, anti-infective, and anti-hypertensive medications, as well as for a variety of different cold and flu remedies. Previously, the Basel cocktail was administered through five different tablets and a liquid formulation, which enabled the phenotyping

of six CYP isoforms responsible for the majority of phase I drug metabolism [11, 12, 15]. However, for phenotyping to become more widely accepted as a routine pre-dosing tool in clinical practice, simplified administration of probe substrates is paramount. The combi-capsule is therefore able to facilitate the intake of probe substrates, while doses of the respective probe drugs can more easily be modified, as the dose of the phenotyping agent is no longer reliant on commercially available drug formulations.

In summary, flurbiprofen did not interact with any probe substrates of the Basel cocktail in primary human hepatocytes in 3D-culture. Hence, in future studies, flurbiprofen can replace losartan as probe substrate for CYP2C9. Furthermore, results of the pilot-study showed that the use of a combi-capsule, containing probe substrates of the modified Basel cocktail in the form of miniature tablets, is feasible. Comparable metabolic ratios were observed when the formulation was compared to earlier studies with the Basel cocktail and to a pilot-study using a prototype combi-pill [11, 12].

Acknowledgements

We would like to thank Urs Duthaler¹, Beatrice Vetter¹, Nathalie Schaub², and Evelyn Durr² for their valuable advice and technical support.

Financial support

SK was supported by a grant of the Swiss National Science Foundation (SNF 31003A_156270).

Conflict of interest

None of the authors reports any conflict of interest regarding this study.

4. References

1. Keates, R.H. and K.A. McGowan, *Clinical trial of flurbiprofen to maintain pupillary dilation during cataract surgery*. Ann Ophthalmol, 1984. **16**(10): p. 919-21.
2. Compendium. *Froben® Fachinformation des Arzneimittel-Kompendium der Schweiz*. 2015 [cited 2016 12.02.2016]; Available from: <http://compendium.ch/mpro/mnr/9886/pdf/de - page1>.
3. Davies, N.M., *Clinical pharmacokinetics of flurbiprofen and its enantiomers*. Clin Pharmacokinet, 1995. **28**(2): p. 100-14.
4. Tracy, T.S., et al., *Role of cytochrome P450 2C9 and an allelic variant in the 4'-hydroxylation of (R)- and (S)-flurbiprofen*. Biochem Pharmacol, 1995. **49**(9): p. 1269-75.
5. Zgheib, N.K., et al., *Evaluation of flurbiprofen urinary ratios as in vivo indices for CYP2C9 activity*. Br J Clin Pharmacol, 2007. **63**(4): p. 477-87.
6. Daali, Y., et al., *Oral flurbiprofen metabolic ratio assessment using a single-point dried blood spot*. Clin Pharmacol Ther, 2012. **91**(3): p. 489-96.
7. Bosilkovska, M., et al., *Geneva cocktail for cytochrome p450 and P-glycoprotein activity assessment using dried blood spots*. Clin Pharmacol Ther, 2014. **96**(3): p. 349-59.
8. Bosilkovska, M., et al., *Simultaneous LC-MS/MS quantification of P-glycoprotein and cytochrome P450 probe substrates and their metabolites in DBS and plasma*. Bioanalysis, 2014. **6**(2): p. 151-64.
9. Zgheib, N.K., et al., *Validation of incorporating flurbiprofen into the Pittsburgh cocktail*. Clin Pharmacol Ther, 2006. **80**(3): p. 257-63.
10. Berger, B., et al., *Comparison of liver cell models using the Basel phenotyping cocktail*. 2016: manuscript.
11. Donzelli, M., et al., *The basel cocktail for simultaneous phenotyping of human cytochrome P450 isoforms in plasma, saliva and dried blood spots*. Clin Pharmacokinet, 2014. **53**(3): p. 271-82.
12. Derungs, A., et al., *Effects of Cytochrome P450 Inhibition and Induction on the Phenotyping Metrics of the Basel Cocktail: A Randomized Crossover Study*. Clin Pharmacokinet, 2016. **55**(1): p. 79-91.
13. Katzenmaier, S., C. Markert, and G. Mikus, *Proposal of a new limited sampling strategy to predict CYP3A activity using a partial AUC of midazolam*. Eur J Clin Pharmacol, 2010. **66**(11): p. 1137-41.
14. Tracy, T.S., et al., *Studies of flurbiprofen 4'-hydroxylation. Additional evidence suggesting the sole involvement of cytochrome P450 2C9*. Biochem Pharmacol, 1996. **52**(8): p. 1305-9.
15. Hewitt, N.J., et al., *Primary hepatocytes: current understanding of the regulation of metabolic enzymes and transporter proteins, and*

pharmaceutical practice for the use of hepatocytes in metabolism, enzyme induction, transporter, clearance, and hepatotoxicity studies. Drug Metab Rev, 2007. **39**(1): p. 159-234.

**7. Cytochrome p450 3A4 and 1A2 phenotyping for the
individualisation of treatment with erlotinib
(or sunitinib) in cancer patients**

Benjamin Berger¹, Massimiliano Donzelli¹, Markus Joerger², Zinnia P. Parra-Guillen³,
Charlotte Kloft³, Stephan Krähenbühl^{1,4}, Manuel Haschke¹

¹Division of Clinical Pharmacology & Toxicology, University Hospital Basel and
Department of Biomedicine, University of Basel, Switzerland

²Department of Medical Oncology, Cantonal Hospital St. Gallen, Switzerland

³Dept. of Clinical Pharmacy and Biochemistry, Institute of Pharmacy,
Freie Universität Berlin, Germany

⁴Swiss Center for Applied Human Research (SCAHT)

Abstract

Bioavailability after oral intake of erlotinib and sunitinib is highly variable due to their dependence on gastrointestinal absorption and first-pass metabolism in the liver. Thus, the uniform dosing strategy currently in place for TKIs is not adequate, as it can result in unacceptable side effects in some patients and under treatment with diminished therapeutic activity in others. Although a number of covariates have been proposed, a substantial interpatient variability in erlotinib (sunitinib) exposure remains unexplained. Since erlotinib and sunitinib are mainly metabolised by CYP3A4 (and erlotinib to a lesser extent also by CYP1A2), differences in the activities of these enzymes might be able to explain a sizeable amount of the observed interpatient variability in the pharmacokinetics of the respective TKIs. In contrast to genotyping, which can only assess genetic polymorphisms, patient phenotyping with probe drugs measures the overall activity of CYP isoforms and is the most promising approach for treatment individualisation of TKI, as has previously been shown with other anti-cancer drugs such as tamoxifen, gefitinib, and imatinib. We were able to demonstrate that low dose orally administered midazolam and caffeine could successfully be utilised in a clinical setting to perform phenotyping of CYP3A4 and CYP1A2. A correlation between CYP3A4/ CYP1A2 phenotype and erlotinib exposure could however not be determined due to lack of reliable exposure markers (i.e. AUC_{0-24h} or C_{trough}). Interestingly, the assessment of treatment-dependent toxicity showed, that patients with slow CYP3A4 metabolism were more likely to develop skin rash than patients with higher CYP3A4 activity. We also investigated the feasibility of drug bioanalysis from dried blood spots (DBS). However, after having measured erlotinib using the current set of DBS samples, we are at present not able to advocate the interchangeability of DBS and conventional plasma measurement.

Before final conclusions can be drawn, a population-PK model which is currently being developed using nonlinear-mixed-effects modelling (NONMEM), which is predominantly used in studies of this manner, has to be evaluated, as it is expected to support meaningful analysis of the gathered data.

Keywords: Erlotinib, Tyrosine-kinase inhibitors (TKI), CYP1A2, CYP3A4, phenotyping, DBS, LC-MS/MS

1. Introduction

Erlotinib (Tarceva[®]; F. Hoffmann-La Roche; Basel, Switzerland) and Sunitinib (Sutent[®]; Pfizer; NY, USA) are among the most frequently used orally active multitargeted tyrosine kinases inhibitors (TKIs). Erlotinib is currently approved for treatment of pancreatic cancer and locally advanced or metastatic non-small cell lung cancer (NSCLC) in patients with activating EGFR mutations, while sunitinib is used to treat metastatic renal cell carcinoma (RCC), gastrointestinal stromal tumours (GIST), and pancreatic neuroendocrine tumours [1, 2]. Erlotinib reversibly and selectively inhibits the intracellular autophosphorylation of tyrosine kinases (TK) in association with the epidermal growth factor receptor (EGFR). On the intracellular domain of the TK, erlotinib is in competition with ATP for binding sites and is thus able to inhibit downstream signalling pathways that can lead to oncogenesis [3-6]. Sunitinib, on the other hand, has been shown to target the inhibition of a number of TKs including the vascular endothelial growth factor receptors (VEGFR - 1,2, and 3), the platelet derived growth factor receptor (PDGFR - α,β), and mast/stem cell growth factor receptor (SCFR/ c-Kit) [7-9].

Although conventional chemotherapy attempts to pinpoint certain macromolecules or enzymes, they do not typically discriminate efficiently between rapidly dividing normal cells – e.g. bone marrow, gastrointestinal tract, or hair follicles – and the tumour cells they are intended to eliminate. They are consequently prone to causing severely toxic adverse events. On the other hand, targeted or cytostatic therapies such as TKIs, which, instead of extinguishing tumour cells, lead to the blocking of tumour cell growth and progression by interfering with a multitude of molecular targets, lead to considerably less toxicity [10-12]. For erlotinib and sunitinib, the most prevalent forms of toxicity are of a cutaneous, hematologic, and gastrointestinal nature [13]. However, potentially life-threatening toxicities, such as interstitial lung disease (erlotinib) and cardiac dysfunction (sunitinib), are becoming increasingly important, as these drugs are being introduced into long-term treatment [14-16].

Erlotinib is metabolised in the liver, mainly by cytochrome P450 3A4 (CYP3A4) and, to a lesser degree, by CYP1A2 to its active metabolite OSI-420, with metabolites primarily excreted in the bile. OSI-420 accounts for approximately 10% of the parent drug while being equipotent in inhibiting EGFR TK activity [17]. Erlotinib is known to be transported via the active efflux pumps P-glycoprotein (MDR1/ ABCB1) and breast cancer resistance protein (BCRP/ ABCG2) [18-20]. Sunitinib is metabolised by CYP3A4 to its equally potent N-desethyl metabolite Su-12662 [7].

The daily-recommended oral dose of erlotinib is 150mg in NSCLC patients and 100mg in pancreatic cancer patients, whereas 50mg of sunitinib is recommended in RCC or GIST patients (for 4 weeks followed by a 2-week hiatus). However, bioavailability after oral intake is highly variable due to its dependence on gastrointestinal absorption and first-pass metabolism in the liver, two processes that show considerable inter-individual differences [21, 22]. Variability in erlotinib pharmacokinetics (PK) can, therefore, have a critical impact on previously reported rates of adverse effects [13, 23-28]. Although a number of covariates have been proposed, i.e. hepatic function, smoking habit, and ABCG2 polymorphisms [25], a substantial inter-patient variability in erlotinib exposure remain unexplained. Thus, the uniform dosing strategy currently in place is inadequate, as it can result in unacceptable side effects in some patients and under treatment with diminished therapeutic activity in others. Since erlotinib and sunitinib are mainly metabolised by CYP3A4 (and, in the case of erlotinib, to a lesser extent also by CYP1A2), differences in the activities of these enzymes might provide an explanation for a sizeable amount of the unexplained observed interpatient variability in the pharmacokinetics of the respective TKIs. In contrast to genotyping, which can only assess genetic polymorphisms, patient phenotyping with probe drugs measures the overall activity of CYP isoforms and is the most promising approach for treatment individualisation of TKI, as has previously been shown with other anticancer drugs such as tamoxifen [29].

The primary aim of this study was to evaluate the relationship between individual CYP3A4 and CYP1A2 phenotype, assessed using oral midazolam and caffeine as phenotyping probes, with erlotinib and sunitinib exposure. Secondary aims were to assess the correlation of individual CYP-phenotype with treatment-related toxicity, as well as to assess the feasibility of using dried blood spots to perform the bioanalysis of erlotinib.

2. Methods

2.1. Clinical study

Patients diagnosed with early or advanced renal cell cancer (RCC), gastrointestinal stromal tumour (GIST) or non-small cell lung cancer (NSCLC), were eligible for entry into the study and were treated according to their indication with either sunitinib or erlotinib (Table 2). All patients taking part in this prospective, nonrandomised, pharmacological cohort study were > 18 years of age, and had adequate laboratory pa-

rameters, as defined by serum creatinine and serum bilirubin $\leq 1.5 \times \text{ULN}$ (upper limit of normal), serum ALT and AST $\leq 2.5 \times \text{ULN}$ (or ≤ 5 in case of liver metastases), and serum calcium $\leq 11,6 \text{ mg/ dl}$ (2.9 mmol/ L). Concurrent radiotherapy or systemic anticancer treatment (with the exception of bisphosphonates and bevacizumab in patients with NSCLC), as well as previous treatment with erlotinib, were regarded as exclusion criteria. Concomitant use of substances known or likely to interfere with either CYP3A4 or CYP1A2 (unless there was no therapeutic alternative available) was not allowed. Patients with a known hypersensitivity to either trial drug or any compounds of the drugs were excluded from the study.

A clinical assessment, including physical examination (blood pressure, WHO performance status, weight), haematological tests (haemoglobin, neutrophils, thrombocyte counts), and blood chemistry tests (ALAT, bilirubin, serum albumin, serum creatinine), was performed on each visit to the clinic, i.e. on day 1 and at 2, 4, 8, and 10-week intervals thereafter.

Adverse events (AE) were coded according to the NCI Common Terminology Criteria for Adverse Events, version 4.0 (CTCAE, National Institutes of Health, Bethesda, MD). AE were treated symptomatically or managed according to appropriate erlotinib/ sunitinib prescribing information; in the case of CTCAE grade 3 toxicity, dosage was lowered and/or completely discontinued in the case of CTCAE grade 4 toxicity.

This study was carried out as part of routine patient care and was conducted in accordance with the Declaration of Helsinki and its amendments. The study was approved by the local ethics committee (Canton St. Gallen, Switzerland) and the national regulatory authority (Swiss agency for the authorisation and supervision of therapeutic products, Swissmedic, ClinicalTrials.gov Identifier: NCT01402089). All patients gave informed written consent before entering the study and agreed to undergo PK-sampling.

2.2. Sample Collection and Phenotyping

After an overnight fast, 2 mg of oral midazolam (in-house formulation; Pharmacy of the cantonal hospital St. Gallen, Switzerland) was administered in tap water as the CYP3A4 probe drug [30]. Blood collected from an antecubital vein was collected into ethylenediaminetetraacetic acid (EDTA) containing vials before and 1, 2, 3, 4, and 6 hours after drug administration, according to the limited sampling strategy previously described [31]. Additionally, CYP1A2 phenotyping was performed after a methylxanthine-free diet over 36h using 100 mg oral caffeine (Mylan Dura GmbH, Darmstadt,

Germany). Blood samples for caffeine and paraxanthine determinations were collected before dosing and 6 hours after the administration of caffeine.

An aliquot of each blood sample was transferred to a different vial and centrifuged (at 1500 g; 10 min; 4°C), after which the residual plasma and the remaining whole blood aliquots were stored at -80°C until analysis.

Patients were treated with either commercially available erlotinib tablets (Tarceva®; Roche Pharma; Basel, Switzerland) with a once daily oral dose of 150 mg or sunitinib maleate hard capsules (Sutent®; Pfizer; NY, USA) with a once daily dose of 50mg for 4 out of 6 weeks, barring disease progression, unacceptable toxicity, or withdrawal of informed consent. On day 1, both sunitinib and erlotinib were sampled at the same time-points as the phenotyping drugs. Subsequently, steady-state plasma concentrations were sampled in weeks 2, 4, 8, and 10. Additionally, DBS were taken by the patient's general practitioner (GP), preferably in week 6 and 10 (for patients still remaining on the study drug). DBS samples were collected through the puncture of a fingertip, using a single-use, disposable lancet device (Accu-Check Softclix Pro; Roche Pharma, Basel, Switzerland). After collecting four droplets of blood per collection card, it was left to dry for at least 2h at room temperature, after which the card was stored at -80°C in a sealable plastic bag containing a desiccant packet until ready for analysis.

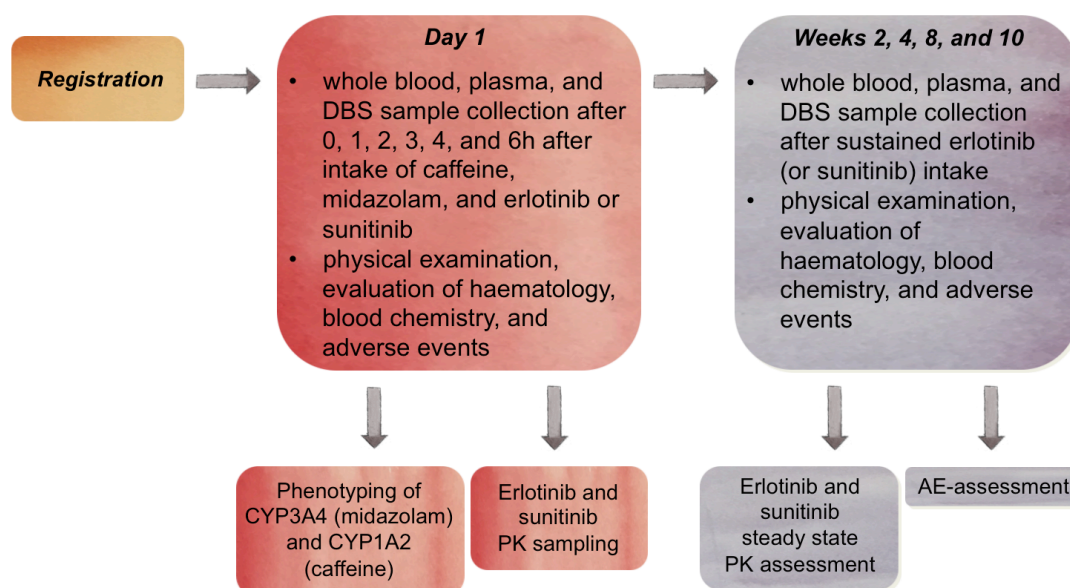


Figure 1. Study Design (adapted from study protocol - clinicaltrials.gov ID: NCT01402089).

2.3. Materials and Reagents

Erlotinib hydrochloride, O-desmethyl erlotinib (OSI-420), sunitinib maleate, N-desethyl sunitinib (Su-12662), as well as the internal standards (erlotinib-d6, sunitinib-d10, caffeine-d9), were purchased from TRC (Toronto, Canada). 1'-hydroxymidazolam and midazolam-d6 were acquired from Lipomed (Arlesheim, Switzerland), whereas midazolam was kindly provided to us by Hoffmann-La Roche, Basel, Switzerland. Caffeine and paraxanthine were obtained from Sigma-Aldrich (Sigma-Aldrich Chemie GmbH, Buchs, Switzerland). Formic acid, DMSO, high-performance liquid chromatography (HPLC)-grade methanol, and HPLC-grade water were purchased from Merck (Darmstadt, Germany). DBS cards (FTA DMPK-C cards), manual hole-punchers (3 mm diameter) and cutting mats were obtained from Whatman (Sanford, ME, USA).

2.4. Bioanalysis

Concentrations of TKIs and phenotyping agents, as well as their main metabolites in plasma, whole blood, and DBS, were determined by LC-MS/MS.

In brief, 50 μ L aliquots of plasma or whole blood were mixed with 150 μ L of an internal standard solution containing deuterated analogues of the respective drugs and phenotyping agents, (at a concentration of 50 ng/mL for midazolam-d6, and 100 ng/mL for erlotinib-d6, sunitinib-d10, and caffeine-d9), was vortex mixed for 30 seconds, and then centrifuged (3200 g; 30 min; 10°C). For DBS analysis, a disc with a diameter of 3 mm was cut out of the centre of the DBS and added to a vial containing 200 μ L of the internal standard solution (methanol/water (1/1, v/v)). The vials were then vortex mixed for 10 minutes and centrifuged (3200 g; 30 min; 10°C). Chromatographic separation was performed on a Shimadzu HPLC system (Shimadzu AG, Reinach, Switzerland), coupled to a triple quadrupole tandem mass spectrometer (API3200 or API4000, AB/MDS Sciex, Concord, ON, Canada) operating in positive electrospray ionisation mode. The selected mass to charge (m/z) ratio transitions of the analytes and internal standards used in selective reaction monitoring mode can be found in Table 1. Analyst software 1.6.2 (AB Sciex, MA, USA) was used to operate the LC-MS/MS system.

Table 1. Multiple Reaction Monitoring (MRM) transitions monitored.

Analyte	Precursor Ion [m/z]	Product Ion [(m/z)]	Ionisation mode
Caffeine	195	138	ESI +
Paraxanthine	181	124	ESI +
Caffeine-d9	204	144	ESI +
Midazolam	326	291	ESI +
OH-Midazolam	342	324	ESI +
Midazolam-d6	332	297	ESI +
Sunitinib	399	326	ESI +
Su-16226	371	283 / 238	ESI +
Sunitinib-d10	409	283	ESI +
Erlotinib	394	278	ESI +
OSI-420	380	278 / 276	ESI +
Erlotinib-d6	400	278	ESI +

A representative chromatogram showing the retention time and separation of the respective analytes can be seen in Figure 2. The total run time was 3.0 minutes.

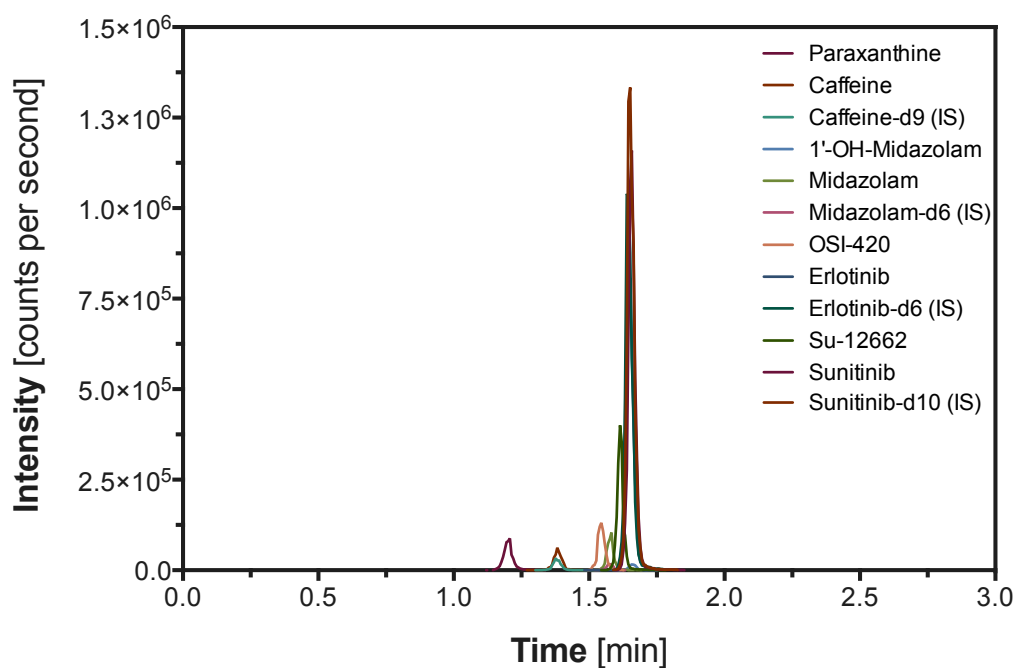


Figure 2. Chromatogram of the analytical method used to analyse erlotinib, sunitinib, midazolam, caffeine, and their metabolites, as well as their respective internal standards (IS).

The linear calibration curve for every measured analyte showed a coefficient of determination greater than 0.99, generated over the respective calibration range. Inter-assay accuracy (determined as the % bias) ranged from -6.5 to 6.5% and inter-assay precision (determined as the CV%) was lower than 12.4% for all analytes. The lower limit of quantification (LLOQ) was 0.25 ng/ml for OSI-420, Su-12662, midazolam, and 1'-hydroxymidazolam; 1.25 ng/ml for erlotinib and sunitinib; and 12.5 ng/ml for paraxanthine and caffeine in plasma and whole blood. LLOQ was 1 ng/mL for midazolam and OSI-420; 5 ng/mL for erlotinib, sunitinib, Su-12662, 1'-hydroxymidazolam, caffeine, and paraxanthine. Stock solutions, calibration spiking solutions, and quality controls were prepared in DMSO. Calibration standards and quality controls were prepared by enriching the respective caffeine-free blank human plasma or whole blood, using the corresponding spiking solutions. Internal standard solutions containing the deuterated compounds were prepared in methanol. For analysis of DBS, the same concentrations of deuterated compounds were dissolved in methanol/water (1/1, v/v).

2.5. Data Analysis

All graphs, figures, and tables make use of erlotinib, OSI-420, sunitinib, Su-12662, midazolam, 1'-hydroxymidazolam, caffeine, and paraxanthine concentrations measured in plasma. The partial area under the concentration-time curve, from time 0 to 6 hours (AUC_{0-6h}) after dosing on day 1, was estimated using the linear trapezoidal method and calculated using Microsoft® Excel 2010 add-on PKsolver [32]. Maximal concentrations (C_{max}) and time to reach C_{max} (T_{max}) were taken directly from observed data. Correlations between single time-point concentration ratios and AUC ratios were tested using linear regression analysis. The relationship between midazolam exposure and erlotinib exposure was examined by Pearson correlation analysis. The unpaired Student's t-test was used to assess the impact of smoking and the intake of PPIs on various pharmacokinetic parameters (C_{ss} , C_{max} , AUC_{0-6h} , etc.), while the paired t-test was used to determine the impact of sustained treatment on erlotinib MR. One-way ANOVA was performed to evaluate the impact of midazolam MR on the severity of skin rash. Bland-Altman analysis was used to compare measurements of erlotinib and OSI-420 between plasma, DBS, and whole blood. All Statistical analysis was performed using GraphPad Prism Software (Version 6.0g, La Jolla, CA, USA). The level of significance was set at $p < 0.05$ for all performed tests.

3. Results

3.1. Patients and Treatment

In total, fifty-two patients took part in the study. Thirty-seven of these patients were treated for NSCLC with erlotinib at the Cantonal Hospital of St. Gallen between February 2012 and May 2015 (Table 2): their median age was 65.5 years (range 52.0-77.8) and 26 patients (70%) were male.

Ten patients included in the study were treated with sunitinib for either gastrointestinal stromal tumour (GIST) or renal cell cancer (RCC) between January 2012 and August 2015. One of the patients being treated with sunitinib abandoned the trial shortly after enlisting and is therefore no longer taken into consideration. However, due to a large number of missing samples in the patient group being treated with sunitinib, meaningful analysis requires a population PK approach, which will be performed at a later point in time.

A further five patients were treated with pazopanib (Votrient®; GlaxoSmithKline; Brentford, United Kingdom). These patients were not included in this body of work and shall be analysed at a later point.

Therefore only results of the patients treated with erlotinib will be discussed in this chapter.

Table 2. Patient demographics and clinical characteristics.

Baseline Screening	Median (range) or Number of patients
Drug	Erlotinib
Number of females	11
Number of males	26
Age (years)	66.5 (52.0 - 77.8)
Weight (kg)	71.0 (37.1 - 96.7)
Tumor Type	
NSCLC	37
Stage of tumour disease (WHO)	
1	2
2	
3	10
4	25
Pretreatment clinical chemistry	
ASAT (IU/L)	20.0 (8.0 - 57.0)
ALAT (IU/L)	14.0 (5.0 - 119)
Total bilirubin (µM/L)	9.0 (4.0 - 27.0)
Serum creatinine (µM/L)	86.0 (38.0 - 267)
Haematocrit (%)	37.0 (26.0 - 46.0)
Serum albumine (g/L)	34.8 (18.7 - 45.9)
TSH (mU/L)	1.5 (0.3 - 23.3)
Patient History	
Prior surgery	7
Prior radiotherapy	15
Prior anticancer drug treatment	36
Smoking Status	
never	4
former	23
current	10

Baseline Screening	Median (range) or Number of patients
Drug	Sunitinib
Number of females	1
Number of males	8
Age (years)	64.4 (54.7 - 70.0)
Weight (kg)	89.2 (57.1 - 105.2)
Tumor Type	
GIST	7
RCC	2
Stage of tumour disease (WHO)	
1	
2	1
3	5
4	3
Pretreatment clinical chemistry	
ASAT (IU/L)	32.0 (6.0 - 61.0)
ALAT (IU/L)	24.0 (55.0 - 78.0)
Total bilirubin (μM/L)	13.0 (6.0 - 34.0)
Serum creatinine (μM/L)	105 (64.0 - 157.0)
Haematocrit (%)	40.0 (33.0 - 45.0)
Serum albumine (g/L)	38.8 (24.2 - 44.9)
TSH (mU/L)	1.6 (0.7 - 4.6)
Patient History	
Prior surgery	9
Prior radiotherapy	2
Prior anticancer drug treatment	2

Twenty-one (57%) of the 37 patients treated with erlotinib were monitored for the entire 10 weeks and 16 (43%) were prematurely discontinued from the study, primarily due to adverse events. One patient died from disease progression during the study. Skin rash, anorexia, and diarrhoea were the principal drug-related toxicities, and these were reported in 70%, 60%, and 46% of the patients, respectively. Other observed toxicities included nausea, hypertension, vomiting, and oral mucositis, all of which were generally of mild to moderate intensity (Table 3).

Table 3. List of reported adverse events (CTCAE grade).

Occurrence of AE		Grade 1 / 2	Grade 3 / 4
Nausea	Day 1	4 / -	- / -
	Week 2	3 / -	2 / -
Hypertension	Day 1	- / -	- / -
	Week 2	- / -	- / -
Anorexia	Day 1	9 / 5	- / -
	Week 2	6 / 4	1 / -
Skin rash	Day 1	- / -	- / -
	Week 2	11 / 7	4 / -
Vomiting	Day 1	- / -	- / -
	Week 2	2 / -	- / -
Diarrhoea	Day 1	1 / 2	- / -
	Week 2	5 / 1	- / -
Oral mucositis	Day 1	2 / 2	- / -
	Week 2	- / -	- / -

Occurrence of AE (at anytime in study)	Grade 1 / 2	Grade 3 / 4
Nausea	7 / 2	3 / 4
Hypertension	- / 1	- / -
Anorexia	11 / 10	1 / -
Skin rash	12 / 10	4 / -
Vomiting	3 / 2	- / -
Diarrhoea	11 / 5	1 / -
Oral mucositis	3 / 3	- / -

Ten patients (27%) were smokers, 23 (62%) were former smokers, while 17 (46%) patients took an acid-inhibiting drug (proton-pump inhibitor (PPI): either omeprazole, esomeprazole, lansoprazole, or pantoprazole) during the course of the study. According to patient diaries and hospital charts, no other medication was taken throughout the study that could have had an impact on erlotinib metabolism. Twenty-eight patients (76%) stayed on the initial dosage regimen of 150 mg erlotinib per day throughout the entire study. Five patients required a dose reduction, and four pa-

tients started treatment with a reduced daily dose (three patients on 100 mg/day; one patient on 75 mg/day). There were no dose escalations.

At baseline, seven study participants already had detectable erlotinib concentrations, and, in one patient, high midazolam concentrations were found at baseline (t=0h). These eight patients were excluded from pharmacokinetic analysis on day 1.

3.2. Erlotinib, midazolam, and caffeine pharmacokinetics

Observed maximal erlotinib concentrations on day 1 (C_{\max}) were 1340 ± 975 ng/mL (median 1100 ng/mL; range 184 - 4290 ng/mL), with a high inter-patient variability (co-efficient of variation 74%). C_{\max} of the main metabolite of erlotinib, OSI-420, was approximately 10-fold lower compared to the parent compound, with C_{\max} averaging 151 ± 164 ng/mL (median 96 ng/mL; range 20 - 848 ng/mL). Average T_{\max} was 3.3 ± 1.6 h (median 3.0h) for erlotinib and 3.7 ± 1.6 h (median 4.0h) for OSI-420. The partial area under the plasma concentration-time curve from time 0 to 6 hours after drug intake on day 1 (AUC_{0-6h}) was 5.7 ± 4.6 $\mu\text{g/ml}\cdot\text{h}$ (median 4.8 $\mu\text{g/ml}\cdot\text{h}$; range 0.8 - 21.2 $\mu\text{g/ml}\cdot\text{h}$) for erlotinib and 0.6 ± 0.5 $\mu\text{g/ml}\cdot\text{h}$ (median 0.4 $\mu\text{g/ml}\cdot\text{h}$; range 0.1 - 2.9 $\mu\text{g/ml}\cdot\text{h}$) for OSI-420. During the 10-week course of erlotinib treatment, C_{ss} values averaged 2069 ± 1101 ng/mL (median 1852; range 671 - 6540 ng/mL; Figure 3).

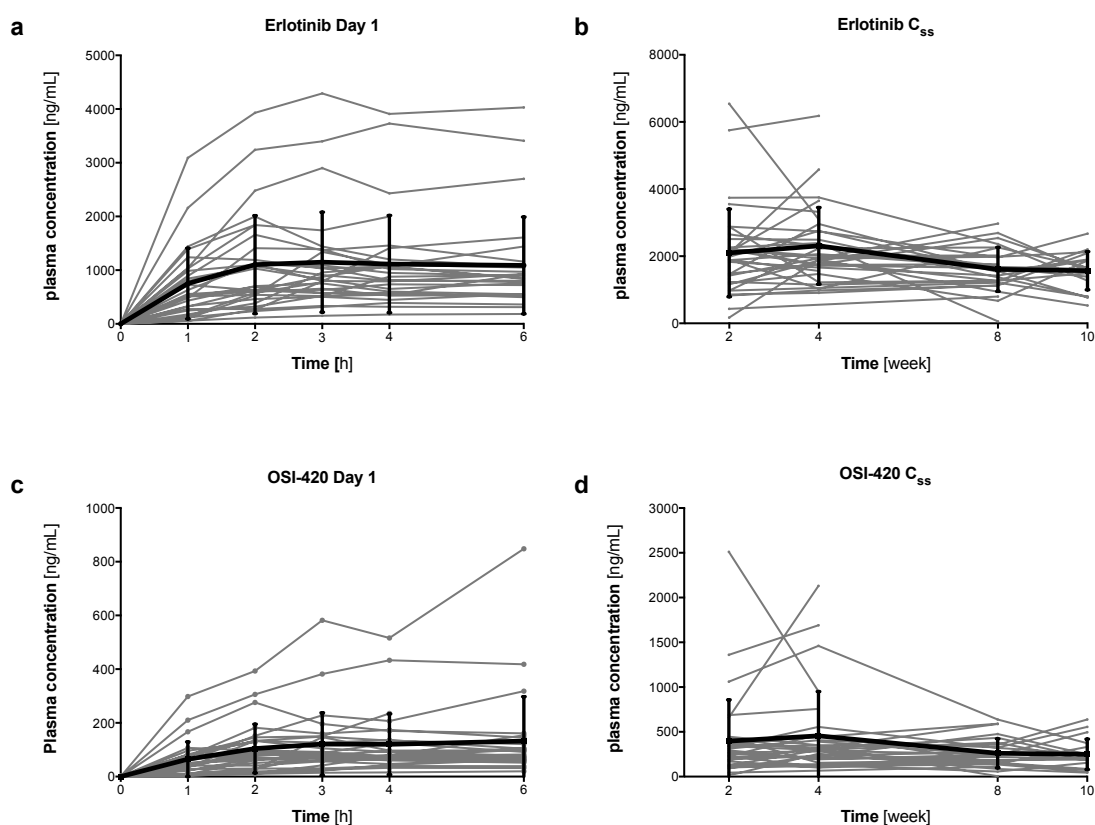


Figure 3. Individual plasma concentration time profiles (grey lines) and mean \pm SD (black line) of (a) erlotinib on day 1 (n=30), (b) OSI-420 on day 1 (n=30), (c) erlotinib after weeks 2, 4, 8, and 10 (n=37), and (d) OSI-420 after weeks 2, 4, 8, and 10 (n=37).

Among all eligible patients, AUC_{0-6h} of midazolam on day one was 20.8 ± 13.9 ng/ml*h (median 19.7 ng/ml*h; range 3.2 - 64.7 ng/ml*h) and 6.8 ± 3.9 ng/ml*h (median 6.2 ng/ml*h; range 1.8 - 19.1 ng/ml*h) for 1'-hydroxymidazolam. C_{max} for midazolam and 1'-hydroxymidazolam was 9.1 ± 5.4 ng/mL (median 8.8 ng/mL; range 2.3 - 24.7 ng/mL) and 3.4 ± 1.8 ng/mL (median 3.07 ng/mL; range 1.2 - 8.4 ng/mL), respectively, while T_{max} was 1.04 ± 0.2 h.

AUC_{0-6h} of caffeine on day one was 12.8 ± 6.3 μ g/ml*h (median 7.3 μ g/ml*h; range 7.3 - 37.4 μ g/ml*h) and 3.8 ± 2.9 μ g/ml*h (median 3.2 μ g/ml*h; range 0.7 - 8.6 μ g/ml*h) for paraxanthine. C_{max} for caffeine and paraxanthine was 3034 ± 1293 ng/mL (median 2580 ng/mL; range 1598 - 7168 ng/mL) and 808 ± 577 ng/mL (median 637 ng/mL; range 171 - 2394 ng/mL), whilst T_{max} was 1.6 ± 1.4 h (median 1h) and 4.8 ± 1.8 h (median 6h), respectively (Figure 4).

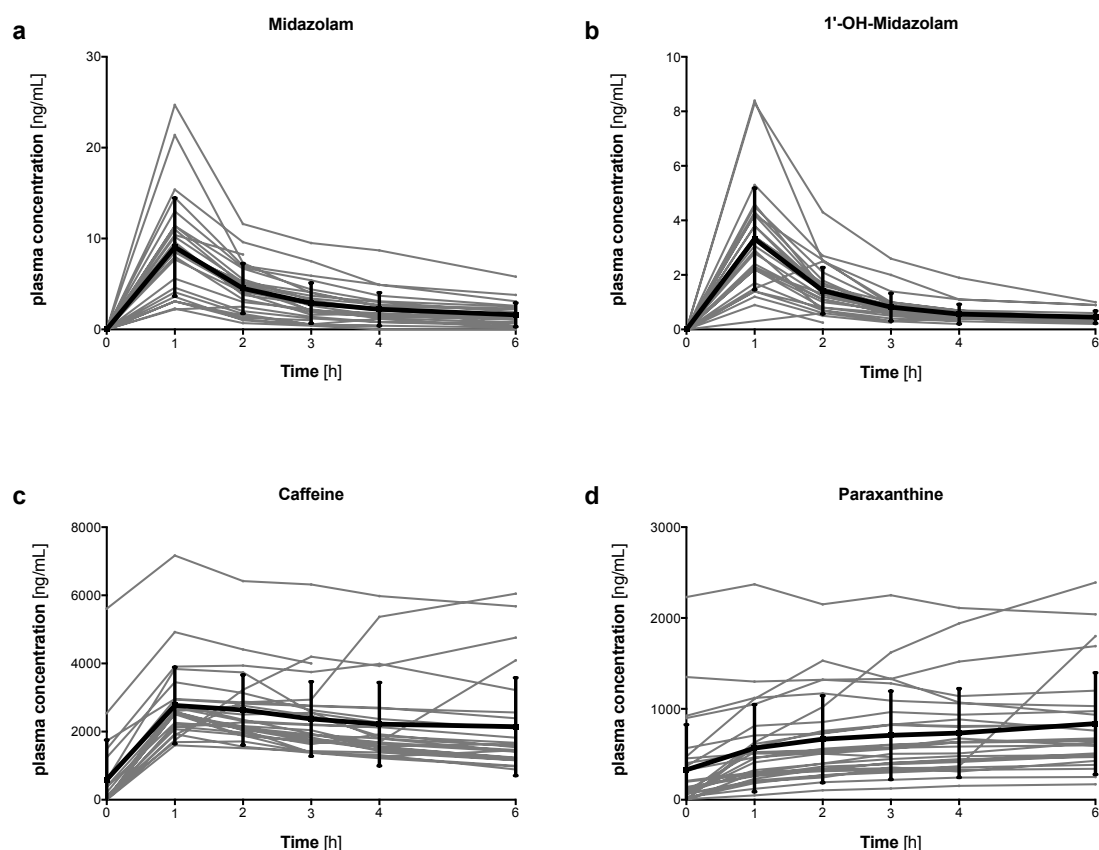


Figure 4. Individual plasma concentration time profiles (grey lines) and mean \pm SD (black line) of **(a)** midazolam (n=29), **(b)** 1'-hydroxymidazolam (n=29), **(c)** caffeine (n=30), and **(d)** paraxanthine (n=30) on day one.

Co-administration of proton pump inhibitors (PPIs) was associated with a statistically significant decrease in erlotinib partial AUC_{0-6h} (Figure 5a) and erlotinib C_{max} (Figure 5b).

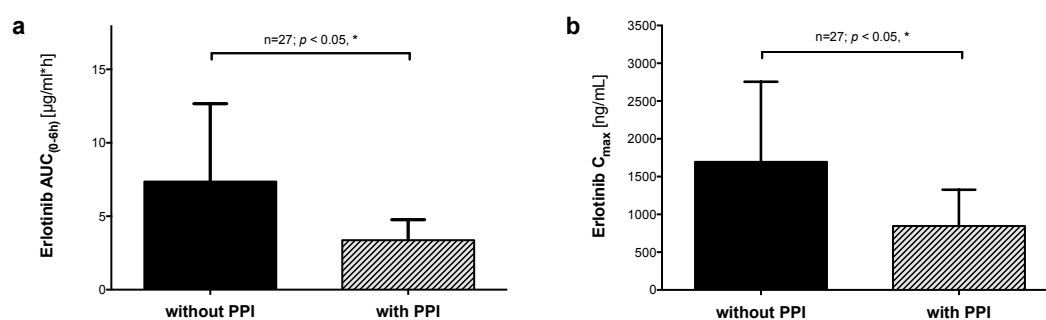


Figure 5. Influence of proton pump inhibitors (PPIs) on **(a)** erlotinib partial AUC_{0-6h}, and **(b)** erlotinib C_{max}. Values are mean \pm SD. The p-values are from unpaired t-tests.

3.2. Correlation between single point ratios and AUC ratios

The single time point parent to metabolite MR, 2h after administration of midazolam, was strongly correlated with the $AUC_{\text{parent (0-6h)}} / AUC_{\text{metabolite (0-6h)}}$ ratio (partial AUC_{0-6h} ratio) (Figure 6a). The same was found for the single time-point concentration of midazolam (2h) and midazolam $AUC_{(0-6h)}$ (Figure 7a). The metabolic ratio (MR) of midazolam showed an 8-fold variation in the study population with a median of 2.9 (range 0.9 to 7.4). As there is no uniformly accepted measure to enable the classification of CYP3A4 slow metabolisers (or extensive metabolisers), we used the 25th and 75th percentile of the 28 patients for whom we were able to calculate the metabolic ratio at 2h. Thus, the seven patients with $MR > 4.1$ were classified to have a slow phenotype, while seven patients with $MR < 2.3$ were accordingly classified to be portraying an extensive phenotype for CYP3A4.

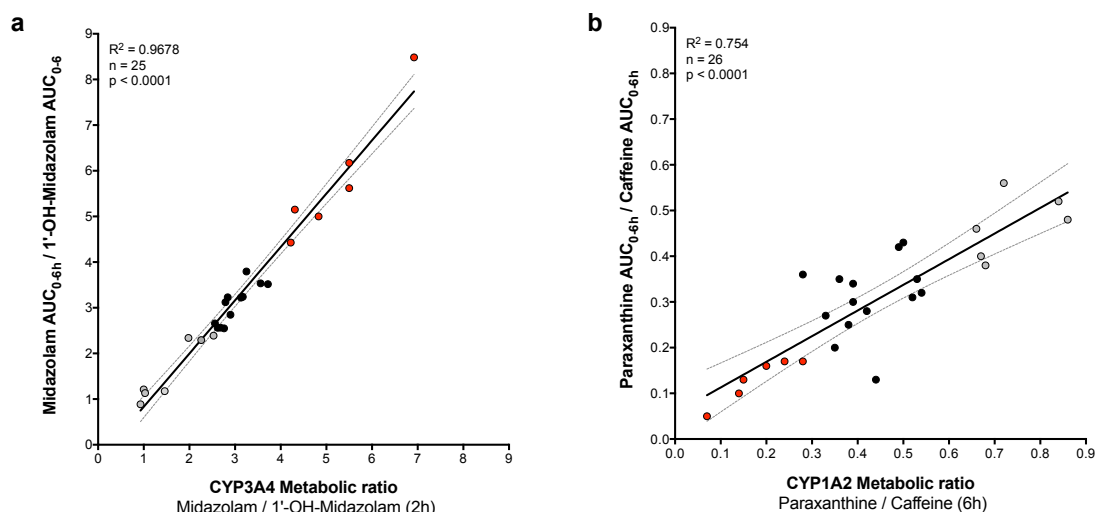


Figure 6. Correlation of MR ratio and AUC_{0-6h} ratio of (a) midazolam, and (b) caffeine. Red dots signify slow metabolisers; black dots signify intermediate metabolisers; grey dots signify fast metabolisers.

The MR of paraxanthine to caffeine at 6h and following a 36h caffeine abstinence, correlated well with the partial AUC_{0-6h} ratio (Figure 6b), while merely using the single time-point concentration of caffeine (6h) and caffeine AUC_{0-6h} also led to a statistically significant correlation (Figure 7b).

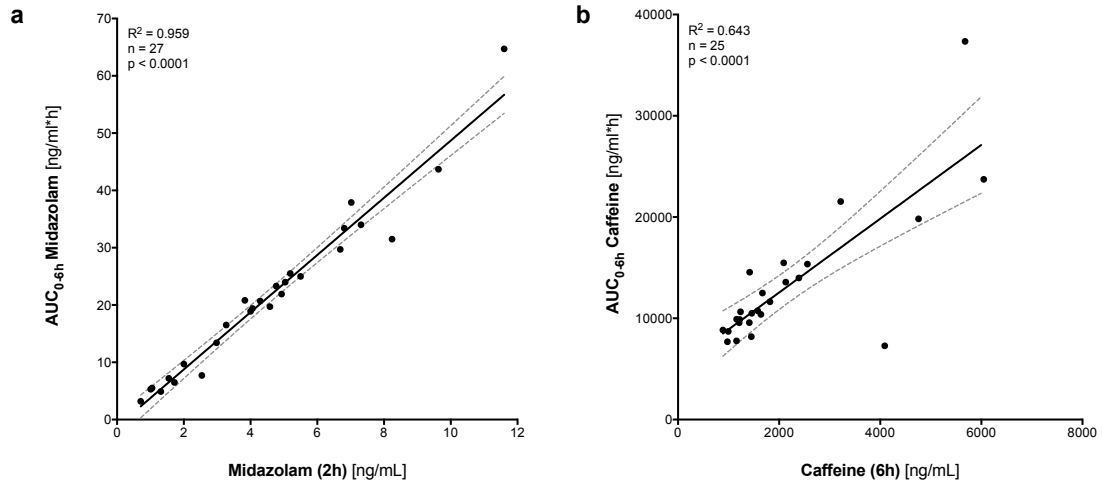


Figure 7. Correlations between AUC_{0-6h} and single time-point measurements for **(a)** midazolam- concentration 2h post-dose, and **(b)** caffeine - concentration 6h post-dose.

The plasma paraxanthine / caffeine ratio showed a 13-fold variation in the study population with a median of 0.41 (range 0.1 to 0.9). The six patients with an MR below 0.3 (25th percentile) were classed as slow metabolisers of CYP1A2, while the six patients with a paraxanthine to caffeine ratio above 0.6 (75th percentile) were assigned to having a fast CYP1A2 phenotype.

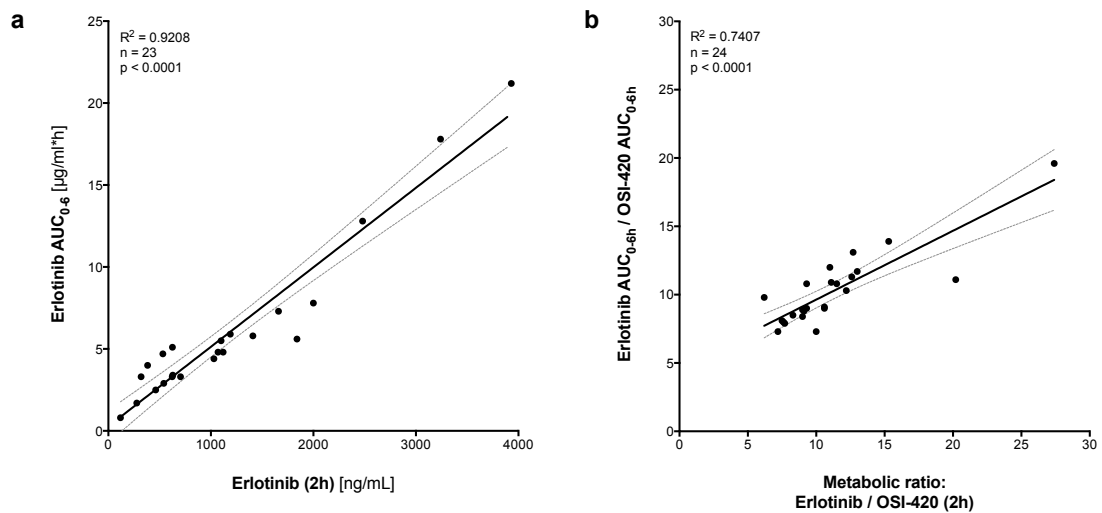


Figure 8. Correlations between **(a)** erlotinib - concentration 2h post-dose and erlotinib AUC_{0-6h} , and **(b)** erlotinib MR and erlotinib partial AUC_{0-6h} ratio.

The single time-point concentration of erlotinib (2h) was strongly correlated with erlotinib partial AUC_{0-6h} (Figure 8a) while using the MR of erlotinib at 2h of erlotinib and erlotinib partial AUC_{0-6h} ratio also led to a statistically significant correlation (Figure 8b).

3.3. Association between CYP3A4 / CYP1A2 phenotype and erlotinib pharmacokinetics

No correlation could be observed between CYP3A4 metabolic ratio (i.e. midazolam to 1'-hydroxymidazolam concentration after 2h), AUC ratio, or midazolam partial AUC_{0-6h} and erlotinib exposure described through erlotinib partial AUC_{0-6h}, erlotinib concentration after 2h (C_{2h}), C_{max}, steady-state concentration after 2 weeks (C_{ss,2w}) (Figure 9a-e). Also, there was no detectable correlation between CYP1A2 metabolic ratio and erlotinib exposure (Figure 9f).

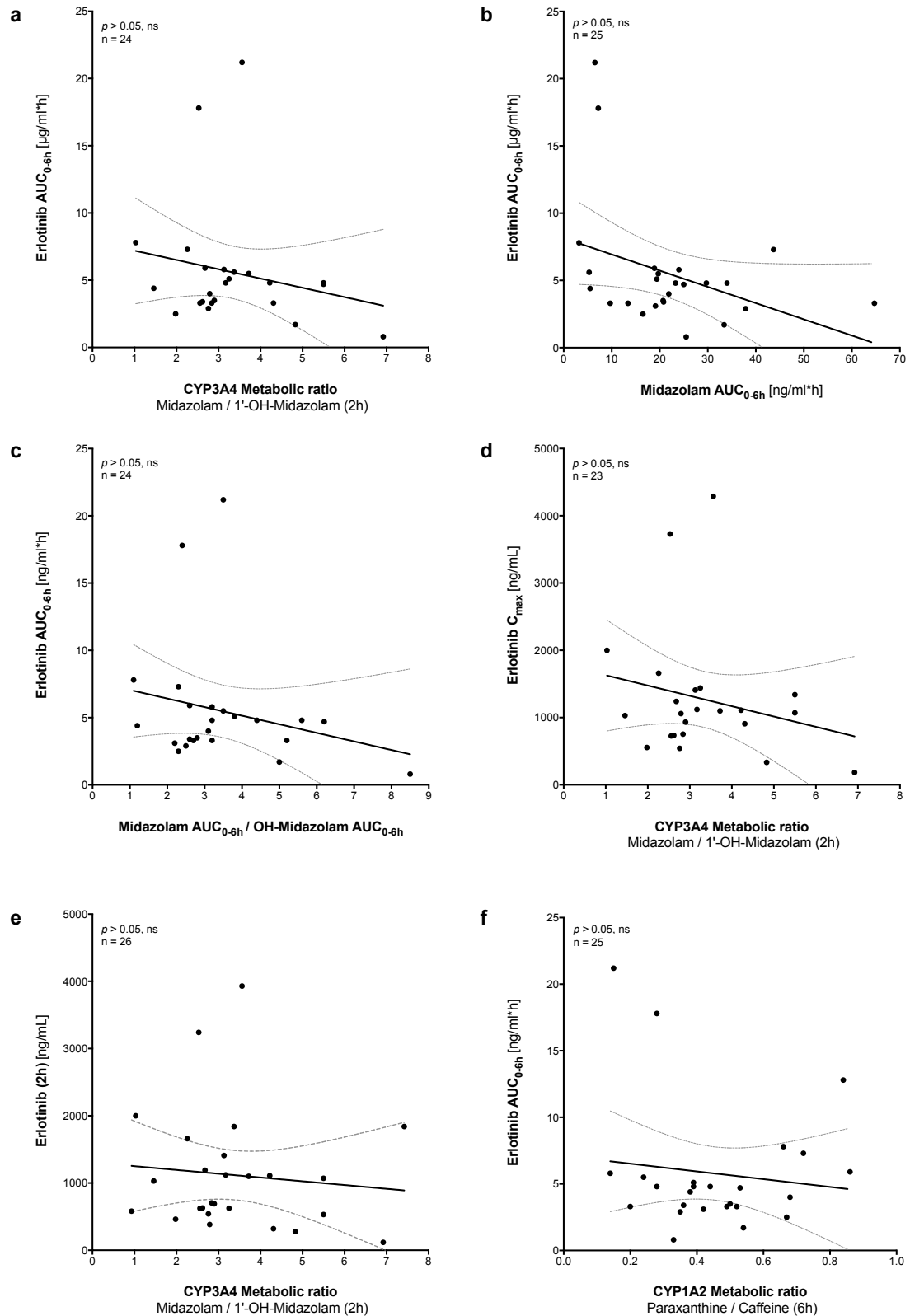


Figure 9. Correlations between **(a)** midazolam MR and erlotinib partial $AUC_{(0-6h)}$, **(b)** midazolam $AUC_{(0-6h)}$ and erlotinib partial $AUC_{(0-6h)}$, **(c)** midazolam $AUC_{(0-6h)}$ ratio and erlotinib partial $AUC_{(0-6h)}$, **(d)** midazolam MR and erlotinib C_{max} , **(e)** midazolam MR and erlotinib concentrations 2h post-dose on day 1, and **(f)** caffeine MR and erlotinib partial $AUC_{(0-6h)}$.

A borderline significant correlation between the metabolic ratio of midazolam and erlotinib was observed (Figure 10a). This result was also shown between the partial AUC_(0-6h) ratio of midazolam/1'-OH-midazolam and partial AUC_(0-6h) ratio of erlotinib/osi-420 (Figure 10b).

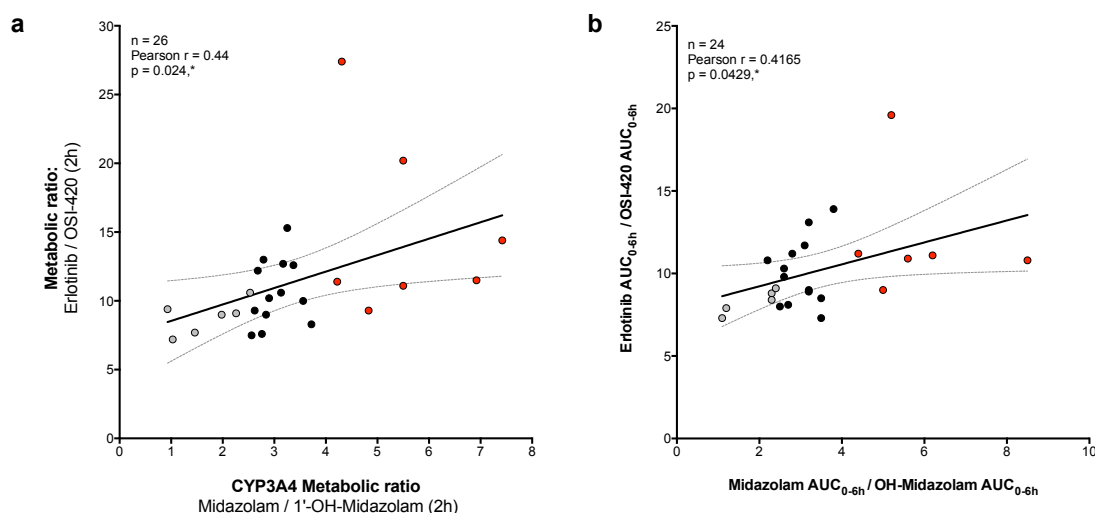


Figure 10. Correlations between MR and AUC_(0-6h) ratios for **a.** midazolam MR and erlotinib MR; and **b.** midazolam AUC ratio_(0-6h) and erlotinib AUC_(0-6h) ratio.

However, after 2 weeks of sustained antineoplastic treatment, the erlotinib/osi-420 metabolic ratio decreased drastically (Figure 11), and the correlation between the MRs of midazolam and erlotinib could not be replicated (Figure 12).

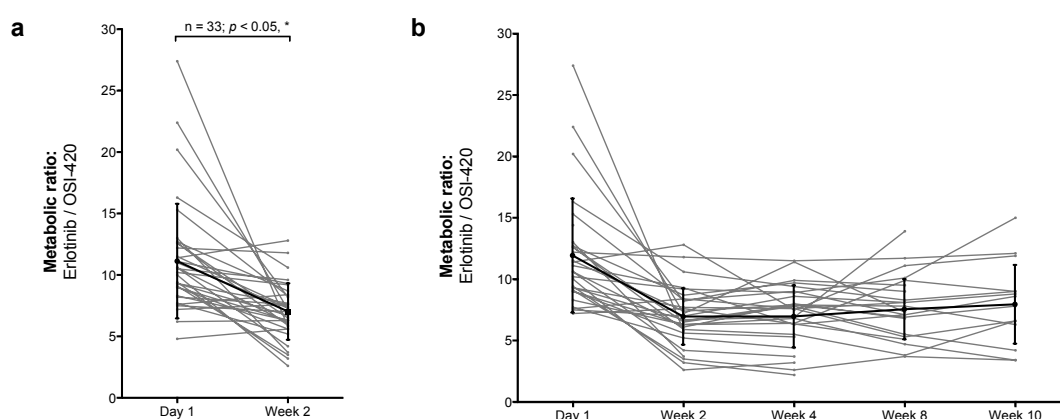


Figure 11. Changes in the MR of erlotinib **(a)** between Day 1 and Week 2, and **(b)** between Day 1 and Week 2, 4, 8, and 10. Results are shown as individual data (grey lines) with mean \pm SD (black line). The p -value is from a paired t -test.

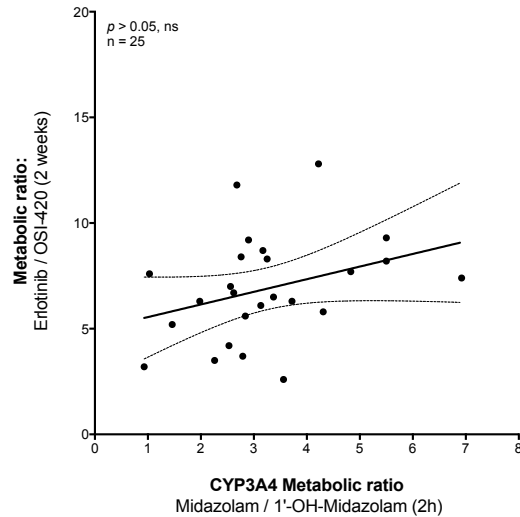


Figure 12. Correlations between (a) midazolam MR and erlotinib MR (after 2 weeks), and (b) midazolam MR and erlotinib $C_{ss,dose}$.

No correlations between erlotinib MR and CYP1A2 phenotype could be observed on day one or after sustained antineoplastic treatment (data not shown).

Although the association between CYP1A2 MR and smoking status bordered on a significant value ($p = 0.062$, Figure 13f), no statistically significant correlation between other evaluated PK parameters or CYP3A4 MR and smoking status could be observed (Figure 13a-e).

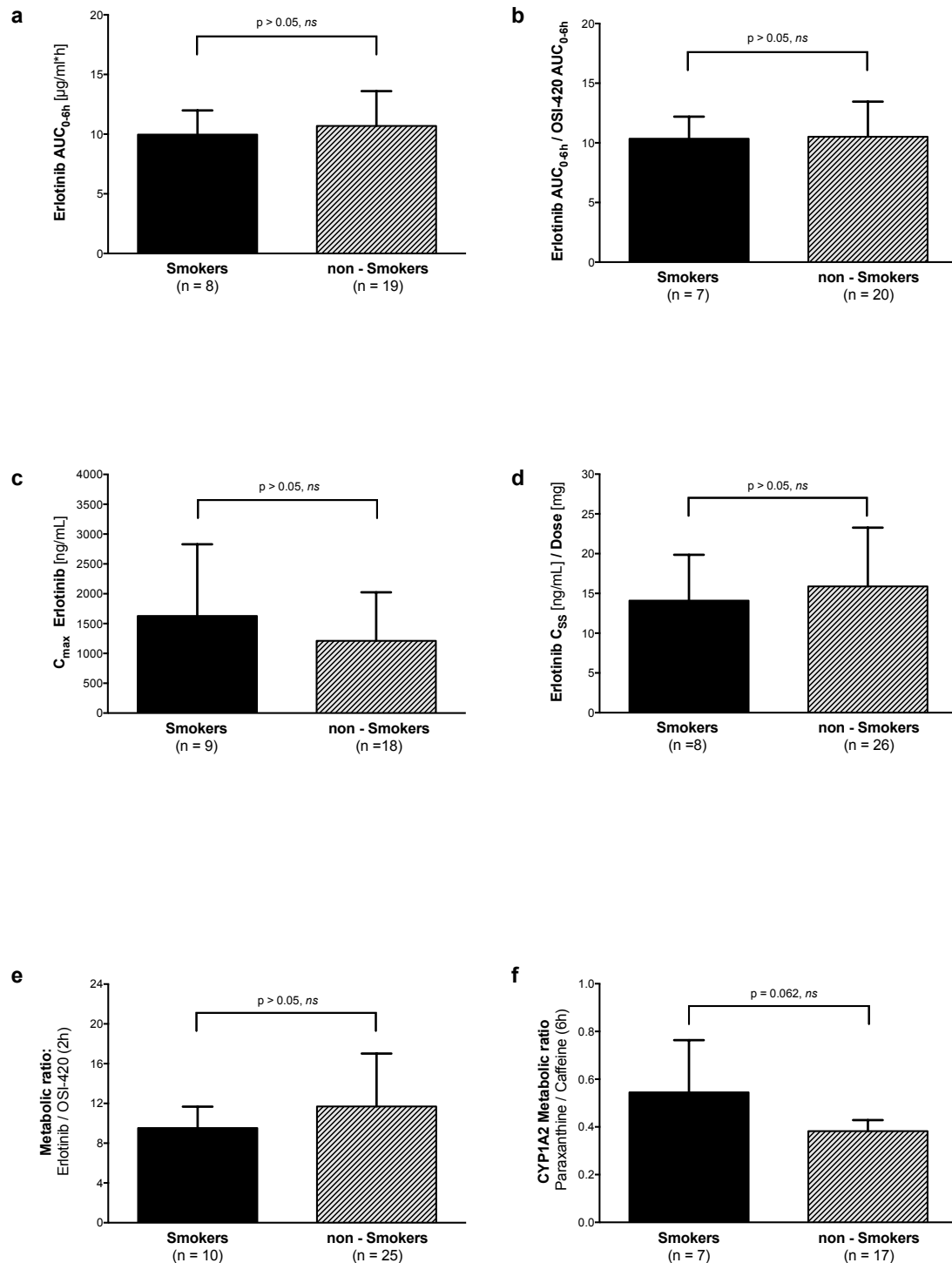


Figure 13. Evaluation of the influence of smoking on (a) erlotinib partial $AUC_{(0-6h)x}$, (b) erlotinib partial $AUC_{(0-6h)}$ ratio, (c) erlotinib C_{max} , (d) erlotinib dose corrected $C_{ss,dose}$, (e) erlotinib MR, and (f) caffeine MR. Values are mean \pm SD. The p -values are from unpaired t -tests.

3.4. Exposure toxicity relationships

The MR of midazolam at 2h shows patients in the 25th percentile (extensive CYP3A4 metabolisers) and interquartile range to have a lower occurrence of skin rash than

the population in the 75th percentile (slow CYP3A4 metabolisers). A similar trend was also observed when comparing the occurrence of skin rash in the 25th and 75th percentile range of the erlotinib/osi-420 ratio on day one (Figure 14a and b).

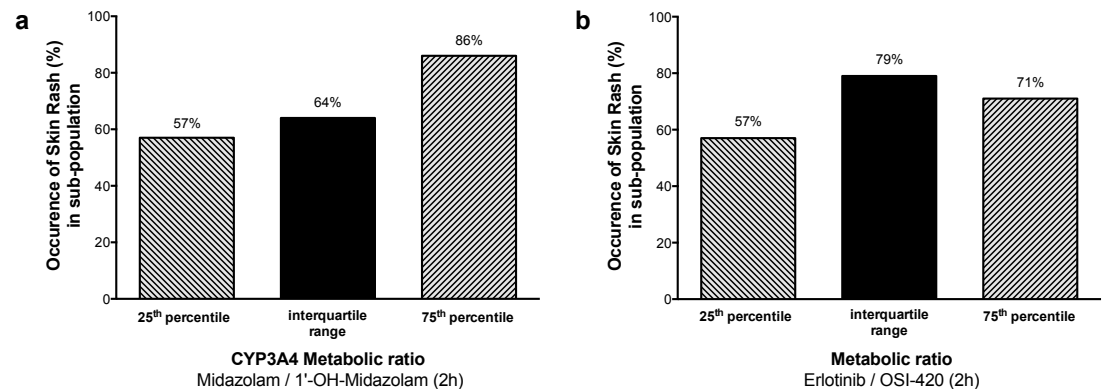


Figure 14. Occurrence of skin rash in 25th percentile (fast CYP3A4 metabolisers), interquartile, and the 75th percentile (slow CYP3A4 metabolisers) in relation to MR of (a) midazolam, and (b) erlotinib.

Therefore, patients with a high MR, being classified as slow metabolisers of CYP3A4 had a statistically significant likelihood of developing CTCAE grade 3 toxicity (Figure 15a). After 2 weeks, patients that developed grade 3 skin toxicity did not show a significant trend towards having higher dose-normalised C_{ss} than patients having developed either grade 1, 2, or no skin toxicity altogether (Figure 15b). Dose-normalised steady-state concentrations of patients that developed skin toxicity after 2 weeks (median 13.9, range 5.5 - 38.3) did not significantly differ from those without skin toxicity (median 12.5, range 5.7-43.6, $p = 0.67$; Figure 16).

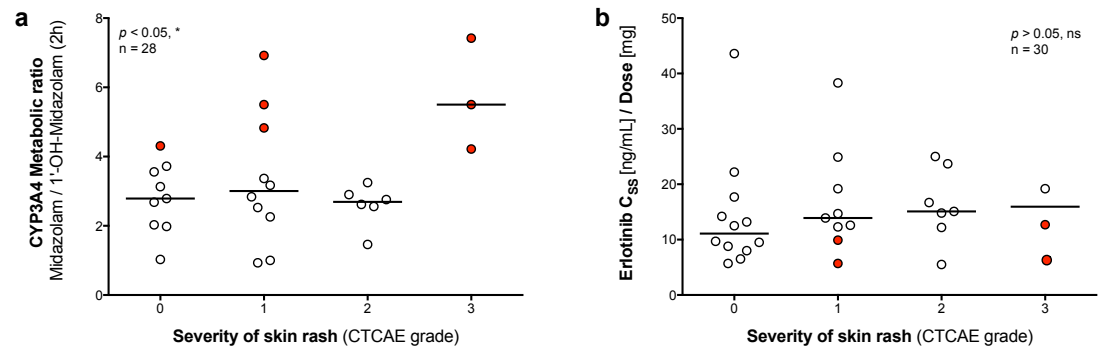


Figure 15. Severity of skin rash (CTCAE grade) in relation to (a) midazolam MR, and (b) erlotinib $C_{ss}/dose$. Red dots signify slow CYP3A4 metabolisers. The p -values are from ordinary one-way anova tests.

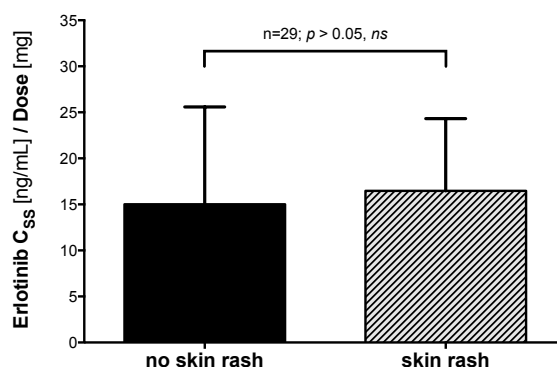


Figure 16. Occurrence of skin rash with regard to erlotinib $C_{ss,dose}$. Values are mean \pm SD. The p -value is from an unpaired t-test.

Using the MR of paraxanthine to caffeine, the 25th and 75th percentile did not lead to any suggestions of likely skin rash development (data not shown).

3.5. Plasma vs. DBS correlations

Using Bland-Altman analysis we compared the data collected in plasma, DBS, and whole blood to assess the level of agreement of concentration measurements obtained from the different sample matrices.

The Bland-Altman blots of erlotinib (Figure 16a) show the bias between plasma and DBS to be around +11%, whereas the 95% limits of agreement (\pm 2SD range) ranged between -31% and 51% (1.11 [0.69 - 1.51]). Consequently, when comparing DBS and plasma extracted samples, 35% of respective samples showed a deviation outside of the \pm 20% threshold, according to the EMEA guideline for cross-validation [33]. Therefore, on average, DBS and plasma values were within the acceptable threshold of \pm 20% in less than 67% of cases, narrowly exceeding the requisite cut-off imposed by the EMEA. No concentration dependent trend was observed between the ratios of the two biospecimens across the entire concentration range. For OSI-420 (Figure 16b), the respective bias and \pm 2SD range was (1.07 [0.53 - 1.61]). In the case of OSI-420, according to the EMEA-guideline for cross-validation, 42% of respective samples showed a deviation outside of the \pm 20% threshold. Bland-Altman blots of the comparison between plasma and whole blood, as well as DBS and whole blood, can be found in the supplementary material (Figures S1 and S2).

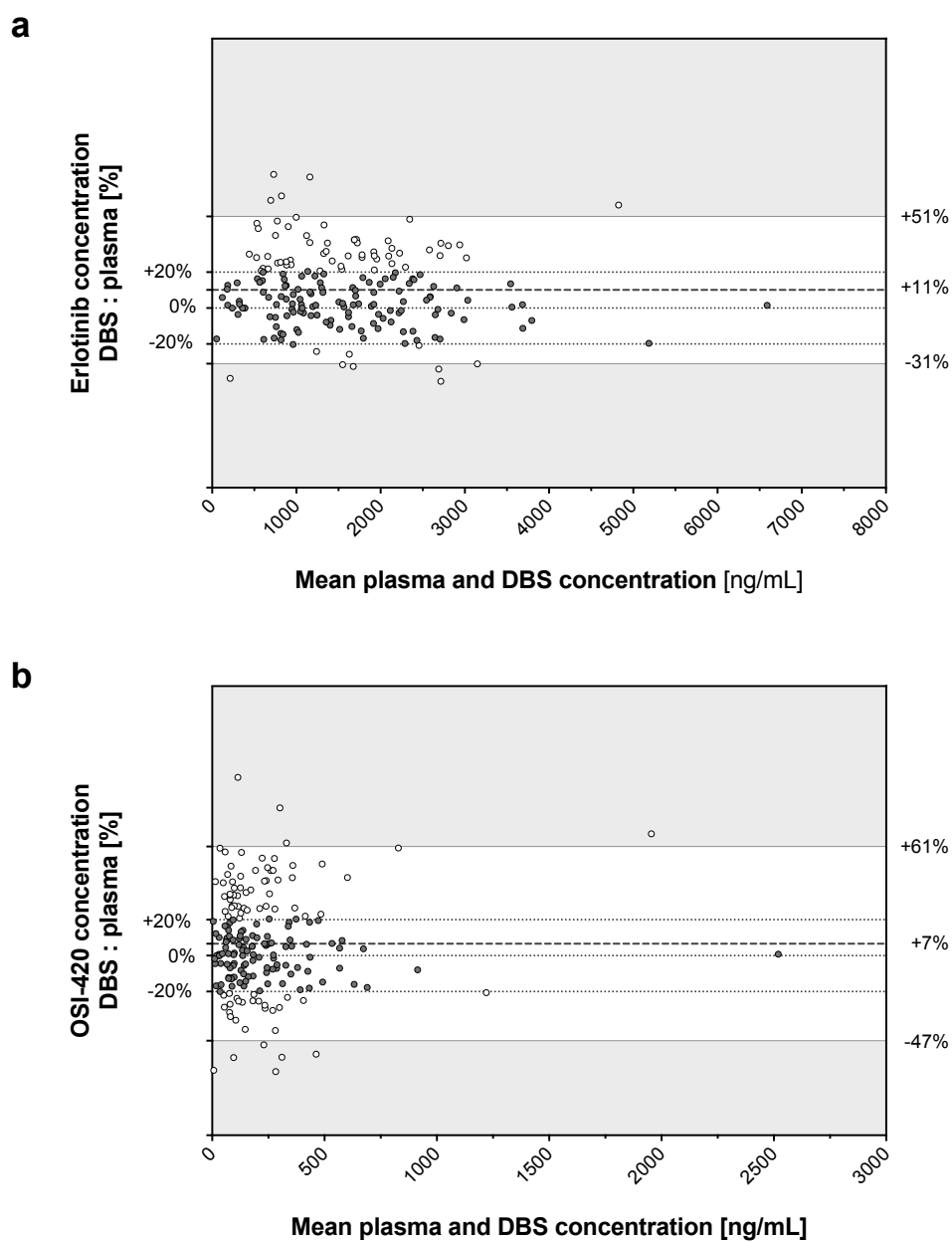


Figure 17. Bland-Altman plots of **(a)** erlotinib, and **(b)** OSI-420, were generated for DBS and plasma samples. Values were coloured grey if the concentration ratio of the two matrices was less than $\pm 20\%$; otherwise, values were coloured white. The white plot area illustrates the 95% limits of agreement. The black dashed line represents the mean concentration ratio of DBS to plasma.

4. Discussion

Although the oral formulation of TKIs is considered to be very convenient for the patient, due to the bioavailability of a number of TKIs being dependent on gastrointestinal absorption and first-pass hepatic metabolism, it does, however, introduce two processes that are prone to considerable variability among individuals [6, 22, 34-37]. In this prospective, non-randomised, pharmacological cohort study in patients treated with erlotinib (Tarceva®) for non-small cell lung cancer (NSCLC), the correlation between CYP3A4 and CYP1A2 phenotype and erlotinib exposure was investigated with the aim of determining whether the degree of variability could be attributed to the metabolic activity of CYP450 enzymes. Treatment-dependent adverse reactions in relation to the respective phenotypes were also evaluated. Furthermore, it was tested whether bioanalysis of erlotinib samples could be performed using dried blood spots. Orally administered midazolam, to assess CYP3A4 activity, has previously been used as a non-invasive phenotyping probe in relation to TKI exposure [38-41]. A significant association was found that accounted for a considerable percentage of pharmacokinetic variability. Results of the present study could not mirror aforementioned study outcomes, as it was not possible to determine a marker of total erlotinib exposure for the following reasons. Firstly, limitations due to the outpatient status of the study patients did not allow for the collection of blood samples at regular intervals up to 24h post dosing, which is necessary to get an adequate estimate of total drug exposure. Hence the elimination constant, which would have permitted the calculation of the half-life could not be estimated due to an insufficient number of samples during the elimination phase. Nevertheless, our partial AUC_{0-6h} values seem plausible when compared to the published AUC_{0-24h} values of erlotinib, while measured C_{max} was also in agreement [37]. Therefore, future studies should try to collect a sufficient number of blood samples, including during the elimination phase of the drug. Secondly, not all samples collected during the follow-up visits were taken at the end of the dosing interval (i.e. trough levels, C_{trough}), as the timing of drug intake, as well as blood collection, appear to differ considerably. Erlotinib is dosed once daily, as its half-life ($t_{1/2}$) at steady state is 18h [37], and therefore a substantial decrease or increase in erlotinib steady state concentration (C_{ss}) can be expected, if collected samples do not correspond to C_{trough} values. Although patients were instructed on how to administer the anticancer drug, a number of other potential explanations remain for the large scattering of C_{ss} values. For instance, typical adherence issues commonly found in elderly patients that include skipped dosing, dose-self adjustment due to side effects,

over-adherence, or inappropriate drug administration, could have played a role. This would corroborate reported adherence rates to therapy, with oral antineoplastic agents ranging from 20 to 100% [42]. Furthermore, it is not clear whether patients swallowed the tablet at least 1h before or 2h after intake of a meal, as food can lead to a substantial increase in erlotinib exposure [17, 36, 43]. Likewise, drugs or dietary components (e.g. grapefruit juice) that inhibit or induce CYP3A4 (and CYP1A2) that were not mentioned in the patient diary, might have been ingested. Additionally, the widespread intake (46% of study population) of proton-pump-inhibitors (PPIs) might have decreased the solubility of erlotinib, by raising the pH of the upper gastrointestinal tract, and thereby reducing absorption [35, 44]. In summary, the lack of reliable estimates for total drug exposure (AUC_{0-24h}), combined with the described uncertainty regarding the steady-state concentrations, require additional modelling efforts before correlations can be analysed. Currently, a population-PK model is being developed using nonlinear-mixed-effects modelling (NONMEM), which is expected to support meaningful analysis of the gathered data. As an example, the inclusion of exact time of dosing and sampling into the model will provide more precise estimates of steady-state concentrations. In addition, a number of other factors associated with the variability of erlotinib exposure (apart from CYP phenotype), such as polymorphisms in breast cancer resistance protein (BCRP; ABCG2) [24, 25, 27], concentrations of α -1-acid glycoprotein [45-47], and hepatic impairment [23, 24, 48], may have to be included as covariates in the model.

An association between the CYP-phenotype and treatment-related toxicity was investigated, as a large number of studies have reported correlations between erlotinib PK exposure parameters, the development of cutaneous toxicity [13, 23-25, 27, 46, 49], and the grade of skin rash [23, 24, 50, 51]. In more detail, it has been reported that patients that went on to develop cutaneous toxicity were found to have higher AUC_{0-24h} values after the intake of their first erlotinib dose, than patients without cutaneous toxicity [13]. Our data (Figure 14a) showed a similar trend, as patients with high metabolic ratios for midazolam (and of erlotinib), classified as ‘slow metabolisers’ of CYP3A4, were more likely to develop cutaneous toxicity and were also more likely to develop grade 3 skin toxicity (Figure 15a), than patients with ‘extensive’ CYP3A4 metabolism.

After having previously characterised the Basel phenotyping cocktail in healthy, male subjects [30, 52], this study represents the first time two of its substrates were used together to gather phenotyping information in elderly, patients of both sexes who were being treated for non-small cell lung cancer (NSCLC). Previous studies have comprehensively shown that instead of full pharmacokinetic profiles, the metabolic

ratios (MRs), i.e. the ratio of parent to metabolite concentrations, can be used to simplify sample collection in phenotyping considerably [31, 53, 54]. The average MRs and AUC_{0-6h} ratios of caffeine and midazolam determined in this study compared well to the corresponding concentration and AUC ratios found in healthy study subjects [52]. Using either the MR at 2h or the partial AUC_{0-6h} ratio of erlotinib, we found a significant association with the midazolam MR and the AUC_{0-6h} ratio. However, the metabolic ratio of midazolam on day one of the study no longer correlated with erlotinib MR measured after 2, 4, 8, and 10 weeks. A limitation of phenotyping is that it represents a “snapshot in time”, meaning that it only describes the activity level of a CYP at the time it is performed. External factors such as diet, co-medication, smoking habits, as well as the deterioration of general health of the patients could have altered the phenotype [34-36, 55, 56]. Similar findings have been reported for imatinib, a related oral tyrosine kinase inhibitor, in which pre-treatment clearance of midazolam correlated with imatinib clearance on day 1, but ceased to correlate after a period of continuous treatment [57]. Importantly, we demonstrated that the single point metabolic concentration ratio between erlotinib and osi-420 decreased considerably after two weeks of treatment (Figure 11), previously also reported in relation to the AUC ratio of erlotinib [27, 58]. This clear change in metabolic ratio is due to auto-induction of CYP3A4 through erlotinib itself [27, 58]. *In vitro* experiments support this assumption, as erlotinib leads to an up regulation of the pregnane X receptor (PXR), a prominent nuclear receptor known to be involved in the induction of CYP3A4 [59, 60].

Tobacco smoke is a known inducer of CYP1A2 [61], which matches the finding that half of the patients classified as CYP1A2 rapid metabolisers were current smokers, while only one out of the six patients classified as slow CYP1A2 metabolisers, was known to be a smoker. However, current smoking status was not significantly correlated with erlotinib metabolism in this study, which does not correspond with previous findings [34]. This could be due to the somewhat unclear divide in subpopulations, the uneven size of subgroups, the lack of information concerning the extent of patients' smoking behaviour, and absent adherence to not smoking.

Recent studies advocate the implementation of therapeutic drug monitoring (TDM) in patients being treated with erlotinib, as a number of arguments show its potential usefulness [27, 37]. Posthoc TDM analysis revealed that average concentrations of erlotinib were around 4 to 6 times higher than the 500ng/mL threshold estimated to provide a level of EGFR inhibition leading to a sufficient degree of antiproliferative activity [13]. Systematic overdosing of patients increases the likelihood of adverse events, as shown by skin rash development [9, 13, 16, 24, 25, 49]. Therefore, our

findings suggest TDM implementation could have been beneficial to patients forced to discontinue treatment (43% of the population), as it could have allowed erlotinib dose-reductions, thereby lessening dose-related cutaneous toxicity, and thus keeping patients on treatment.

Minimally invasive sampling procedures, such as dried blood spots (DBS) could further increase the attractiveness and ease of performing TDM for TKIs. Suitably instructed patients would even be able to collect a sample at home: without the necessity of travelling to the hospital or their GP's office, they could simply send the DBS through regular mail to the analytical laboratory. Therefore, the feasibility of implementing therapeutic drug monitoring through drug bioanalysis from patients' DBS could be evaluated. Erlotinib and OSI-420 have not previously been measured using DBS. In our study, comparisons of erlotinib concentrations in DBS and plasma showed the bias of the respective biospecimens to be marginal, whereas a considerable degree of scattering was observed (bias $\pm 2SD$: 1.11 [0.69-1.51]). Visual inspection of DBS showed that inappropriate spot formation (e.g. size, volume, shape) led to spot inhomogeneity, which can have a significant impact on accuracy and precision of measurements [62]. Hence, improving '*good blood spotting practice*' through more vigorous training of hospital staff is of great importance. Literature data also suggests that improvements to the analytical method, such as spraying the internal standard directly on to the blood spots, could lead to an increase in accuracy and precision of the DBS measurements [63-65]. The use of an automated DBS extraction system could also prove advantageous (see *chapter 8*). By incorporating these improvements, we deem it feasible for future studies to demonstrate the implementation of the bioanalysis of erlotinib in DBS, especially recently, four different TKIs, namely imatinib, dasatinib, nilotinib, and pazopanib have been shown to yield reliable and reproducible results when measured in either plasma or DBS samples [66, 67].

In conclusion, we were able to demonstrate that low dose, orally administered midazolam and caffeine could successfully be utilised in a clinical setting to perform phenotyping of CYP3A4 and CYP1A2. However, a correlation between CYP3A4/CYP1A2 phenotype and erlotinib exposure could not be determined due to a lack of reliable exposure markers (i.e. AUC_{0-24h} or C_{trough}). Interestingly, the assessment of treatment-dependent toxicity showed that patients with slow CYP3A4 metabolism were more likely to develop skin rashes than patients with higher CYP3A4 activity. Posthoc data analysis furthermore suggested that implementation of TDM guided dose adjustment could have helped to avoid toxicity-related treatment discontinuation. After having performed bioanalysis of erlotinib using the current set of DBS

samples, we are at present not able to recommend the interchangeability of DBS and conventional plasma measurement.

Before final conclusions can be drawn, a population pharmacokinetic analysis (NONMEM), which is predominantly used in studies of this manner [23, 25, 27, 39, 43], might be able to clarify some of the as yet unanswered questions.

Acknowledgements

We would like to thank Urs Duthaler, Beatrice Vetter, and Daria Winogradova for their valuable advice and technical support.

Financial support

SK was supported by a grant of the Swiss National Science Foundation (SNF 31003A_156270).

Conflict of interest

None of the authors reports any conflict of interest regarding this study.

5. References

1. EMEA. *Sutent (Sunitinib): European Public Assessment Report - Summary of opinion (post authorisation)*. 2014 26.02.2016]; EMEA/H/C/000687:[Available from: http://www.ema.europa.eu/docs/en_GB/document_library/EPAR_-_Summary_for_the_public/human/000687/WC500057689.pdf.
2. EMEA. *Tarceva (Erlotinib): European Public Assessment Report - Summary of opinion (post authorisation)*. 2015 17.12.2015 26.02.2016]; Available from: http://www.ema.europa.eu/docs/en_GB/document_library/Summary_of_opinion/human/000618/WC500199001.pdf.
3. Moyer, J.D., et al., *Induction of apoptosis and cell cycle arrest by CP-358,774, an inhibitor of epidermal growth factor receptor tyrosine kinase*. Cancer Res, 1997. **57**(21): p. 4838-48.
4. Arora, A. and E.M. Scholar, *Role of tyrosine kinase inhibitors in cancer therapy*. J Pharmacol Exp Ther, 2005. **315**(3): p. 971-9.
5. Krause, D.S. and R.A. Van Etten, *Tyrosine kinases as targets for cancer therapy*. N Engl J Med, 2005. **353**(2): p. 172-87.
6. Harari, P.M., G.W. Allen, and J.A. Bonner, *Biology of interactions: antiepidermal growth factor receptor agents*. J Clin Oncol, 2007. **25**(26): p. 4057-65.
7. Adams, V.R. and M. Leggas, *Sunitinib malate for the treatment of metastatic renal cell carcinoma and gastrointestinal stromal tumors*. Clin Ther, 2007. **29**(7): p. 1338-53.
8. Pfizer. *Pfizer Fact Sheet*. 2012 26.02.2016]; Available from: http://www.pfizer.com/files/news/asco/sutent_fact_sheet.pdf.
9. Josephs, D.H., et al., *Clinical pharmacokinetics of tyrosine kinase inhibitors: implications for therapeutic drug monitoring*. Ther Drug Monit, 2013. **35**(5): p. 562-87.
10. Aggarwal, S., *Targeted cancer therapies*. Nat Rev Drug Discov, 2010. **9**(6): p. 427-428.
11. The National Cancer Institute. *Targeted Cancer Therapies Fact Sheet*. 2014 25.04.2014 03.09.2016]; Available from: <http://www.cancer.gov/about-cancer/treatment/types/targeted-therapies/targeted-therapies-fact-sheet>.
12. Yim, K.L. and D. Cunningham, *Targeted drug therapies and cancer*. Recent Results Cancer Res, 2011. **185**: p. 159-71.
13. Hidalgo, M., et al., *Phase I and pharmacologic study of OSI-774, an epidermal growth factor receptor tyrosine kinase inhibitor, in patients with advanced solid malignancies*. J Clin Oncol, 2001. **19**(13): p. 3267-79.

14. Hahn, V.S., D.J. Lenihan, and B. Ky, *Cancer therapy-induced cardiotoxicity: basic mechanisms and potential cardioprotective therapies*. J Am Heart Assoc, 2014. **3**(2): p. e000665.
15. Gupta, R. and M.L. Maitland, *Sunitinib, hypertension, and heart failure: a model for kinase inhibitor-mediated cardiotoxicity*. Curr Hypertens Rep, 2011. **13**(6): p. 430-5.
16. ter Heine, R., et al., *Fatal interstitial lung disease associated with high erlotinib and metabolite levels. A case report and a review of the literature*. Lung Cancer, 2012. **75**(3): p. 391-7.
17. Ling, J., et al., *Metabolism and excretion of erlotinib, a small molecule inhibitor of epidermal growth factor receptor tyrosine kinase, in healthy male volunteers*. Drug Metab Dispos, 2006. **34**(3): p. 420-6.
18. Li, J., et al., *Association of variant ABCG2 and the pharmacokinetics of epidermal growth factor receptor tyrosine kinase inhibitors in cancer patients*. Cancer Biol Ther, 2007. **6**(3): p. 432-8.
19. Shi, Z., et al., *Erlotinib (Tarceva, OSI-774) antagonizes ATP-binding cassette subfamily B member 1 and ATP-binding cassette subfamily G member 2-mediated drug resistance*. Cancer Res, 2007. **67**(22): p. 11012-20.
20. Marchetti, S., et al., *Effect of the ATP-binding cassette drug transporters ABCB1, ABCG2, and ABCC2 on erlotinib hydrochloride (Tarceva) disposition in in vitro and in vivo pharmacokinetic studies employing Bcrp1-/-/Mdr1a/1b-/- (triple-knockout) and wild-type mice*. Mol Cancer Ther, 2008. **7**(8): p. 2280-7.
21. van Erp, N.P., H. Gelderblom, and H.J. Guchelaar, *Clinical pharmacokinetics of tyrosine kinase inhibitors*. Cancer Treat Rev, 2009. **35**(8): p. 692-706.
22. Klumpen, H.J., et al., *Moving towards dose individualization of tyrosine kinase inhibitors*. Cancer Treat Rev, 2011. **37**(4): p. 251-60.
23. Lu, J.F., et al., *Clinical pharmacokinetics of erlotinib in patients with solid tumors and exposure-safety relationship in patients with non-small cell lung cancer*. Clin Pharmacol Ther, 2006. **80**(2): p. 136-45.
24. Rudin, C.M., et al., *Pharmacogenomic and pharmacokinetic determinants of erlotinib toxicity*. J Clin Oncol, 2008. **26**(7): p. 1119-27.
25. Thomas, F., et al., *Population pharmacokinetics of erlotinib and its pharmacokinetic/pharmacodynamic relationships in head and neck squamous cell carcinoma*. Eur J Cancer, 2009. **45**(13): p. 2316-23.
26. Lind, J.S., et al., *A multicenter phase II study of erlotinib and sorafenib in chemotherapy-naïve patients with advanced non-small cell lung cancer*. Clin Cancer Res, 2010. **16**(11): p. 3078-87.
27. Fukudo, M., et al., *Population pharmacokinetics/pharmacodynamics of erlotinib and pharmacogenomic analysis of plasma and cerebrospinal fluid drug concentrations in Japanese patients with non-small cell lung cancer*. Clin Pharmacokinet, 2013. **52**(7): p. 593-609.

28. Bardin, C., et al., *Therapeutic drug monitoring in cancer--are we missing a trick?* Eur J Cancer, 2014. **50**(12): p. 2005-9.
29. de Graan, A.J., et al., *Dextromethorphan as a phenotyping test to predict endoxifen exposure in patients on tamoxifen treatment.* J Clin Oncol, 2011. **29**(24): p. 3240-6.
30. Donzelli, M., et al., *The basal cocktail for simultaneous phenotyping of human cytochrome P450 isoforms in plasma, saliva and dried blood spots.* Clin Pharmacokinet, 2014. **53**(3): p. 271-82.
31. Katzenmaier, S., C. Markert, and G. Mikus, *Proposal of a new limited sampling strategy to predict CYP3A activity using a partial AUC of midazolam.* Eur J Clin Pharmacol, 2010. **66**(11): p. 1137-41.
32. Zhang, Y., et al., *PKSolver: An add-in program for pharmacokinetic and pharmacodynamic data analysis in Microsoft Excel.* Comput Methods Programs Biomed, 2010. **99**(3): p. 306-14.
33. EMEA. *Guideline on bioanalytical method validation.* 2011 01.03.2016]; Available from: http://www.ema.europa.eu/docs/en_GB/document_library/Scientific_guideline/2011/08/WC500109686.pdf.
34. Hamilton, M., et al., *Effects of smoking on the pharmacokinetics of erlotinib.* Clin Cancer Res, 2006. **12**(7 Pt 1): p. 2166-71.
35. Kletzl, H., et al., *Effect of gastric pH on erlotinib pharmacokinetics in healthy individuals: omeprazole and ranitidine.* Anticancer Drugs, 2015. **26**(5): p. 565-72.
36. Ling, J., et al., *Effect of food on the pharmacokinetics of erlotinib, an orally active epidermal growth factor receptor tyrosine-kinase inhibitor, in healthy individuals.* Anticancer Drugs, 2008. **19**(2): p. 209-16.
37. Petit-Jean, E., et al., *Erlotinib: another candidate for the therapeutic drug monitoring of targeted therapy of cancer? A pharmacokinetic and pharmacodynamic systematic review of literature.* Ther Drug Monit, 2015. **37**(1): p. 2-21.
38. Wong, M., et al., *CYP3A5 genotype and midazolam clearance in Australian patients receiving chemotherapy.* Clin Pharmacol Ther, 2004. **75**(6): p. 529-38.
39. Li, J., et al., *CYP3A phenotyping approach to predict systemic exposure to EGFR tyrosine kinase inhibitors.* J Natl Cancer Inst, 2006. **98**(23): p. 1714-23.
40. Swaisland, H.C., et al., *Exploring the relationship between expression of cytochrome P450 enzymes and gefitinib pharmacokinetics.* Clin Pharmacokinet, 2006. **45**(6): p. 633-44.
41. de Wit, D., et al., *Midazolam as a phenotyping probe to predict sunitinib exposure in patients with cancer.* Cancer Chemother Pharmacol, 2014. **73**(1): p. 87-96.

42. Partridge, A.H., et al., *Adherence to therapy with oral antineoplastic agents*. J Natl Cancer Inst, 2002. **94**(9): p. 652-61.
43. White-Koning, M., et al., *Population analysis of erlotinib in adults and children reveals pharmacokinetic characteristics as the main factor explaining tolerance particularities in children*. Clin Cancer Res, 2011. **17**(14): p. 4862-71.
44. Compendium. *Tarceva® Fachinformation des Arzneimittel-Kompendium der Schweiz*. 2014 25.04.2014 26.02.2016]; Available from: <https://compendium.ch/mpro/mnr/15104/html/de>.
45. Tan, A.R., et al., *Evaluation of biologic end points and pharmacokinetics in patients with metastatic breast cancer after treatment with erlotinib, an epidermal growth factor receptor tyrosine kinase inhibitor*. J Clin Oncol, 2004. **22**(15): p. 3080-90.
46. Twelves, C., et al., *Erlotinib in combination with capecitabine and docetaxel in patients with metastatic breast cancer: a dose-escalation study*. Eur J Cancer, 2008. **44**(3): p. 419-26.
47. Raizer, J.J., et al., *A phase II trial of erlotinib in patients with recurrent malignant gliomas and nonprogressive glioblastoma multiforme postradiation therapy*. Neuro Oncol, 2010. **12**(1): p. 95-103.
48. Miller, A.A., et al., *Phase I and pharmacokinetic study of erlotinib for solid tumors in patients with hepatic or renal dysfunction: CALGB 60101*. J Clin Oncol, 2007. **25**(21): p. 3055-60.
49. Government, A., *Australian Public Assessment Report for Erlotinib*, D.o.H.a.A.T.G. Administration, Editor. 2010, Australian Government.
50. Yamamoto, N., et al., *Phase I dose-finding and pharmacokinetic study of the oral epidermal growth factor receptor tyrosine kinase inhibitor Ro50-8231 (erlotinib) in Japanese patients with solid tumors*. Cancer Chemother Pharmacol, 2008. **61**(3): p. 489-96.
51. Mita, A.C., et al., *Erlotinib 'dosing-to-rash': a phase II inpatient dose escalation and pharmacologic study of erlotinib in previously treated advanced non-small cell lung cancer*. Br J Cancer, 2011. **105**(7): p. 938-44.
52. Derungs, A., et al., *Effects of Cytochrome P450 Inhibition and Induction on the Phenotyping Metrics of the Basel Cocktail: A Randomized Crossover Study*. Clin Pharmacokinet, 2016. **55**(1): p. 79-91.
53. Link, B., et al., *Pharmacokinetics of intravenous and oral midazolam in plasma and saliva in humans: usefulness of saliva as matrix for CYP3A phenotyping*. Br J Clin Pharmacol, 2008. **66**(4): p. 473-84.
54. Zadoyan, G., et al., *Effect of Ginkgo biloba special extract EGb 761(R) on human cytochrome P450 activity: a cocktail interaction study in healthy volunteers*. Eur J Clin Pharmacol, 2012. **68**(5): p. 553-60.

55. Rivory, L.P., K.A. Slaviero, and S.J. Clarke, *Hepatic cytochrome P450 3A drug metabolism is reduced in cancer patients who have an acute-phase response*. Br J Cancer, 2002. **87**(3): p. 277-80.
56. Slaviero, K.A., S.J. Clarke, and L.P. Rivory, *Inflammatory response: an unrecognised source of variability in the pharmacokinetics and pharmacodynamics of cancer chemotherapy*. Lancet Oncol, 2003. **4**(4): p. 224-32.
57. Judson, I., et al., *Imatinib pharmacokinetics in patients with gastrointestinal stromal tumour: a retrospective population pharmacokinetic study over time*. EORTC Soft Tissue and Bone Sarcoma Group. Cancer Chemother Pharmacol, 2005. **55**(4): p. 379-86.
58. Kraut, E.H., et al., *Phase I and pharmacokinetic study of erlotinib (OSI-774) in combination with docetaxel in squamous cell carcinoma of the head and neck (SSCHN)*. Cancer Chemother Pharmacol, 2011. **67**(3): p. 579-86.
59. Harmsen, S., et al., *Nuclear receptor mediated induction of cytochrome P450 3A4 by anticancer drugs: a key role for the pregnane X receptor*. Cancer Chemother Pharmacol, 2009. **64**(1): p. 35-43.
60. Harmsen, S., et al., *PXR-mediated P-glycoprotein induction by small molecule tyrosine kinase inhibitors*. Eur J Pharm Sci, 2013. **48**(4-5): p. 644-9.
61. Gunes, A. and M.L. Dahl, *Variation in CYP1A2 activity and its clinical implications: influence of environmental factors and genetic polymorphisms*. Pharmacogenomics, 2008. **9**(5): p. 625-37.
62. Timmerman, P., et al., *EBF recommendation on the validation of bioanalytical methods for dried blood spots*. Bioanalysis, 2011. **3**(14): p. 1567-75.
63. Jager, N.G., et al., *Procedures and practices for the validation of bioanalytical methods using dried blood spots: a review*. Bioanalysis, 2014. **6**(18): p. 2481-514.
64. van Baar, B.L., et al., *IS addition in bioanalysis of DBS: results from the EBF DBS-microsampling consortium*. Bioanalysis, 2013. **5**(17): p. 2137-45.
65. Meesters, R., et al., *Impact of internal standard addition on dried blood spot analysis in bioanalytical method development*. Bioanalysis, 2011. **3**(20): p. 2357-64.
66. Kralj, E., et al., *Simultaneous measurement of imatinib, nilotinib and dasatinib in dried blood spot by ultra high performance liquid chromatography tandem mass spectrometry*. J Chromatogr B Analyt Technol Biomed Life Sci, 2012. **903**: p. 150-6.
67. de Wit, D., et al., *Dried blood spot analysis for therapeutic drug monitoring of pazopanib*. J Clin Pharmacol, 2015. **55**(12): p. 1344-50.

Supplementary material

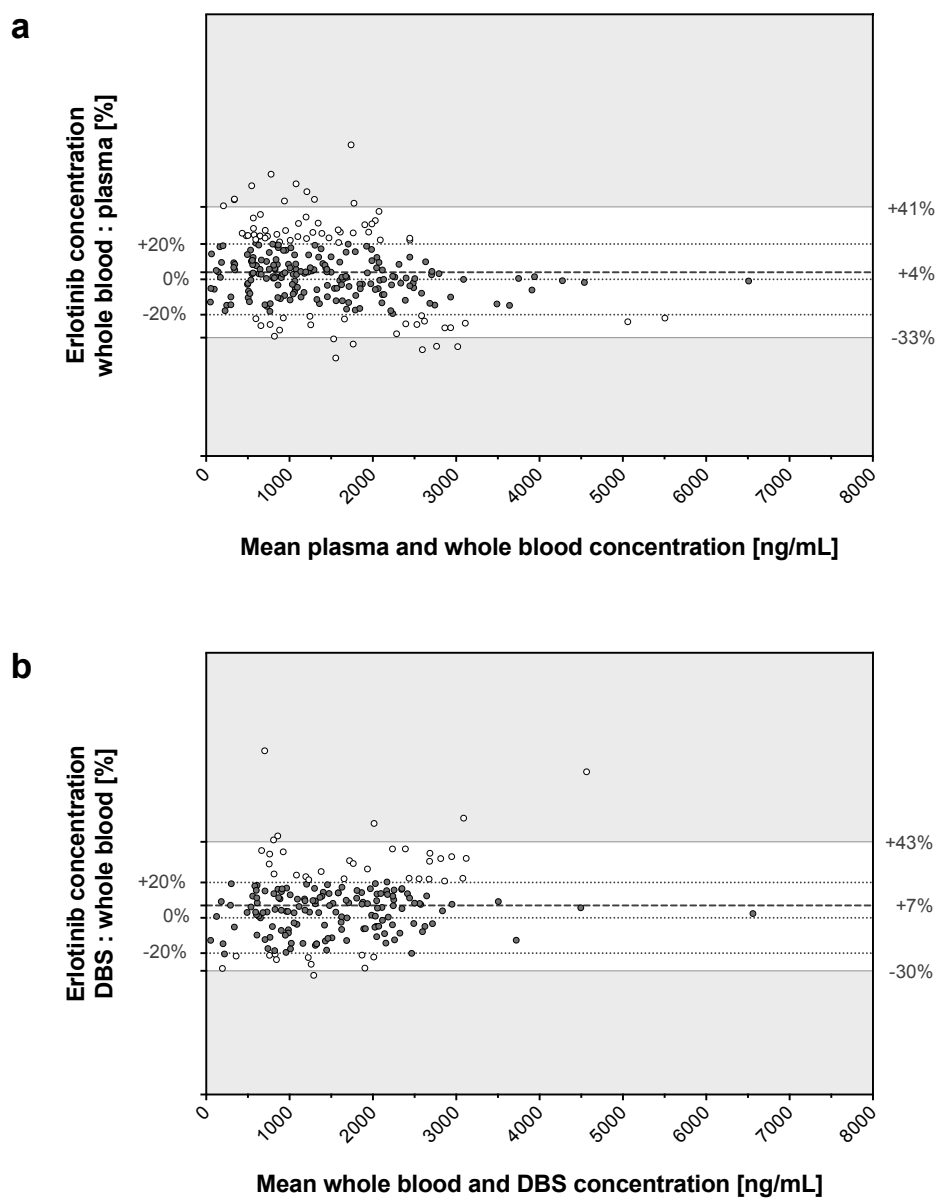


Figure S1. Bland-Altman plots generated for erlotinib concentrations in **(a)** whole blood and plasma samples, and in **(b)** DBS and whole blood samples. Values were coloured grey if the concentration ratio of the two matrices was less than $\pm 20\%$; otherwise, values were coloured white. The white plot area illustrates the 95% limits of agreement. The black dashed line represents the mean concentration ratio of DBS to plasma.

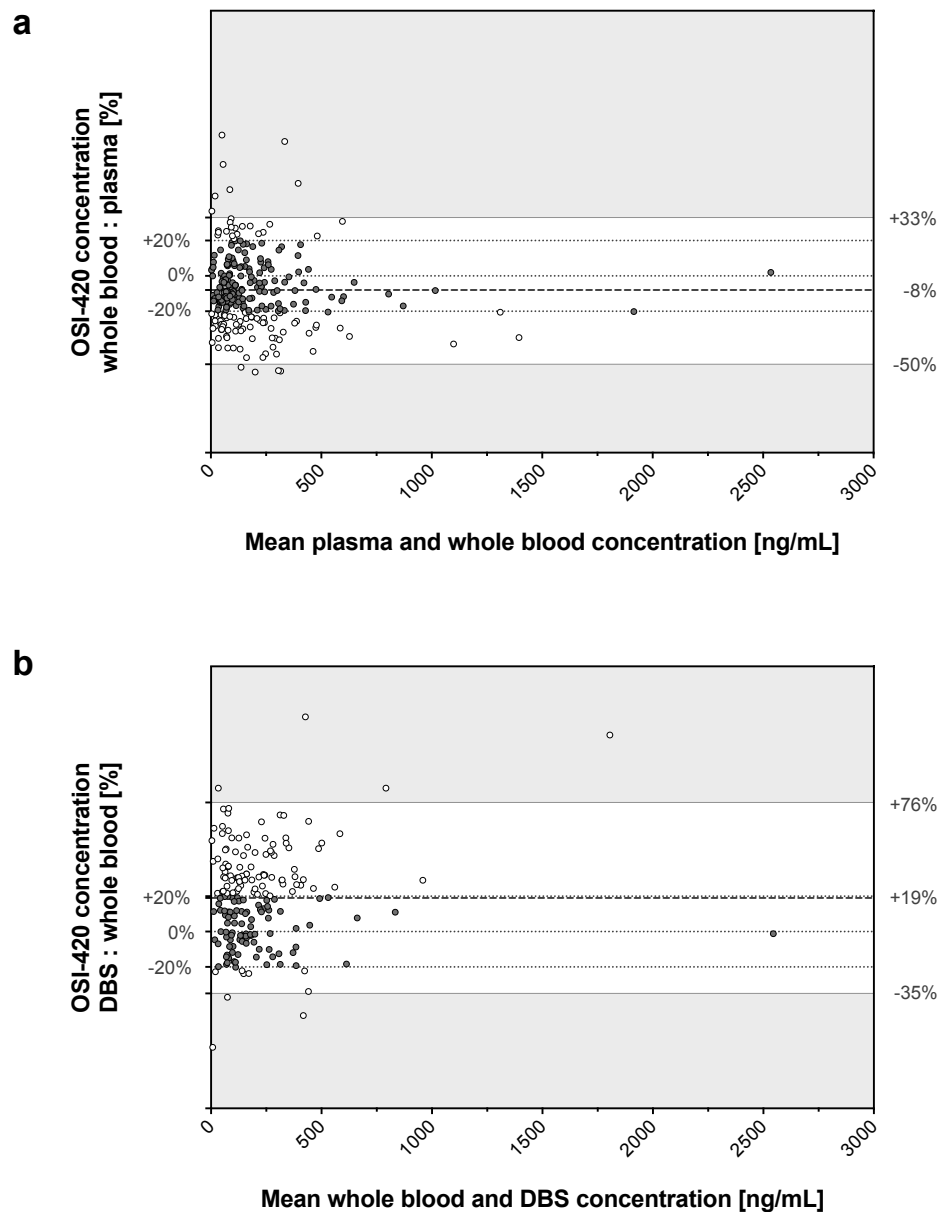


Figure S2. Bland-Altman plots generated for OSI-420 concentrations in **(a)** whole blood and plasma samples, and in **(b)** DBS and whole blood samples. Values were coloured grey if the concentration ratio of the two matrices was less than $\pm 20\%$; otherwise, values were coloured white. The white plot area illustrates the 95% limits of agreement. The black dashed line represents the mean concentration ratio of DBS to plasma.

8. Therapeutic drug monitoring of antiretroviral drugs using a fully automated dried blood spot extraction method to measure samples from a clinical study in rural Tanzania

Benjamin Berger¹, Urs Duthaler¹, Stefan Erb², Manuel Battegay², Stefan Gaugler³,
Stephan Krähenbühl^{1,4}, Manuel Haschke¹

¹Division of Clinical Pharmacology & Toxicology, University Hospital Basel and
Department of Biomedicine, University Hospital Basel, Switzerland

²Division of Infectious Diseases and Hospital Epidemiology, Departments of
Medicine and Clinical Research, University Hospital Basel, Switzerland

³ CAMAG, Muttenz, Switzerland

⁴Swiss Center for Applied Human Research (SCAHT)

Abstract

For therapeutic drug monitoring (TDM) in remote settings, obtaining dried blood spots (DBS) is particularly advantageous, as blood is withdrawn after a simple finger prick and the ensuing DBS sample is generally stable at room temperature. However, factors such as variable haematocrit and the small sample volume pose a challenge for the development of reliable and sensitive bioanalytical methods. The aim of this study was to develop and validate an automated extraction method for the analysis of nevirapine, efavirenz, and lopinavir in DBS samples, thereby circumventing drawbacks of conventional DBS methodology. To test the feasibility of using DBS within the framework of a clinical adherence assessment study in HIV patients in rural Tanzania, concentrations of antiretrovirals found in DBS samples were compared with conventional plasma samples.

From 299 patients, DBS and plasma samples for the analysis of nevirapine (n=192), efavirenz (n=482), and lopinavir (n=66) were collected. DBS samples were extracted with methanol:H₂O (70:30 v/v), using a CAMAG DBS-MS-500 autosampler, which was coupled with an LC-MS/MS system. The analytes were detected through multiple reaction monitoring with electrospray ionisation in positive (nevirapine and lopinavir) or negative (efavirenz) mode. Analytes were separated within a 3 minute run time on a pentafluorophenyl phase analytical column, using methanol and water, both of which were supplemented with 0.1% formic acid as mobile phases.

The method was linear between 10-25'000ng/ml ($R^2 > 0.99$) for all three analytes. Recoveries and matrix effects were consistent between different donors and were independent of concentration. A mean recovery of 70%, 63%, and 60% was determined for nevirapine, efavirenz, and lopinavir respectively. Higher haematocrit values reduced the extraction recovery by approximately 10-25%. This could be compensated by spraying the internal standard directly onto the DBS before analysis. Inter- and intra-assay accuracy and precision deviations were $\leq 15\%$. A correction factor was implemented for the relationship of blood spot area and haematocrit, which improved the overall reliability of the DBS analysis. Under accelerated storage conditions (4 weeks, 40°C, 75%rH), only lopinavir demonstrated a time-dependent degradation of approximately 20%. Manual and automated extractions showed good agreements with deviations of less than 9%. No bias between DBS and plasma concentrations was detected for nevirapine (bias $\pm 2SD$ range: 1.05 [0.73-1.36]). By contrast, concentrations in DBS were approximately 50% lower, compared to plasma, for efavirenz (0.59 [0.43-0.74]) and lopinavir (0.48 [0.28-0.67]). In the case of

efavirenz, the bias could be removed by correcting the DBS concentrations with patient-specific haematocrit values and plasma protein binding (0.91 [0.66-1.16]). Our study highlights that concentrations of nevirapine and efavirenz can be reliably determined by automated extraction in DBS samples, obtained in the challenging setting of rural Africa. This facilitates high throughput DBS analysis of large sample numbers and confirms that DBS are a suitable alternative to conventional plasma samples for future studies conducted in remote settings without reliable cold chains.

Keywords: *Dried blood spots, automated extraction, nevirapine, efavirenz, lopinavir, haematocrit, therapeutic drug monitoring, LC-MS/MS*

1. Introduction

The dried blood spots (DBS) technique is a microsampling tool, whereby capillary blood is spotted onto a filter paper, leading to a more or less homogeneously distributed blood spot. After complete drying, a fixed blood spot area can be punched out for drug analysis, thereby avoiding exact pipetting [1]. Contrasting against conventional plasma sampling, the DBS technique does not require a trained phlebotomist. Only a few drops of blood are withdrawn after a simple and minimally invasive finger prick: a process that could be performed by patients who have been given adequate instruction [2]. Moreover, DBS samples minimise biohazardous risk during further sample handling and are generally stable at room temperature, making the maintenance of cold chains unnecessary [3]. Hence, the collection of DBS samples is especially attractive for field studies in remote or resource-constrained settings, where uninterrupted cold chains cannot be guaranteed [4].

Worldwide, an estimated 37 million people are HIV-positive, of which the majority reside in Sub-Saharan Africa [5]. Adherence to antiretroviral therapy has been strongly correlated with viral suppression, increase in survival, and improved quality of life [6, 7]. Patients with suboptimal adherence are at risk of HIV progression and the development of drug resistance, which consequently narrows options for future treatment [6, 8, 9]. However, particularly in developing countries, adherence assessment by healthcare providers is performed infrequently [6, 8, 10]. The previously mentioned DBS qualities, therefore, make it an ideal tool for adherence assessments in such environments.

However, the development of bioanalytical DBS methods is more complex than those used in conventional liquid matrices, as variable haematocrit values not only alter the analyte recovery, but also the extent of blood diffusion within the filter paper, thereby impacting the reliability of the DBS analysis [11]. On the other hand, the small amount of blood collected on a blood collection card complicates the development of highly sensitive bioanalytical methods [11]. Finally, concentrations found in DBS must be compared to conventional plasma samples to be able to correctly interpret results from DBS measurements [12-15].

DBS and plasma samples of patients treated with combined antiretroviral therapy (cART) were collected in the framework of an adherence assessment study in Tanzania (Ifakara) [16]. Treatments with two non-nucleoside reverse transcriptase inhibitors, efavirenz and nevirapine, and a protease inhibitor, lopinavir, were monitored in this study. In contrast to previous studies, which used manual DBS extraction for the measurement and validation of the respective cART compounds

[17-21], we extracted DBS using a fully automated CAMAG DBS-MS-500 autosampler [22]. A number of different approaches enabling the automated handling of DBS have been developed, thereby facilitating the laborious manual DBS work-up [23-26]. The DBS-MS-500 autosampler exhibits a TLC based extraction head, with a circular plunger that seals a vent of 4 mm inner diameter (ID) on the blood spot. The extraction solvent passes horizontally from the inlet capillary, through the blood spot to the outlet capillary, and into a sample loop (unilateral extraction). Thus, in contrast to other online DBS extraction systems, the extraction solvent is not forced vertically through the filter paper (flow-through extraction) [27]. The autosampler is connected to the LC-MS/MS system, features 500 DBS card slots, takes an image of the blood spot before and after the extraction process, and works with a low volume (~25 µL) of extraction solvent.

The aim of the present study was to develop and validate a fully automated DBS extraction method for the analysis of nevirapine, efavirenz, and lopinavir, with sufficient robustness to handle a large number of samples from a field study in rural Tanzania (Ifakara). We demonstrate that methodological drawbacks of DBS analysis can be partially overcome with the applied automated extraction system. Feasibility of the automated procedure was demonstrated by comparing concentrations obtained after automated DBS extraction with concentrations after manual DBS extractions. Furthermore, the agreement of plasma and DBS concentrations was determined.

2. Materials and Methods

2.1. Chemicals, reagents and reference compounds

Gradient grade water and methanol for liquid chromatography as well as formic acid (98-100%) were purchased from Merck (Darmstadt, Germany). Dimethyl sulfoxide (DMSO) was obtained from Sigma-Aldrich (St. Louis, USA). The reference compounds, nevirapine, efavirenz, and lopinavir and its deuterated internal standards (IS) – nevirapine-d3, efavirenz-d5, and lopinavir-d8 – were products of Toronto Research Chemicals (Toronto, Canada). Dried blood spot cards (grade 226 filter paper) were kindly provided by CAMAG (Muttens, Switzerland). Fresh whole blood was obtained from the blood donation centre (Basel, Switzerland).

2.2. LC–MS/MS Instrumentation and settings

Chromatography was performed on a modular HPLC system from Shimadzu (Kyoto, Japan); it contained a system controller (CBM-20A), four pumps (2x LC-20AD and 2x LC-20AD XR), a degasser (DGU-20A5), and a column oven (CTO-20A). A CTC HTS PAL autosampler (CTC analytics, Zwingen, Switzerland) was used to perform manual extraction of DBS samples. Automated extractions were carried out with a DBS-MS 500 autosampler (CAMAG, Muttenz, Switzerland). Analytes were separated on a Kinetex 2.6 μ F5 100 Å (50x2.1 mm) analytical column (Phenomenex, Torrance, USA). A filter frit (SS 0.5 μ m 0.62x0.65, Ercatech AG, Bern, Switzerland) was connected upstream to the analytical column. Mobile phase A consisted of water plus 0.1% formic acid, while methanol supplemented with 0.1% formic acid was used as mobile phase B. The following stepwise gradient was applied: 5% (0-0.25 min), 5%-60% (0.25-0.4 min), 60%-80% (0.4-2.0 min), 80%-95% (2.0-2.2 min), 95% (2.2-3.0 min), 5% (3.0-3.3 min). The flow rate was set at 0.5 mL/min at 45°C. HPLC liquid stream was connected to an API 4000 Q-trap tandem mass spectrometer (ABSciex, MA, USA) between minute 0.6 and 2.5 of each run to reduce system contamination. The analytical run was divided into three multiple reaction monitoring (MRM) periods, whereas electrospray ionisation was switched from positive to negative ionisation between minute 1.3 and 1.7 (period 2) of each run. The following mass transitions and compound specific settings were used: 267→226 m/z for nevirapine (declustering potential [DP]: 76 V, collision energy [CE]: 20 V, entrance potential [EP]: 10 V, collision cell exit potential [CXP]: 16 V), 270→229 m/z for nevirapine-d3 (DP: 121 V, CE: 37 V, EP: 10 V, CXP: 16 V), 314→244 m/z for efavirenz (DP: -95 V, CE: -26 V, EP: -10 V, CXP: -13 V), 319→248 m/z for efavirenz-d5 (DP: -75 V, CE: -28 V, EP: -1 V, CXP: -15 V), 629→155 m/z for lopinavir (DP: 111 V, CE: 35 V, EP: 10 V, CXP: 10 V), and 637→163 m/z for lopinavir-d8 (DP: 66V, CE: 75 V, EP: 10 V, CXP: 10 V). The general settings of the mass spectrometer were as follows: Ion source gas-1 60 L/min (N₂), Ion source gas-2 50 L/min (N₂), curtain gas 10 L/min, collision gas 4 L/min, ion spray voltage 5500 V (positive mode) and -4200 V (negative mode), and a source temperature of 350°C. Analyst software 1.6.2 (AB Sciex, MA, USA) was used to operate the LC-MS/MS system.

2.3. Preparation of standards and extraction solvents

Nevirapine, efavirenz, and lopinavir stock solutions were prepared in DMSO (10 mg/mL) and stored at -20°C. Stock solutions were pooled and serially diluted with

DMSO to cover a range from 2500 to 1 µg/mL. The dilution series for calibrators and QC samples originated from different weightings. Internal standard (IS) stock solutions were likewise prepared in DMSO at a final concentration of 1 mg/mL. The extraction solvent was a mixture of methanol and water (70:30 v/v). In the case of the automated extractions, the IS was dissolved in methanol at a concentration of 1 µg/mL for nevirapine-d3 and at 2 µg/mL for efavirenz-d5 and lopinavir-d8.

2.4. Preparation of calibration and quality control samples

Fresh collected human blood was obtained from the local blood donation centre (Basel, Switzerland). EDTA was used as an anticoagulation agent (vacutainer tubes, BD, Allschwil, Switzerland). Calibrators and Quality control (QC) samples were prepared by spiking blank blood with the analyte dilution series in a ratio of 1:100 (v/v). Calibration samples encompassed a range from 10-25'000 ng/mL. QC samples were prepared at the lower limit of quantification (LLOQ, 10 ng/mL), as well as at low (50 ng/mL), medium (500 ng/mL), and high (5000 ng/mL) concentration levels. In the case of manual extractions, the LLOQ was set to 50 ng/mL. Spiked blood samples were gently mixed and agitated on a roll-agitator (RM 5, CAT, Staufen, Switzerland), after which 15 µL aliquots were spotted onto CAMAG DBS cards (CAMAG, Muttenz, Switzerland). DBS cards were dried at room temperature for at least 2h and were subsequently stored at -20°C in sealed plastic bags containing desiccants. Each calibration set consisted of one blank sample (DBS sample processed without IS), one zero sample (DBS sample processed with IS), and eleven calibrators (nine calibrators in the case of manual extractions). Calibration lines were established by linear regression of the nominal analyte concentration against the analyte:IS peak area ratio using a weighting factor of $1/x^2$.

2.5. Dried blood spots sample procession

2.5.1. Automated extraction

The DBS cards were photographed with the built-in camera of the CAMAG-DBS 500 autosampler before and after each run to check for the presence of a blood spot and to adjust the extraction head to the centre of each spot. 10 µL of internal standard was sprayed in a homogenous layer onto each spot. After a 20 second drying time, the samples were extracted with a volume of 25 µL and a 40 µL/min flow rate. As a

20 µL loop was installed, the first 5 µL of the extract were discarded. To complete the automated DBS extraction cycle, the system was first rinsed for 20 seconds with a methanol:acetonitrile:isopropanol:water (1:1:1:1 v/v) mixture, after which it was cleaned for a further 20 seconds with water containing 0.1% formic acid.

2.5.2. Manual extraction

10 µL of internal standard was sprayed using the internal spraying device of the CAMAG autosampler onto each spot. The card was then removed, left to dry at room temperature, and then a disc, 3 mm in diameter, was manually punched out, using a manual hole puncher (Whatman, Sanford, ME, USA), from the centre of each spot and transferred to a 0.75 mL autosampler matrix tube (Thermo Scientific, Reinach, Switzerland). Then, 200 µL extraction solvent, methanol:water (70:30 v/v), was added to each blood disc. The samples were mixed for 3 minutes and afterwards, centrifuged (30min; 3220 g; 10°C, Eppendorf, Hamburg, Germany), and kept at 10°C in the autosampler. To perform the analysis, an aliquot of 20 µL supernatant was introduced into the LC-MS/MS system. Subsequently, the system was washed with methanol and a methanol:water mixture (1:1 v/v).

2.6. Method validation

The automated DBS extraction LC-MS/MS method was validated following the FDA guidance for bioanalytical method validation for industry. The method was validated in terms of selectivity, sensitivity, accuracy, precision, linearity, extraction recovery, matrix effect, and analyte stability.

2.6.1. Selectivity and sensitivity

Blank DBS samples from seven different subjects were examined for interfering endogenous matrix components. The signal at the designated LLOQ was set to be at least five times higher than the noise signal, with a bias in precision of less than 20%, and accuracy of 80-120%.

2.6.2. Intra- and inter-day accuracy and precision experiments

The accuracy and precision of the method were determined by analysing QC samples from seven different subjects at four concentration levels (LLOQ, low, medium, and high level QC). Placing the QC samples between two calibration lines, one spot was analysed per condition (n=28 QC samples, n=22 calibrators). Precision and accuracy were evaluated within a single validation run (intra-day) as well as between three runs recorded at different days (inter-day). The precision was calculated as the percentage relative standard deviation (CV, %) for each QC concentration within an analytical run (intra-day precision) and over all three runs (inter-day precision). A precision of <15% (<20% at the LLOQ) was accepted in our study. The accuracy was assessed from the overall mean of each QC concentration divided by its nominal value (bias, %). A mean accuracy of 85-115% (LLOQ: 80–120%) was acceptable; however, at least 67% of the QC samples of each concentration level had to be within the acceptance range.

2.6.3. Linearity

The coefficients of variation (R^2) of the linear regression, between the analyte peak area, normalised by the internal standard peak area and the nominal concentration, had to be ≥ 0.99 . At least 75% of the calibration samples had to be in within $\pm 15\%$ (LLOQ: $\pm 20\%$) of the nominal value.

2.6.4. Recovery and matrix effect

The extraction recovery of the DBS-MS 500 autosampler was investigated for DBS samples of seven different subjects. Furthermore, the influence of varying haematocrit values on recovery was analysed over a range of 20 to 50% (same preparation as described in Section 2.6.5). DBS spots at 50, 500, 5000 ng/mL were prepared for the recovery experiments. Each spot was extracted six times for medium and high concentration samples (500 and 5000 ng/mL), while low concentration samples (50 ng/mL) were extracted three times. Between two extractions, a drying time of approximately 15 minutes was programmed. Spots were visually inspected to ascertain whether the extraction head always locked onto the same area of the blood spot. The recovery was finally estimated as the percentage ratio of the analyte peak area of the first extraction to the sum of the peak areas of all conducted extractions.

Blank DBS samples from seven different subjects were prepared to quantify the effect of the blood matrix itself on the analyte signal intensity. The extraction solvent was spiked with 10, 100, or 1000 ng/mL nevirapine, efavirenz, and lopinavir. Each blank DBS sample, and a corresponding card without a blood spot, were processed at each concentration level. The matrix effect was calculated as the ratio of the analyte peak areas measured, following extraction of filter cards containing a blank DBS, to the peak areas of filter cards without matrix.

2.6.5. Impact of the haematocrit value and the applied blood volume

Haematocrit levels in the study population ranged from 20 to 50%, with a mean haematocrit of 35%. Therefore, blood samples with haematocrit values of 20%, 25%, 30%, 35%, 40%, 45%, and 50% were prepared by adding or removing plasma from blood with a known haematocrit [28]. Modified haematocrit values were verified for quality control reasons using a haematology analyser (Sysmex KX-21N, Kobe, Japan). The correlation between the haematocrit value and the resulting blood spot area was evaluated by measuring the area of 12 blood spots per haematocrit level. This experiment was carried out by pipetting three different volumes of blood (10, 15, and 20 μ L). Blood spots were photographed using the built-in camera of the CAMAG autosampler, and the areas were digitally measured with GIMP software (GNU Image Manipulation Program 2.8.10). The relationship between the spot area, normalised to the applied volume of blood and the respective haematocrit value, was analysed by linear regression.

DBS spots using 15 μ L and 30 μ L blood were prepared at LLOQ, low, medium, and high concentration levels. Additionally, the change in concentration of 15 μ L to 30 μ L spots was calculated. A deviation of $\leq 15\%$ ($\text{LLOQ} \leq 20\%$) implied that the method does not depend on the applied volume of blood.

2.6.6. Stability

Stability tests of nevirapine, efavirenz, and lopinavir were performed under different conditions at a medium concentration level of 500 ng/mL. Stability was evaluated under accelerated storage conditions, aimed at mimicking weather conditions in Tanzania, at 40°C and 75% relative humidity after 1 day and, again, after 1, 2, 3, and 4 weeks. Stability in the fridge (4°C) and the freezer (-20°C) was tested after 4 weeks

of storage. Five replicates were analysed per condition and compared to a set of QC samples, prepared on the day of analysis.

2.7. Method application

DBS and plasma samples (nevirapine n=192, efavirenz n=482, lopinavir n=66) were collected from within the framework of an adherence assessment study in Tanzania, which included 299 patients [16]. Ethical approval was obtained from the Institutional Review Board of the Ifakara Health Institute, Dar es Salaam, Tanzania (IRB reference no. IHI 28-2013).

2.7.1. Comparison of automated/manual DBS extraction and plasma/ DBS samples

Clinical application of the LC-MS/MS method was demonstrated by analysing 50 randomly chosen DBS samples for each analyte, which were processed by automated and manual extraction. In both cases, the IS was sprayed onto the DBS. Bland-Altman plots were created with GraphPad Prism 6.04 (La Jolla, CA, USA) to compare the two extraction methods [29]. In so doing, a mean ratio plot was generated including the mean ratio bias and the 95% limits of agreement (± 2 standard deviations).

Furthermore, 192 nevirapine, 482 efavirenz, and 66 lopinavir plasma, and their corresponding DBS samples, were analysed and compared using Bland-Altman plots. DBS samples were extracted using the CAMAG-500 autosampler. An aliquot of 50 μ L plasma was precipitated with 500 μ L methanol, containing the IS (nevirapine-d3: 50 ng/mL, efavirenz-d5: 100 ng/mL, and lopinavir-d8: 100 ng/mL). After centrifugation (3220 g, 30 min, 10° C), 5 μ L supernatant was injected (CTC PAL autosampler, Zwingen, Switzerland) into the LC-MS/MS system. EMEA Criteria set for the cross-validation of two methods were applied in this study, meaning at least 67% of the samples had to be within $\pm 20\%$ limits: *“For study samples, the difference between the two values obtained should be within 20% of the mean for at least 67% of the repeats”* [30].

3. Results and Discussion

3.1. Method development

Assessment of adherence to antiretroviral therapy is essential to assure sufficient viral suppression and thus improve survival and quality of life. While therapeutic drug monitoring (TDM) is part of the standard of care in industrialised nations, less is known about adherence to antiretroviral treatments in developing countries. Using DBS to perform TDM, instead of conventional plasma or serum sampling, does entail several method-specific drawbacks. When working with DBS, the preparation of calibrator and QC samples, alongside the extraction procedure, is more laborious. Moreover, the small amount of blood available in the DBS sample is a challenge for the development of particularly sensitive methods. Finally, technical difficulties, such as variations in haematocrit, can lead to variable blood spot areas, while the haematocrit can also be the reason for variable analyte recovery that can further complicate accurate quantification. Here we demonstrate that these challenges can be partially overcome by using the CAMAG DBS-MS 500 autosampler for the analysis of nevirapine, efavirenz, and lopinavir.

In the first stage of method development, mass spectrometer voltages were adjusted to maximise the peak response of the parent mass and the product ions for each compound. The best results were obtained when using the transitions 267→226 m/z, 314→244 m/z, and 629→155 m/z for nevirapine, efavirenz, and lopinavir, respectively. Similar transitions were used for the internal standards, with the addition of the respective amount of deuterium atoms (nevirapine-d3: 270→229 m/z, efavirenz-d5: 319→248 m/z, lopinavir-d8: 637→163 m/z). The same MS/MS transitions were also utilised in other published methods [17, 18, 21, 31].

Nevirapine and lopinavir were optimised in positive ionisation mode, while efavirenz was optimised in negative ionisation mode. Therefore, efavirenz had to be chromatographically separated from nevirapine and lopinavir, as negative and positive ionisation modes cannot be run in parallel with the employed mass spectrometer. Figure 1 illustrates that baseline separation of all analytes was efficiently achieved within a 3 minute running time, using a core-shell pentafluorophenyl phase column. Peak symmetry was reasonable using methanol and water supplemented with formic acid (0.1%) as mobile phase.

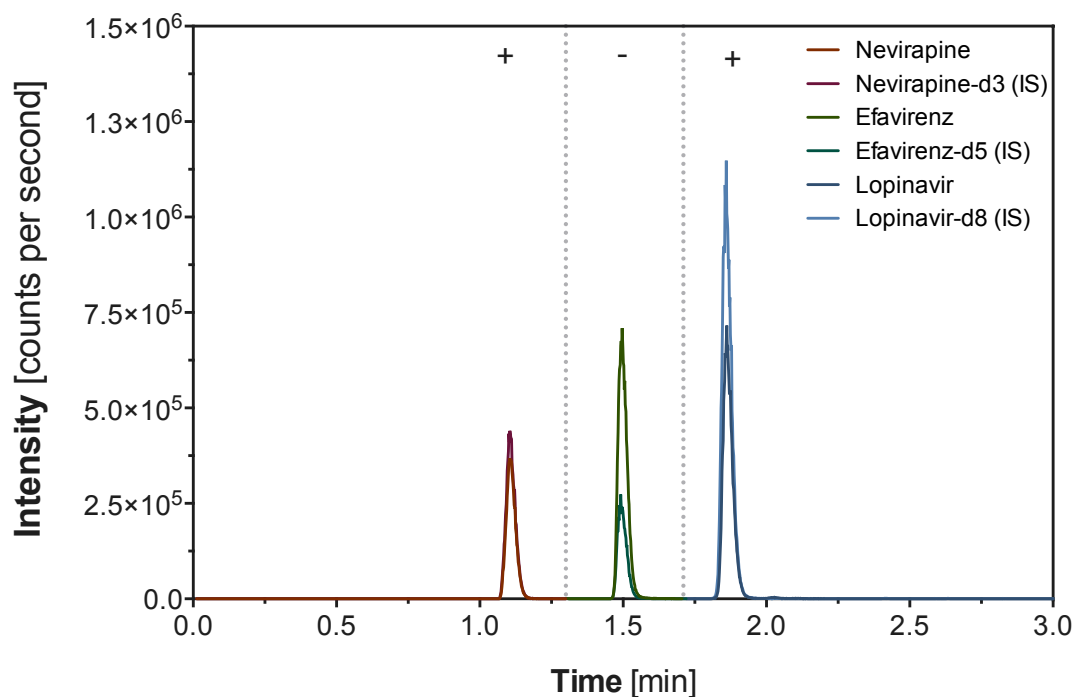


Figure 1. Chromatogram of a high concentration QC sample of nevirapine, efavirenz, lopinavir, and their respective internal standards. Polarity was switched to negative ionisation mode between 1.3 and 1.7 minutes.

The emphasis of method development focused on improving the automated extraction. The main adjustable instrument parameters for this process consisted of the amount of IS sprayed onto the DBS, the extraction-flow, -volume, and -solvent composition. Parameters giving the highest signal intensities, best precisions, and optimal peak shapes were selected (Figure 2), and extraction parameter optimisation was investigated at low and high QC levels ($n=4$).

First, different methanol:water mixtures (50:50, 60:40, 70:30, 80:20, and 90:10 v/v) were tested. A high water amount increased the risk of clogging the extraction head, as presumably more biomolecules and cellular components are removed from the dried spot. Extraction robustness was thereby limited. Overall a mixture of 70:30 methanol:water resulted in the highest signal intensities and showed good precisions. Peak symmetry was disturbed by methanol concentrations exceeding 80% in the extraction solvent. Replacing methanol with acetonitrile did not improve extraction yield and worsened peak shapes. The extraction volume was increased stepwise from 20 to 70 μL (20, 25, 30, 40, 50, 60 and 70 μL), while the last 20 μL of each extraction were trapped in the sample loop. Signal intensities decreased with larger extraction volumes to about 80-90% of the initial value. Almost 50% is extracted within the first 10 μL of the extraction fraction. An extraction volume of 25 μL was

selected because the precision was enhanced compared to 20 μL and the signal intensity was only marginally lower. As extraction flow did not seem to have a significant impact, the standard setting of 40 $\mu\text{L}/\text{min}$ flow was used to perform automated extraction.

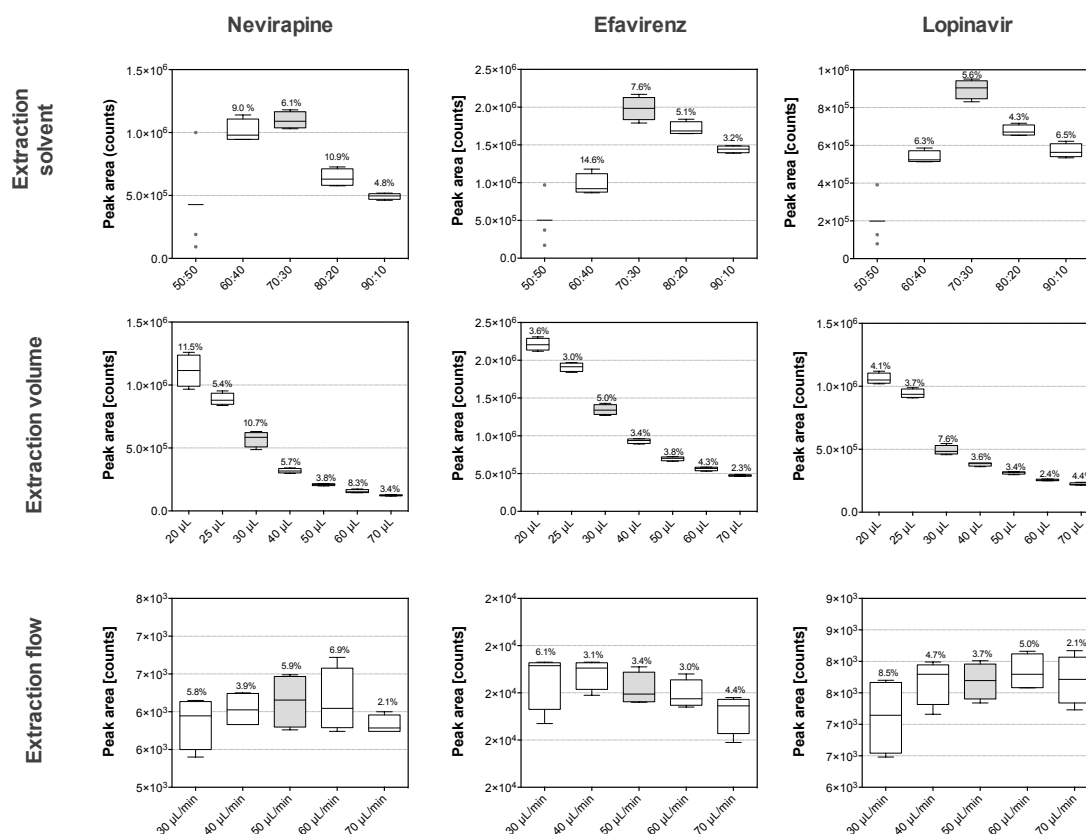


Figure 2. Optimisation of the DBS-MS 500 method for the extraction of nevirapine, efavirenz, and lopinavir from DBS samples. High concentration QC samples ($n=4$) were extracted for every extraction condition. The effects of the methanol:water mixture, extraction volume, and extraction flow on the extraction yield were evaluated. Conditions with grey coloured box plots were selected for the extraction method.

The wash cycle had to be optimised in order to reduce analyte carry-over. In the case of nevirapine and efavirenz, the signal in a blank sample after injection of the highest calibrator was ten times lower than the signal detected at LLOQ. However, the carry-over of lopinavir led to signal intensities around three to four times lower than the signal at LLOQ. Nevertheless, through a sequential injection of another blank sample, the interference was removed, meaning that carry-over of lopinavir is manageable.

3.2. Method validation

3.2.1. Selectivity and Sensitivity

Selectivity of the method was tested for interfering matrix components in seven blank human DBS samples (Figure 3). Noise level baselines of the blank samples did not show co-eluting peaks at the retention time of nevirapine (1.1 min), efavirenz (1.5 min), or lopinavir (1.9 min). Moreover, internal standards that were sprayed onto blank DBS spots did not cause interfering signals. Hence, the developed method is selective for the analysis of the investigated antiretrovirals.

A sensitivity of 10 ng/mL was achieved for all analytes. Based on published data, we expect this quantification limit to be sufficient to perform therapeutic monitoring of nevirapine, efavirenz, and lopinavir [32]. Figure 3 illustrates that the signal intensity at LLOQ is at least five times higher than the background noise level.

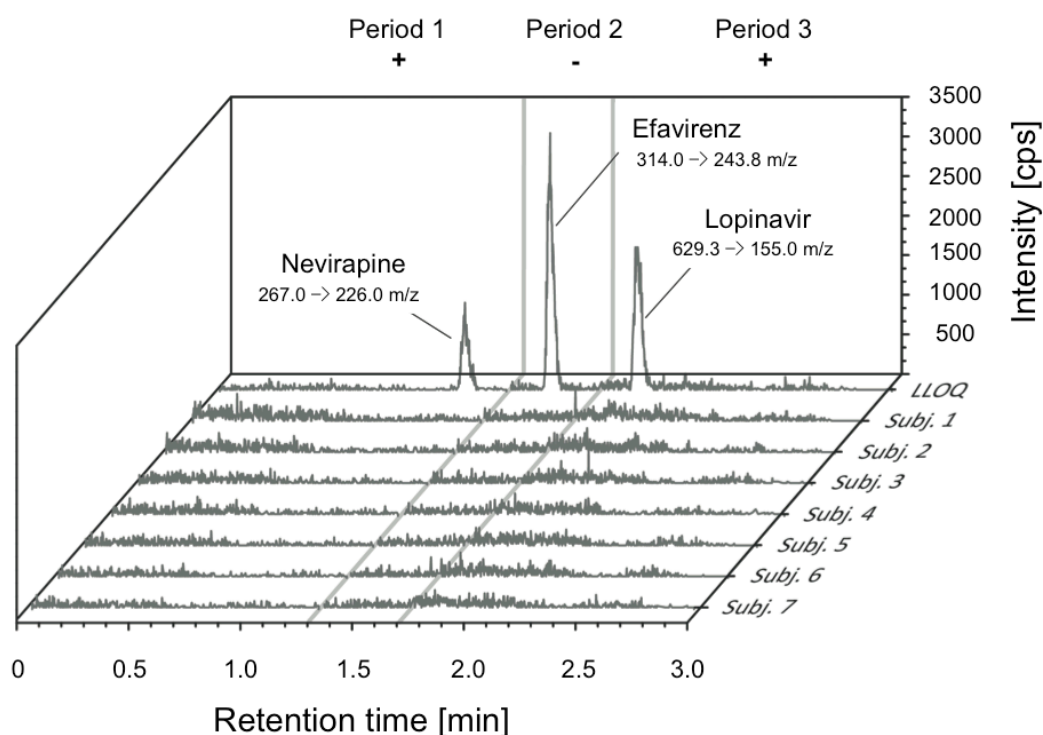


Figure 3. Chromatograms of blank DBS samples ($n=7$ donors) were placed next to a LLOQ sample. The method is selective for the quantification of nevirapine, efavirenz, and lopinavir in DBS samples.

3.2.2. Linearity

Linearity was attained over a calibration range of 10 to 25'000 ng/ml for all analytes. Taking all validation experiments into account, the coefficient of variation (R^2) was always >0.99 for each respective analyte. The upper limit of quantification also

encompasses high therapeutic concentrations [33], which is especially important for the automated extraction of DBS, as dilution of the DBS samples cannot be easily performed. Thus, clinically occurring concentrations can be quantified by linear regression within the chosen calibration range.

3.2.3. Accuracy and Precision

Intra- and inter-day accuracy and precision data are summarised in Table 1. QC samples were derived from seven donors with haematocrit values varying between 39-44%. An intra-day precision of less than 14.8%, 12.0%, and 13.9% was found for nevirapine, efavirenz, and lopinavir respectively. Inter-day precisions were $\leq 11.3\%$. Mean inter-day accuracies were between 88.9-106.8% for nevirapine, 91.3-104.6% for efavirenz, and 90.1-108.5% for lopinavir. On all occasions, not more than two out of the seven QC samples per concentration were outside the 85-115% (LLOQ: 80-120%) limits. Overall, results were consistent with conditions specified by regulatory guidelines.

Table 1. Intra- and inter-assay accuracy and precision of nevirapine, efavirenz, and lopinavir analysed in DBS samples.

Analyte	QC Level [ng/mL]	Intra-assay						Inter-assay	
		Day 1		Day 2		Day 3		Day 1-3	
		Conc. found at [ng/mL]	Accuracy \pm CV [%]	Conc. found at [ng/mL]	Accuracy \pm CV [%]	Conc. found at [ng/mL]	Accuracy \pm CV [%]	Conc. found at [ng/mL]	Accuracy \pm CV [%]
Nevirapine	10	9.3	93.2 \pm 7.4	9.7	96.9 \pm 7.4	10.7	106.8 \pm 8.3	9.9	99 \pm 9.5
	50	44.4	88.9 \pm 8.6	47.1	94.1 \pm 14.8	47.9	95.9 \pm 7.3	46.5	93 \pm 10.7
	500	469.8	94 \pm 5.9	474.1	94.8 \pm 5.4	482.1	96.4 \pm 7	475.3	95.1 \pm 5.9
	5000	4753.9	95.1 \pm 8.3	4772.5	95.4 \pm 6	4941	98.8 \pm 10.4	4822.5	96.4 \pm 8.2
Efavirenz	10	9.1	91.3 \pm 7.1	9.7	96.9 \pm 11	10.5	104.6 \pm 10.6	9.8	97.7 \pm 11
	50	46.7	93.4 \pm 9.1	47.4	94.8 \pm 12	50.1	100.1 \pm 9.7	48.1	96.1 \pm 10.3
	500	480.4	96.1 \pm 5.9	480.5	96.1 \pm 5.5	495.5	99.1 \pm 7	485.5	97.1 \pm 6.1
	5000	4779.6	95.6 \pm 9.2	4655.2	93.1 \pm 8.6	4934.1	98.7 \pm 9.7	4789.7	95.8 \pm 9.1
Lopinavir	10	9.7	96.5 \pm 5.8	10.2	98.4 \pm 12.8	10.9	108.5 \pm 8.7	10.2	101.1 \pm 10.5
	50	45.9	91.8 \pm 10.7	45.9	91.8 \pm 13.9	47.2	94.4 \pm 10.5	46.3	92.7 \pm 11.3
	500	482.4	96.5 \pm 7.8	455.7	91.1 \pm 7.2	464.2	92.8 \pm 7.9	467.5	93.5 \pm 7.7
	5000	4723.2	94.5 \pm 10.3	4506.4	90.1 \pm 9.5	4618.2	92.4 \pm 12.8	4615.9	92.3 \pm 10.6

3.2.4. Recovery and Matrix effect

The relative recovery and matrix effect were determined in four different donors at low, medium, and high concentrations. In addition, the recovery of the analytes was assessed in dried water spots. The highest mean recovery was achieved for nevirapine with 70%, followed by efavirenz (63%), and lopinavir (60%). A bias in recovery of less than 7.2% was determined between subjects, indicating high consistency in the sample extraction process (Figure 4). Recovery at low

concentration was overestimated by around 10% compared to medium and high concentration samples, as the limit of quantification was already reached after three instead of six consecutive extractions. The recovery of dried water spots was >97%, which implies that blood acts as an extraction barrier. For this reason, the influence of the haematocrit on extraction recovery was additionally investigated (see section 3.2.5).

The signal intensity of nevirapine and lopinavir was only suppressed by about 8% and 6% respectively, through the DBS matrix. However, a significant suppressive matrix effect was observed for efavirenz, where the signal was reduced to approximately 50% due to the biological matrix. Importantly, the matrix effect was independent of concentration, as its deviation was $\leq 10.4\%$ at different concentrations, and did not vary between subjects (CV $\leq 11.0\%$).

Table 2. Matrix effect (ME) of nevirapine, efavirenz, and lopinavir in DBS samples.

	Nevirapine		Efavirenz		Lopinavir	
	ME \pm CV [%]	Mean \pm CV [%]	ME \pm CV [%]	Mean \pm CV [%]	ME \pm CV [%]	Mean \pm CV [%]
10ng/mL	92.2 \pm 1.0	92.0 \pm 0.4	52.7 \pm 4.9	54.8 \pm 10.4	100.6 \pm 2.0	94 \pm 6.2
100ng/mL	91.5 \pm 1.8		50.4 \pm 5.4		91.5 \pm 2.0	
1000ng/mL	92.1 \pm 3.4		61.2 \pm 11.0		89.7 \pm 2.0	

Hence, the matrix of different donors did not alter the reliability of the method. Online solid phase purification of DBS extracts, via column switching or through more thorough separation of efavirenz and blood ingredients, may eliminate suppressive matrix effects [27, 34]. All in all, the automated extraction was eminently reproducible and delivered consistent matrix effects.

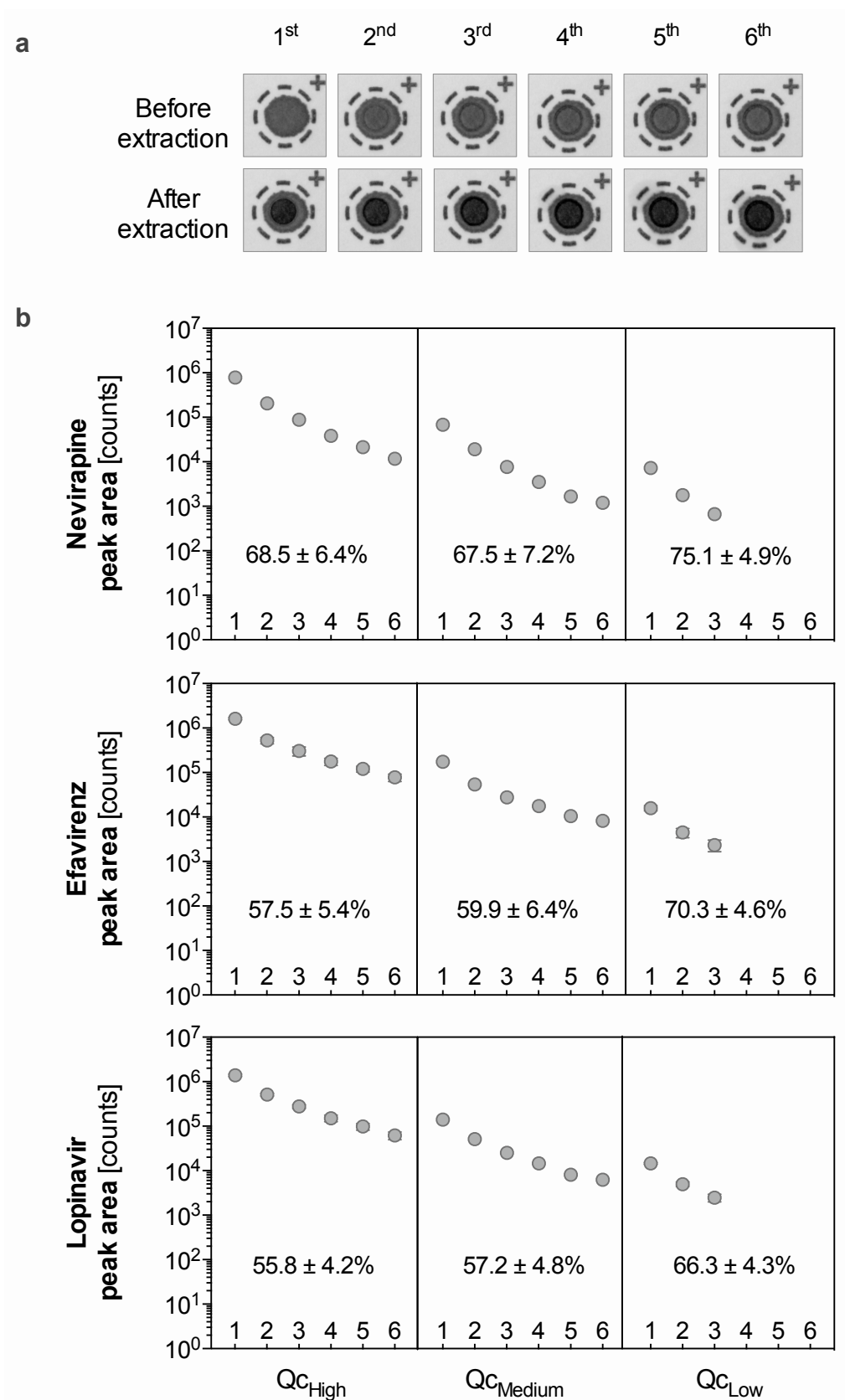


Figure 4. (a) Pictures of DBS before and after six consecutive extractions. The extraction head was always aimed onto the same coordinates on the blood spot. **(b)** Extraction recovery of nevirapine, efavirenz, and lopinavir determined at low, medium, and high concentrations of four different donors. Decrease in peak areas after six (medium and high QC) or three (low QC) repetitive extractions are shown. Recoveries were consistent between different subjects and over different concentrations.

3.2.5. Impact of the haematocrit value and the applied blood volume

It is comprehensively described that the blood haematocrit can affect the reliability of DBS methods, as the diffusion behaviour is altered by its magnitude [11]. Blood spot area on the filter paper grade 226 decreased in a linear manner ($R^2 \geq 0.93$), with increasing haematocrit values, as shown in Supplementary Figure S1. A linear relationship between haematocrit and spot size has also been described for other brands of filter paper [12]. QC sample concentrations differed by less than 5.7% when 30 μ L instead of 15 μ L blood was spotted onto cards. Hence, the applied blood volume produced reproducible, volume-dependent spot areas and, therefore, importantly, did not affect accuracy and precision of the analysis (Table S1 and Figure S2). To counteract the haematocrit-area bias the following correction formula for the applied filter paper grade 226 was established, based on the observed linear regression between area and haematocrit (Figure S2b):

$$DBS\ area = -1.157 \times HCT + 261.8$$

Accordingly, the haematocrit value of the calibrator and of the TDM sample must be known before the correction can be applied. A clear tendency, for DBS samples spotted with a haematocrit below or above that of the calibrators (HCT 35%), to under- or overestimate the actual concentration is shown in Figure 5. A significant linear correlation between haematocrit and the deviation from the calibration haematocrit was observed. Overall, 24% (nevirapine), 46% (efavirenz), and 22% (lopinavir) of the QC samples (n=54) exhibited a bias of >15%. After correction, this proportion was reduced to 2% for nevirapine, 20% for efavirenz, and 9% for lopinavir. Thus, only efavirenz demonstrated a significant haematocrit-driven bias. It is, therefore, conceivable, that the haematocrit might additionally influence the diffusion behaviour of efavirenz, leading to a haematocrit dependent concentration gradient across the spot (e.g. volcano effect) [35].

Moreover, higher haematocrit values complicate analyte recovery and thereby diminish the area-haematocrit bias [36]. In the case of nevirapine, efavirenz, and lopinavir a change in haematocrit from 20 to 50% decreased the extraction recovery by 7.7 to 27.4% over the tested concentration range (QC_{low} , QC_{med} , QC_{high}). Importantly, the recovery of the IS solution, which was sprayed on top of each spot, declined by roughly the same degree (Table S2). To spray the IS onto the DBS, instead of adding it to the extraction solvent, has been shown to reduce the recovery-haematocrit bias, which is in line with our findings [36]. Crucially, if the haematocrit of the DBS sample were to be unknown, it could be estimated by measuring the

potassium concentration, which has been shown to correlate with the haematocrit and therefore enables haematocrit corrected DBS analysis [37].

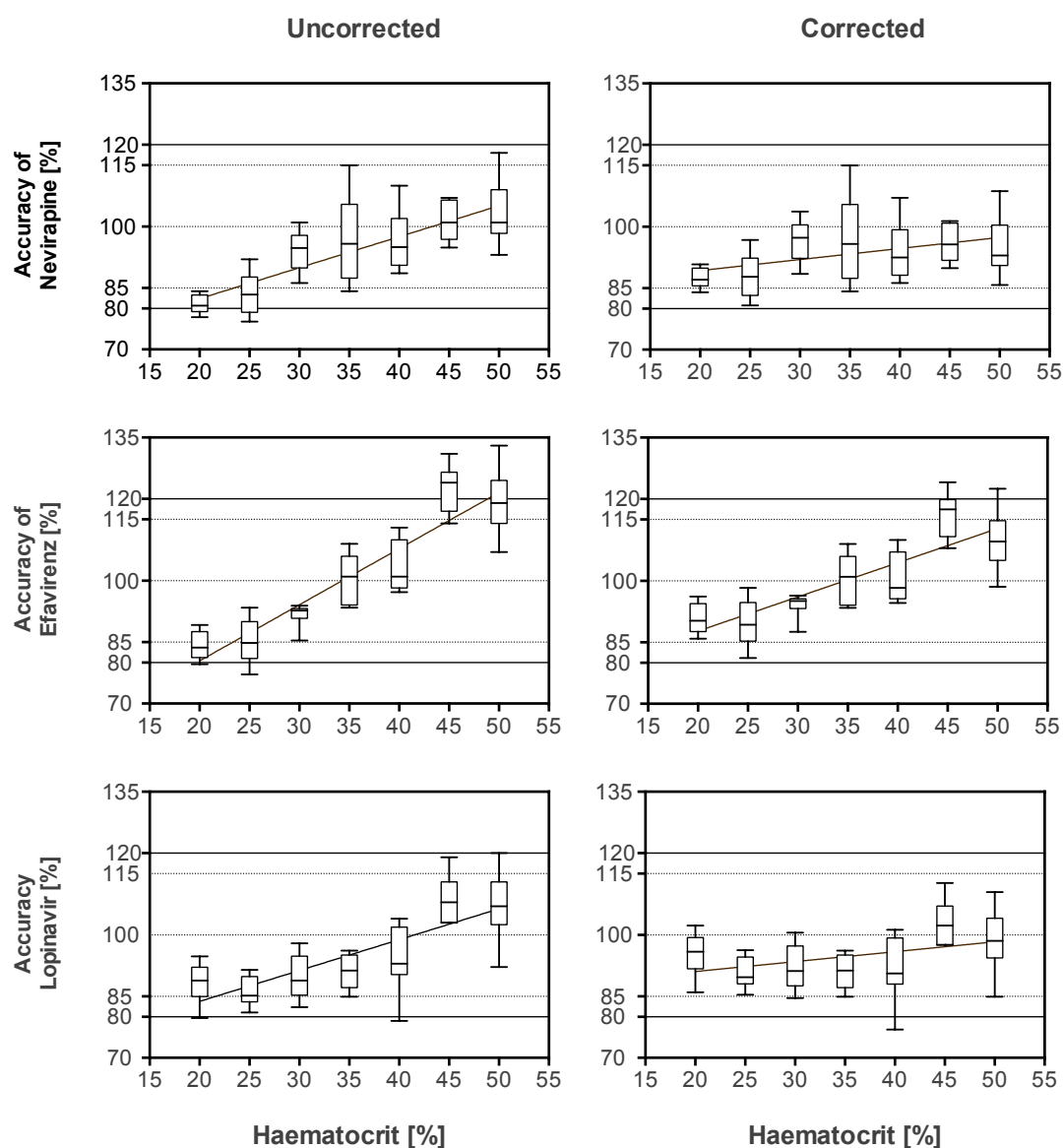


Figure 5. Relationship between haematocrit and the deviation related to a haematocrit of 35% determined for nevirapine, efavirenz, and lopinavir. The DBS of the calibrators exhibited a haematocrit of 35%. Each Box-plot included low, medium, and high QC samples (n=3 each). White Box-plots are before correction and grey box-plots are before correction with the area-haematocrit correction formula. The upper and lower limits of the boxes correspond to the interquartile range and the middle line is the median of the data set. The limits of the whiskers are the minimum and maximum values. Linear regression through the mean-value of the boxes was established.

3.2.6. Stability

Stability data are summarised in Table 3. The data implied that analytes were stable in DBS for four weeks at -20°C or 4°C, as the change in concentration compared to a freshly prepared DBS sample was less than 6.1%. Nevirapine and efavirenz were

also stable, if temperature and relative humidity were increased to 40°C and 75%rH, respectively. Previous studies demonstrated that efavirenz was stable for at least 7 months [21], and nevirapine for 15 months at room temperature [31]. Under accelerated storage conditions (e.g. 40°C/75rH), we observed a time-dependent degradation from -5.7% to -24.3% for lopinavir over the course of four weeks. That lopinavir is stable for one week at 30°C, as determined by Heine et al., was in line with our data as it required an additional three weeks at 40°C/75rH to degrade >15% of lopinavir [18]. In summary, it is important that DBS samples containing lopinavir, especially if collected in tropical countries, should be kept in a fridge or freezer for prolonged storage. Moreover, and by contrast, our data shows that nevirapine and efavirenz are not likely to be degraded through storage outside of the cold chain.

Table 3. Stability of nevirapine, efavirenz, and lopinavir evaluated under different conditions for DBS samples at a concentration of 500ng/mL.

Condition	Nevirapine			Efavirenz			Lopinavir		
	Conc. [ng/mL]	Accuracy ± CV [%]	Change in Conc. [ng/mL]	Conc. [ng/mL]	Accuracy ± CV [%]	Change in Conc. [ng/mL]	Conc. [ng/mL]	Accuracy ± CV [%]	Change in Conc. [ng/mL]
RT, normal rH	519.5	103.9 ± 3.6	-	481.6	96.3 ± 6.1	-	532.7	106.5 ± 3.3	-
24 h, 40°C, 75%rH	540.9	108.2 ± 3.9	4.1	486.4	97.3 ± 2.5	1	502.5	100.5 ± 6.9	-5.7
1 week, 40°C, 75%rH	540.7	108.1 ± 8.2	4.1	486	97.2 ± 9	0.9	492.4	98.5 ± 6.5	-7.6
2 weeks, 40°C, 75%rH	529.3	105.9 ± 5.2	1.9	489.7	97.9 ± 5.8	1.7	460.7	92.1 ± 6.2	-13.5
3 weeks, 40°C, 75%rH	531.8	106.4 ± 4.4	2.4	507.6	101.5 ± 3.7	5.4	427.7	85.5 ± 4.2	-19.7
4 weeks, 40°C, 75%rH	533	106.6 ± 6.9	2.6	495.2	99 ± 6.5	2.8	403.2	80.6 ± 4.3	-24.3
4 weeks, 4°C	532.4	106.5 ± 7.3	2.5	511.1	102.2 ± 8.8	6.1	537.2	107.4 ± 8.2	0.8
4 weeks, -20°C	517.4	103.5 ± 7.2	-0.4	477.7	95.5 ± 8.2	-0.8	559.2	111.8 ± 6.7	5

3.3. Method application

TDM samples (n=740), which were collected in the framework of a drug adherence study in Ifakara (Tanzania), were analysed in Basel (Switzerland). 50 DBS samples of each analyte were extracted, manually as well as automatically, using the DBS-MS 500 autosampler. Nevirapine concentrations in DBS were between 3360 and 19'000 ng/mL, efavirenz concentrations were between 262 and 15'000 ng/mL, and lopinavir concentrations between 41.8 and 16'100 ng/mL; thus the selected calibration range (10 to 25'000 ng/mL) was suitable for the quantification of all collected TDM samples of this study. Sample dilution was therefore not necessary, which is relevant because it cannot be easily performed through automated extraction.

Overall, automated and manual extractions were in strong agreement (Figure 6). Mean bias of automated to manual extractions was -9% for nevirapine, -8% for

efavirenz, and -1% for lopinavir. 95% limits of agreement were narrow with a range smaller than $\pm 24\%$ (nevirapine: -30 to +11%; efavirenz: -32% to +16%; lopinavir: -24% to +22%). Consequently, when comparing automated and manually extracted samples, not more than 16% of respective samples showed a deviation outside of the $\pm 20\%$ threshold, according to the EMEA guideline for cross-validation [30]. No concentration-dependent trend was observed between the ratios of the two extraction methods across the entire concentration range. Overall, automated extraction was 5 times more sensitive than manual extraction, which is mainly due to DBS being extracted with less solvent through the automated sample workup (25 μL vs. 150 μL) resulting in more concentrated samples. Both extraction procedures achieved similar results and the data obtained were in agreement with aforementioned criteria [30].

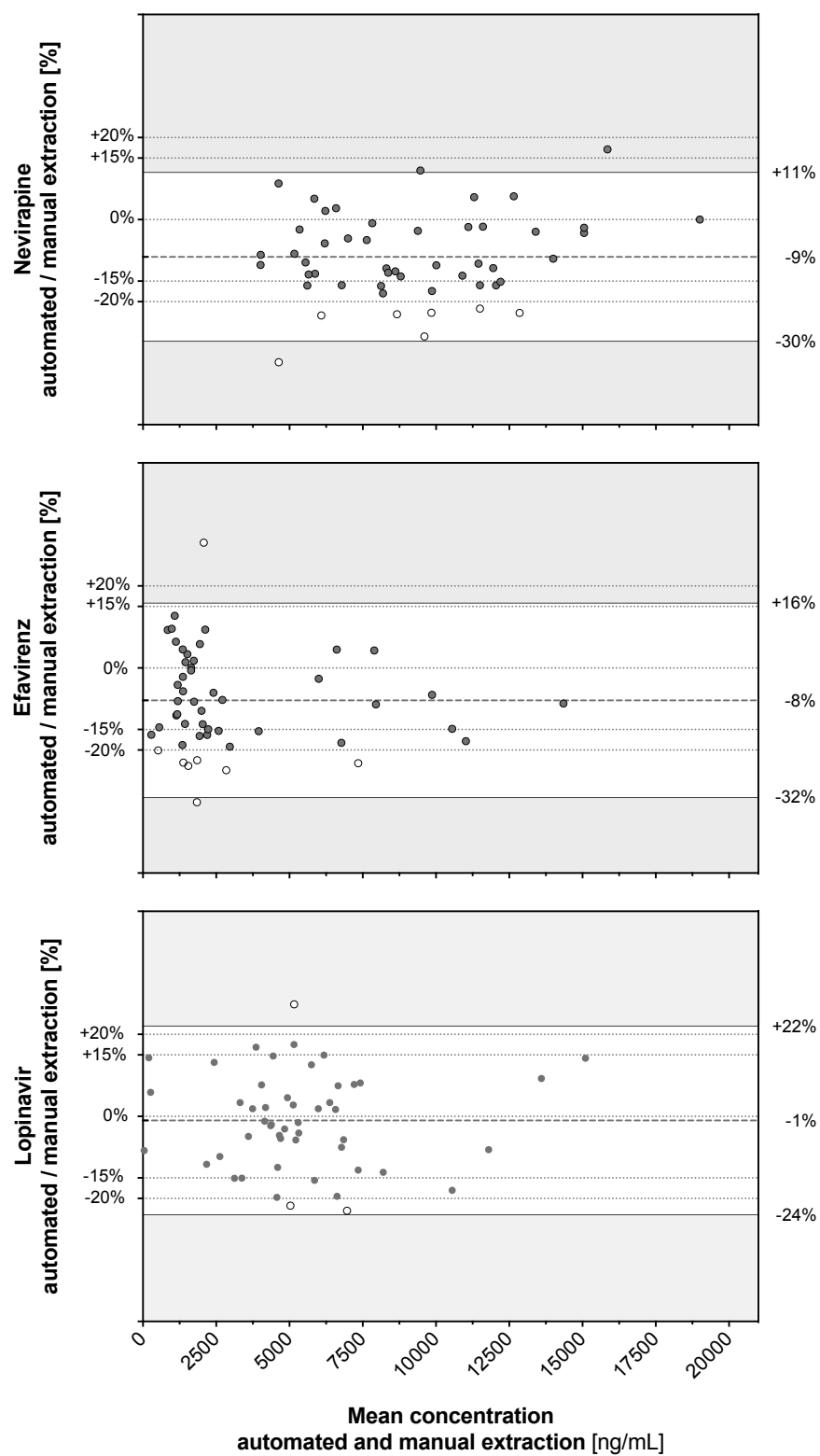


Figure 6. Bland-Altman plots of nevirapine, efavirenz, lopinavir were generated for automated and manual DBS extractions. Values were coloured grey if the concentration ratio of the two extraction methods was less than $\pm 20\%$; otherwise values were coloured white. The white plot area illustrates the 95% limits of agreement. The black dashed line describes the mean ratio of automated to manual extraction.

A negligible mean bias of +5% between DBS and plasma concentrations was detected for nevirapine. The 95% limits of agreement reached from -27% to +36%, and only 11.9% of the nevirapine samples were outside $\pm 20\%$ limits (Figure 7). In contrast, DBS concentrations were about 50% lower, as in plasma samples for efavirenz (bias $\pm 2SD$ range: 0.59 [0.43-0.74]) and lopinavir (bias $\pm 2SD$ range: 0.48 [0.28-0.67]). In the case of efavirenz the bias could be greatly reduced by correcting the DBS concentration with the corresponding haematocrit value and protein binding (bias $\pm 2SD$ range: 0.91 [0.66-1.16]), as previously described by Kromdijk et al. and Li et al. [14, 21]. After correcting the efavirenz values through the formula – $([DBS_{(analyte)}] / (1 - \text{haematocrit})) \times f_{b_{pp}}$ – the percentage of samples outside the $\pm 20\%$ limits was reduced from 99.2% to 18.7%. Furthermore, applying the same correction formula to lopinavir samples improved the agreement between DBS and plasma considerably (bias $\pm 2SD$ range: 0.73 [0.44-1.03]). Nevertheless, 71.9% of the DBS samples still demonstrated a deviation of more than 20%. In conclusion, DBS analysis of nevirapine and efavirenz align with criteria set for cross-validation of two methods, whereas lopinavir concentrations determined in DBS samples are, on average, about 25% lower than in plasma [30].

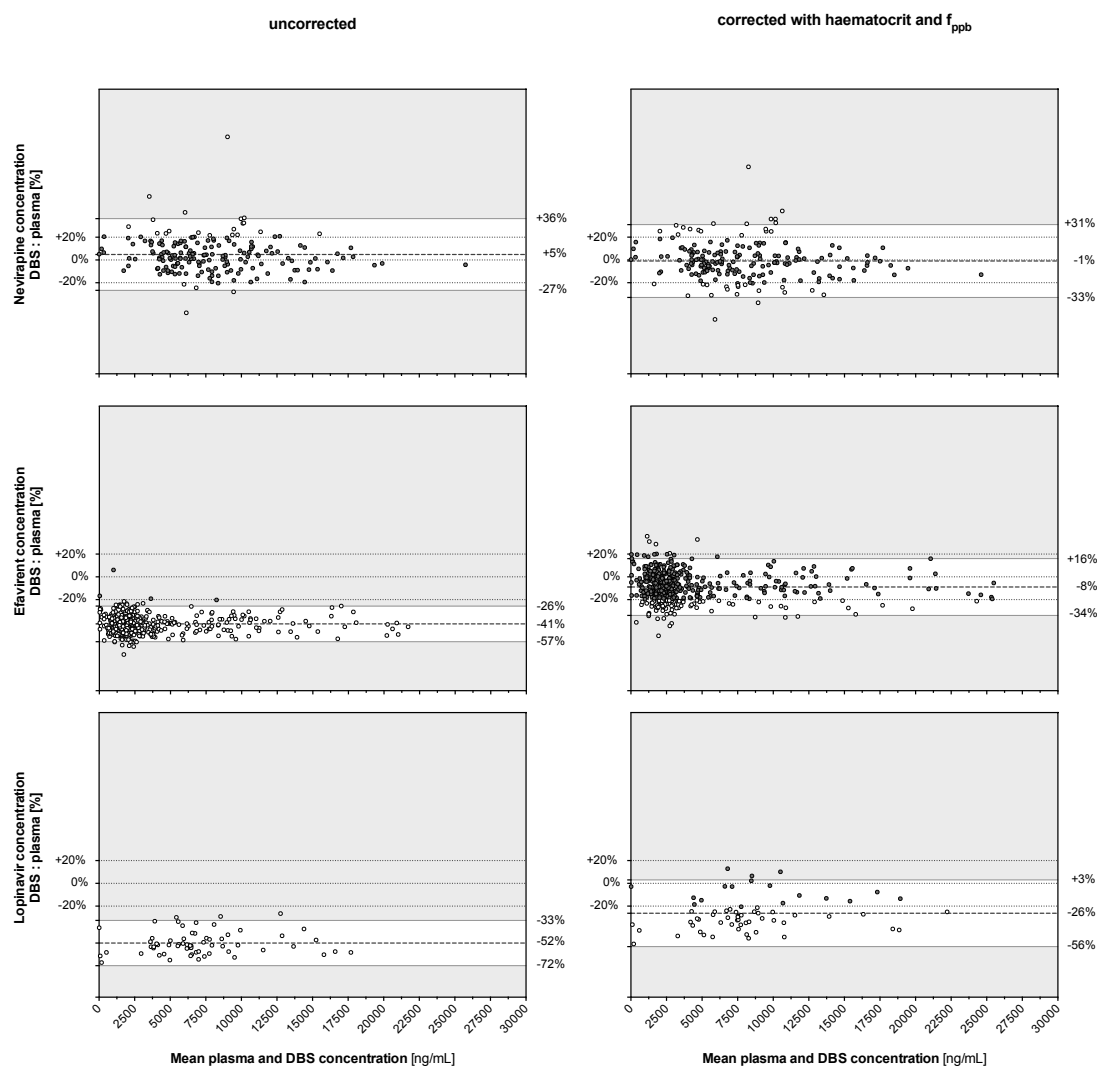


Figure 7. Bland-Altman plots of nevirapine, efavirenz, lopinavir were generated for DBS and plasma samples. Values were coloured grey if the concentration ratio of the two matrices was less than $\pm 20\%$; otherwise values were coloured white. The white plot area illustrates the 95% limits of agreement. The black dashed line represents the mean concentration ratio of DBS to plasma. In the case of the plots depicted on the right side, DBS concentrations were corrected with haematocrit and with plasma protein binding (f_{ppb}).

In summary, an innovative automated LC-MS/MS method was developed and validated for the quantification of nevirapine, efavirenz, and lopinavir DBS samples. It took approximately 3-4 minutes to extract and analyse one DBS sample. Automated DBS extraction resulted in extremely consistent inter-individual recoveries and matrix effects. Validation parameters were in accordance with specifications put in place by regulatory guidelines. Through the spraying of IS onto the DBS, the haematocrit-recovery bias could be minimised. Furthermore, by making use of the installed camera in the autosampler, a correction function between the haematocrit and the blood spot area could be established, thereby reducing the haematocrit-area bias. The method was successfully applied to analyse TDM samples. Results obtained by automated and manual extraction were comparable. However, the sample

processing time and method sensitivity was improved by the DBS-500 autosampler. Automated DBS extraction was reliable and will facilitate analysis of large sample numbers. Our study confirms that TDM of nevirapine and efavirenz in DBS is a suitable alternative to conventional plasma analysis, especially when samples have to be collected in resource-limited settings.

Acknowledgements

We would like to thank Beatrice Vetter¹ and Massimiliano Donzelli¹ for their valuable advice and technical support.

Financial support

SK was supported by a grant of the Swiss National Science Foundation (SNF 31003A_156270).

Conflict of interest

None of the authors reports any conflict of interest regarding this study.

4. References

1. Pandya, H.C., N. Spooner, and H. Mulla, *Dried blood spots, pharmacokinetic studies and better medicines for children*. Bioanalysis, 2011. **3**(7): p. 779-86.
2. Spooner, N., *A dried blood spot update: still an important bioanalytical technique?* Bioanalysis, 2013. **5**(8): p. 879-83.
3. Edelbroek, P.M., J. van der Heijden, and L.M. Stolk, *Dried blood spot methods in therapeutic drug monitoring: methods, assays, and pitfalls*. Ther Drug Monit, 2009. **31**(3): p. 327-36.
4. Smit, P.W., et al., *An overview of the clinical use of filter paper in the diagnosis of tropical diseases*. Am J Trop Med Hyg, 2014. **90**(2): p. 195-210.
5. WHO HIV/AIDS - Fact sheet N°360 (Updated November 2015). 2015.
6. Bangsberg, D.R., *Less than 95% adherence to nonnucleoside reverse-transcriptase inhibitor therapy can lead to viral suppression*. Clin Infect Dis, 2006. **43**(7): p. 939-41.
7. Burkhart, P.V. and E. Sabate, *Adherence to long-term therapies: evidence for action*. J Nurs Scholarsh, 2003. **35**(3): p. 207.
8. Schneider, J., et al., *Better physician-patient relationships are associated with higher reported adherence to antiretroviral therapy in patients with HIV infection*. J Gen Intern Med, 2004. **19**(11): p. 1096-103.
9. Meesters, R.J., et al., *Incurred sample reanalysis comparison of dried blood spots and plasma samples on the measurement of lopinavir in clinical samples*. Bioanalysis, 2012. **4**(3): p. 237-40.
10. Paterson, D.L., et al., *Adherence to protease inhibitor therapy and outcomes in patients with HIV infection*. Ann Intern Med, 2000. **133**(1): p. 21-30.
11. De Kesel, P.M., et al., *Hemato-critical issues in quantitative analysis of dried blood spots: challenges and solutions*. Bioanalysis, 2013. **5**(16): p. 2023-41.
12. Denniff, P. and N. Spooner, *The effect of hematocrit on assay bias when using DBS samples for the quantitative bioanalysis of drugs*. Bioanalysis, 2010. **2**(8): p. 1385-95.
13. Jager, N.G., et al., *Procedures and practices for the validation of bioanalytical methods using dried blood spots: a review*. Bioanalysis, 2014. **6**(18): p. 2481-514.
14. Li, W. and F.L. Tse, *Dried blood spot sampling in combination with LC-MS/MS for quantitative analysis of small molecules*. Biomed Chromatogr, 2010. **24**(1): p. 49-65.
15. Timmerman, P., et al., *EBF recommendation on the validation of bioanalytical methods for dried blood spots*. Bioanalysis, 2011. **3**(14): p. 1567-75.

16. Erb S, L.E., Elzi L, Hatz C, Klimkait T, Manuel Haschke, Berger B, Duthaler U, Langewitz W, Tanner M, Battegay M, , *Adherence assessment in HIV-infected patients treated with combination antiretroviral therapy (cART) in rural Tanzania*. (manuscript in preparation), 2016.
17. Koal, T., et al., *Quantification of antiretroviral drugs in dried blood spot samples by means of liquid chromatography/tandem mass spectrometry*. Rapid Commun Mass Spectrom, 2005. **19**(21): p. 2995-3001.
18. ter Heine, R., et al., *Quantification of protease inhibitors and non-nucleoside reverse transcriptase inhibitors in dried blood spots by liquid chromatography-triple quadrupole mass spectrometry*. J Chromatogr B Analyt Technol Biomed Life Sci, 2008. **867**(2): p. 205-12.
19. Ter Heine, R., et al., *Clinical evaluation of the determination of plasma concentrations of darunavir, etravirine, raltegravir and ritonavir in dried blood spot samples*. Bioanalysis, 2011. **3**(10): p. 1093-7.
20. Meesters, R.J., et al., *Ultrafast and high-throughput mass spectrometric assay for therapeutic drug monitoring of antiretroviral drugs in pediatric HIV-1 infection applying dried blood spots*. Anal Bioanal Chem, 2010. **398**(1): p. 319-28.
21. Kromdijk, W., et al., *Use of dried blood spots for the determination of plasma concentrations of nevirapine and efavirenz*. J Antimicrob Chemother, 2012. **67**(5): p. 1211-6.
22. Abu-Rabie, P. and N. Spooner, *Direct quantitative bioanalysis of drugs in dried blood spot samples using a thin-layer chromatography mass spectrometer interface*. Anal Chem, 2009. **81**(24): p. 10275-84.
23. Deglon, J., et al., *Automated system for on-line desorption of dried blood spots applied to LC/MS/MS pharmacokinetic study of flurbiprofen and its metabolite*. J Pharm Biomed Anal, 2011. **54**(2): p. 359-67.
24. Deglon, J., et al., *Direct analysis of dried blood spots coupled with mass spectrometry: concepts and biomedical applications*. Anal Bioanal Chem, 2012. **402**(8): p. 2485-98.
25. Ganz, N., et al., *Development and validation of a fully automated online human dried blood spot analysis of bosentan and its metabolites using the Sample Card And Prep DBS System*. J Chromatogr B Analyt Technol Biomed Life Sci, 2012. **885-886**: p. 50-60.
26. Daali, Y., et al., *Oral flurbiprofen metabolic ratio assessment using a single-point dried blood spot*. Clin Pharmacol Ther, 2012. **91**(3): p. 489-96.
27. Wagner, M., et al., *The use of mass spectrometry to analyze dried blood spots*. Mass Spectrom Rev, 2014.
28. Koster, R.A., et al., *What is the right blood hematocrit preparation procedure for standards and quality control samples for dried blood spot analysis?* Bioanalysis, 2015. **7**(3): p. 345-51.

29. Bland, J.M. and D.G. Altman, *Measuring agreement in method comparison studies*. Stat Methods Med Res, 1999. **8**(2): p. 135-60.
30. EMEA. *Guideline on bioanalytical method validation*. 2011 01.03.2016]; Available from: http://www.ema.europa.eu/docs/en_GB/document_library/Scientific_guideline/2011/08/WC500109686.pdf.
31. Olagunju, A., et al., *Validation and clinical application of a method to quantify nevirapine in dried blood spots and dried breast-milk spots*. J Antimicrob Chemother, 2015. **70**(10): p. 2816-22.
32. Schoenenberger, J.A., et al., *The advantages of therapeutic drug monitoring in patients receiving antiretroviral treatment and experiencing medication-related problems*. Ther Drug Monit, 2013. **35**(1): p. 71-7.
33. Back, D., S. Gibbons, and S. Khoo, *An update on therapeutic drug monitoring for antiretroviral drugs*. Ther Drug Monit, 2006. **28**(3): p. 468-73.
34. Singleton, C., *Recent advances in bioanalytical sample preparation for LC-MS analysis*. Bioanalysis, 2012. **4**(9): p. 1123-40.
35. Cobb, Z., et al., *In-depth study of homogeneity in DBS using two different techniques: results from the EBF DBS-microsampling consortium*. Bioanalysis, 2013. **5**(17): p. 2161-9.
36. Abu-Rabie, P., et al., *Investigation of different approaches to incorporating internal standard in DBS quantitative bioanalytical workflows and their effect on nullifying hematocrit-based assay bias*. Anal Chem, 2015. **87**(9): p. 4996-5003.
37. den Burger, J.C., et al., *Haematocrit corrected analysis of creatinine in dried blood spots through potassium measurement*. Anal Bioanal Chem, 2015. **407**(2): p. 621-7.

Supplementary files

Table S1. Deviation between DBS samples using 15 μ L or 30 μ L blood spot volume.

QC Level	Nevirapine			Efavirenz			Lopinavir		
	Concentration found at [ng/mL]		Change [%]	Concentration found at [ng/mL]		Change [%]	Concentration found at [ng/mL]		Change [%]
	15 μ L	30 μ L		15 μ L	30 μ L		15 μ L	30 μ L	
QC _{LLOQ}	9.3	9.4	1.1	9.1	9.7	5.7	9.1	9.7	5.7
QC _{Low}	46.3	45.8	-1.1	48	46.3	-3.5	48	46.3	-3.5
QC _{Mid}	470	482	2.5	480	481	0.2	480	481	0.2
QC _{High}	4881	5011	2.7	4919	4824	-1.9	4919	4824	-1.9

Table S2. Recovery determined for nevirapine, efavirenz, and lopinavir.

HCT [%]	Nevirapine [%]				Efavirenz [%]				Lopinavir [%]			
	QC _{Low}	QC _{Mid}	QC _{High}	IS	QC _{Low}	QC _{Mid}	QC _{High}	IS	QC _{Low}	QC _{Mid}	QC _{High}	IS
20	90.5	87	90.5	92.3	76.2	77.3	76.2	88.1	73.6	69.8	66.5	88.2
25	83.3	87	82.5	87.2	75.6	75.1	69.3	82.2	67	72.5	62.3	83.7
30	79.6	76.5	77.9	87.8	68.7	64.1	67.8	83.4	63.2	64.9	61.8	83.4
35	69.7	76.1	68.6	85	60.2	67.4	58.6	77.2	60.7	65.5	55.6	82
40	63.4	58.8	67	82.8	57.7	56.2	56.8	81.8	58.6	57.4	56.7	80.1
45	64.2	66.6	66.1	77.5	56.9	60.4	57.6	72.9	60.8	63.3	58.8	76.7
50	66.5	67.6	63.1	77.3	59.5	61.6	53.4	71.5	60.3	62.2	53.7	76.7
20-50	24	19.3	27.4	14.9	16.7	15.8	22.8	16.5	13.3	7.7	12.9	11.5

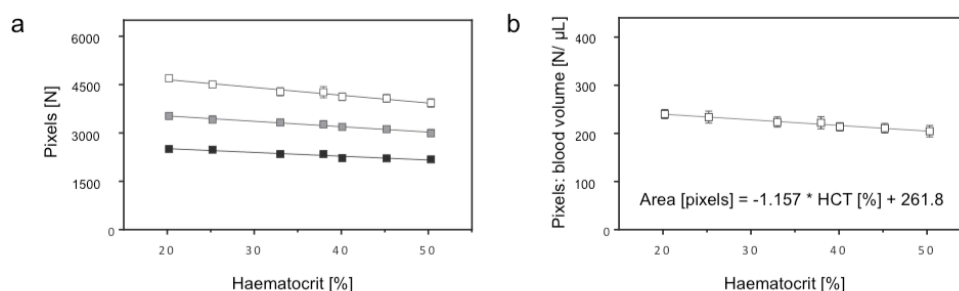


Figure S1. (a) Linear relationship between spot areas, measured in pixels per spot, and the haematocrit was determined. 10, 15, and 20 μ L were spotted onto the filter paper ($R^2 > 0.93$). (b) For grade 226 filter paper, the following formula was established between DBS area, normalised to the spotted blood volume, and the haematocrit: DBS Area = $-1.157 \times \text{HCT} + 261.8$.

9. General conclusions and outlook

The main goal of the presented projects in this thesis was to gain insight and contribute to procedures that are useful in personalised drug treatment.

The first four studies furthered previous work that involved the development, validation, and implementation of a novel *in vivo* phenotyping cocktail. From the two published Basel cocktail studies [15, 16], a number of questions arose that required further evaluation. In a first step, the metabolism of the six CYP450 isoforms, characterised by the *in vivo* Basel cocktail, was further characterised in a variety of different *in vitro* liver cell models, using the same probe drugs as in the *in vivo* studies. We were able to demonstrate that the Basel cocktail substrates can be used not only *in vivo* [15, 16], but also that our *in vitro* results, obtained with these substrates, aligned with trials performed with classic *in vitro* substrates. An especially interesting model involved the co-culture of human cryopreserved hepatocytes with mouse embryo 3T3 fibroblasts, enabling the hepatocytes to reside in an *in vivo*-like 3D environment. By comparing hepatocytes from an identical batch, cultured in a 2D and 3D milieu, we found a number of advantageous properties of 3D-culture. Among the four evaluated liver cell models, results obtained with the 3D co-culture model under induced conditions came closest to the *in vivo* situation [15]. This underscores that 3D-culture techniques open up new possibilities for *in vitro* metabolism and toxicological studies, as they have the capability of overcoming longstanding functional and temporal limitations of traditional 2D-hepatocyte culture.

Having characterised the Basel phenotyping cocktail in both *in vivo* and *in vitro* settings makes it unique, as such data is usually unavailable. In two further studies, we were able to demonstrate *in vitro* that the α -hydroxylation pathway of metoprolol, which has been considered to be exclusively mediated by CYP2D6 [32, 33], is also mediated by CYP3A4, especially after pre-treatment with the CYP inducer rifampicin. Quantitatively, however, the amount of α -hydroxymetoprolol produced by CYP3A4 is irrelevant, both *in vitro* and *in vivo* [15], where no significant increase of α -hydroxymetoprolol after induction was found. This could either be explained by a more pronounced clearance of α -hydroxymetoprolol in the urine or by a more pronounced degradation of metoprolol through CYP3A4 mediated demethylation- and dealkylation pathways. This hypothesis was confirmed *in vitro*, where we could show that the production of the O-desmethyl metabolite of metoprolol was indeed increased under induction treatment with rifampicin. Regardless, these findings do

not impede the utilisation of metoprolol as a phenotyping agent of CYP2D6, as the contribution of CYP3A4 is negligible, even after induction, when CYP2D6 activity is not evaluated, since CYP2D6 has previously been shown not to be inducible [37-42].

Previously, losartan was used as a CYP2C9 probe drug in the *in vivo* Basel cocktail [15]. In plasma, however, the losartan metabolic ratio did not reflect induction after pre-treatment with the inducer rifampicin, and therefore losartan needed to be replaced by another CYP2C9 probe drug. Instead of performing an expensive and time-consuming clinical study, the replacement of losartan with flurbiprofen was evaluated, together with the remaining probe drugs of the Basel cocktail, using the already characterised 3D co-culture *in vitro* model. The data showed that flurbiprofen did not cause a significant change in the enzyme activity of any of the other five CYP450 isoforms, thus enabling its inclusion into the cocktail.

For phenotyping to become more widely accepted as a routine tool in clinical practice, simplified administration of the probe drugs is of great importance. Based on the *in vitro* results showing that flurbiprofen does not interfere with the other five Basel cocktail probe drugs, a previously developed combination-capsule (combi-capsule) was adapted to contain the probe drugs of the modified Basel cocktail (including flurbiprofen instead of losartan), in the form of miniature tablets, and tested in a pilot study (n=2). The obtained PK profiles proved the feasibility of this concept and will serve as the basis for the design of a future clinical study comparing the new combi-capsule to the intake of the six probe drugs as individual commercially available formulations in healthy volunteers.

In recent years, molecularly targeted drug therapy in oncology has become one of the main focus areas through which personalised medicine has been implemented by pharmaceutical and biotechnology companies. For instance, in the past two years (2014 - 2015) alone, 28 new antineoplastic drugs have been approved by the FDA, of which the vast majority are targeted drug therapies that can either be classified as monoclonal antibodies (mAbs) or small molecule protein kinase inhibitors [61-64]. TKIs are predominantly metabolised through CYP450 enzymes, resulting in high inter-individual variability. This, therefore, makes uniform drug intake – the current recommendation – an inadequate dosing strategy to safeguard against potentially avoidable side effects and under-treatment with diminished therapeutic activity.

In the study described in Chapter 7, the correlation between CYP3A4 and CYP1A2 phenotype and pharmacokinetic parameters of erlotinib and sunitinib was evaluated. Single time-point metabolic ratios of midazolam (CYP3A4) and caffeine (CYP1A2) were successfully applied in order to phenotype elderly patients being treated for non-small cell lung cancer (n=37). Although with the present analysis, no clear correlation could be found relating individual metabolic status of CYP3A4 and CYP1A2 to erlotinib exposure, it is anticipated that, with the help of a population pharmacokinetic model (NONMEM) being developed by Parra-Guillen ZA et al. (Department of Clinical Pharmacy and Biochemistry, Freie Universität, Berlin), a more precise assessment of this correlation will be possible, as has previously been accomplished for a number of other TKIs [65-67]. The main goal will be to build an integrated covariate model on erlotinib pharmacokinetics and help define a dosing algorithm based on the individual CYP450-phenotype.

Previously, therapeutic drug monitoring (TDM) has been routinely used in cancer therapy; for instance, to measure methotrexate concentrations [68]. Thus far, however, it has not been widely used to measure TKIs [69]. The apparent link between concentration, toxicity, and therapeutic response, its narrow therapeutic range, large PK variability, and the need of adhering to the treatment long-term, all point towards erlotinib being a promising candidate for TDM [70, 71]. According to de Wit et al., one of the general criteria for dose individualisation of TKIs includes “a validated dose-adaptation strategy” [46]. They argue that an impending challenge of TDM remains the “patient unfriendly and time-consuming exposure-efficacy/ toxicity relations based on AUCs” and that to make TDM feasible in clinical practice, efforts should, therefore, be undertaken to determine surrogate PK markers – e.g. C_{trough} or limited sampling – that show a good correlation with AUC. Preliminary recommendations on how to implement dosage adjustments have been postulated by Petit-Jean et al. [71]. In our clinical study, we found a good correlation between erlotinib single time-point concentration and partial AUC, which could in future be used for limited sampling.

Dried blood spots (DBS) exemplify another approach to simplify sampling for TDM or PK studies. As erlotinib has not been previously evaluated in DBS, we compared erlotinib concentrations measured in DBS to plasma samples. However, using the current set of DBS samples, we were not able to find a sufficient correlation between plasma and DBS concentrations to be able to recommend using DBS instead of conventional plasma samples for TDM. This contrasts with recent work that demonstrated that samples collected in either plasma or DBS containing the TKIs

dasatinib, nilotinib, imatinib, and pazopanib can be interchangeably measured [72, 73]. It is, therefore, possible that through a number of methodological modifications and implementation of *good spotting practice* [74] (both previously alluded to in *Chapter 8*), the replacement of conventional plasma sampling through DBS sample collection may also be achieved for erlotinib.

The application of DBS sampling for TDM of antiretroviral drugs was evaluated within the framework of an HIV-adherence study conducted in Tanzania. For TDM in remote settings, obtaining dried blood spots (DBS) is particularly beneficial, as drug concentrations in DBS are generally stable at room temperature, making cold chains unnecessary. Performing TDM using DBS is a patient-friendly alternative to conventional plasma sampling, since it does not require a trained phlebotomist, and, simultaneously, the DBS sample does not yield a further biohazardous risk [75-78]. As a micro-sampling technique, DBS use considerably less blood than conventional blood sampling techniques [79], making DBS an interesting sampling method with which to perform clinical trials as well as the aforementioned TDM in resource-limited settings [53, 55, 59, 80]. Furthermore, in South Africa, which has the world's largest HIV-positive population, as well as in other African countries, DBS have recently been used to screen for HIV-1 DNA by PCR in infants whose mothers are HIV-positive [81]. Therefore, the use of DBS is already familiar to trained hospital personnel in several Sub-Saharan African countries and can, according to Johannesen et al., "serve as a model for further expansion of DBS monitoring in such settings" [78]. In Tanzania alone, HIV and AIDS is a serious health issue, as more than 2 million people are living with HIV/AIDS (prevalence 3.1%) [82]. Both the introduction of combined antiretroviral therapy (cART) and a massive global health campaign aiming for universal access to cART, has led to the dramatic decline in morbidity and mortality rates in HIV/ Aids patients [83]. A report highlighted that even in the short period between 2011 and 2014, the coverage of people having access to HIV antiretroviral treatment has more than doubled, from 18 to 43% [84]. It is, therefore, all the more important to make sure that patients, who now have access to drugs, are upholding compliance/adherence recommendations of health care professionals. We therefore successfully developed and validated an automated LC-MS/MS method with which TDM DBS samples collected in rural Tanzania could be analysed. Compared to manual DBS extraction, sample processing time and method sensitivity could be improved using an automated DBS extraction method. Automated DBS extraction was reliable and facilitated analysis of the large numbers of samples for this study. Our data confirmed that the TDM of nevirapine and efavirenz in DBS is a suitable alternative to conventional plasma analysis.

10. General References

1. Chainuvati, S., et al., *Combined phenotypic assessment of cytochrome p450 1A2, 2C9, 2C19, 2D6, and 3A, N-acetyltransferase-2, and xanthine oxidase activities with the "Cooperstown 5+1 cocktail"*. Clin Pharmacol Ther, 2003. **74**(5): p. 437-47.
2. Ryu, J.Y., et al., *Development of the "Inje cocktail" for high-throughput evaluation of five human cytochrome P450 isoforms in vivo*. Clin Pharmacol Ther, 2007. **82**(5): p. 531-40.
3. Sharma, A., et al., *A convenient five-drug cocktail for the assessment of major drug metabolizing enzymes: a pilot study*. Br J Clin Pharmacol, 2004. **58**(3): p. 288-97.
4. Christensen, M., et al., *The Karolinska cocktail for phenotyping of five human cytochrome P450 enzymes*. Clin Pharmacol Ther, 2003. **73**(6): p. 517-28.
5. Zgheib, N.K., et al., *Validation of incorporating flurbiprofen into the Pittsburgh cocktail*. Clin Pharmacol Ther, 2006. **80**(3): p. 257-63.
6. Turpeinen, M., et al., *Multiple P450 substrates in a single run: rapid and comprehensive in vitro interaction assay*. Eur J Pharm Sci, 2005. **24**(1): p. 123-32.
7. Spaggiari, D., et al., *A cocktail approach for assessing the in vitro activity of human cytochrome P450s: an overview of current methodologies*. J Pharm Biomed Anal, 2014. **101**: p. 221-37.
8. Walsky, R.L. and R.S. Obach, *Validated assays for human cytochrome P450 activities*. Drug Metab Dispos, 2004. **32**(6): p. 647-60.
9. Testino, S.A., Jr. and G. Patonay, *High-throughput inhibition screening of major human cytochrome P450 enzymes using an in vitro cocktail and liquid chromatography-tandem mass spectrometry*. J Pharm Biomed Anal, 2003. **30**(5): p. 1459-67.
10. Dierks, E.A., et al., *A method for the simultaneous evaluation of the activities of seven major human drug-metabolizing cytochrome P450s using an in vitro cocktail of probe substrates and fast gradient liquid chromatography tandem mass spectrometry*. Drug Metab Dispos, 2001. **29**(1): p. 23-9.
11. Kim, M.J., et al., *High-throughput screening of inhibitory potential of nine cytochrome P450 enzymes in vitro using liquid chromatography/tandem mass spectrometry*. Rapid Commun Mass Spectrom, 2005. **19**(18): p. 2651-8.
12. Lahoz, A., et al., *A new in vitro approach for the simultaneous determination of phase I and phase II enzymatic activities of human hepatocyte preparations*. Rapid Commun Mass Spectrom, 2008. **22**(2): p. 240-4.
13. Zientek, M., et al., *Development of an in vitro drug-drug interaction assay to simultaneously monitor five cytochrome P450 isoforms and performance assessment using drug library compounds*. J Pharmacol Toxicol Methods, 2008. **58**(3): p. 206-14.

14. Gomez-Lechon, M.J., J.V. Castell, and M.T. Donato, *An update on metabolism studies using human hepatocytes in primary culture*. Expert Opin Drug Metab Toxicol, 2008. **4**(7): p. 837-54.
15. Derungs, A., et al., *Effects of Cytochrome P450 Inhibition and Induction on the Phenotyping Metrics of the Basel Cocktail: A Randomized Crossover Study*. Clin Pharmacokinet, 2016. **55**(1): p. 79-91.
16. Donzelli, M., et al., *The basel cocktail for simultaneous phenotyping of human cytochrome P450 isoforms in plasma, saliva and dried blood spots*. Clin Pharmacokinet, 2014. **53**(3): p. 271-82.
17. Ohkura, T., et al., *Evaluation of human hepatocytes cultured by three-dimensional spheroid systems for drug metabolism*. Drug Metab Pharmacokinet, 2014. **29**(5): p. 373-8.
18. Grammaticos, P.C. and A. Diamantis, *Useful known and unknown views of the father of modern medicine, Hippocrates and his teacher Democritus*. Hell J Nucl Med, 2008. **11**(1): p. 2-4.
19. Michl, S., *Inventing Traditions, Raising Expectations. Recent Debates on "Personalized Medicine"*. 2015. **7**: p. 45-60.
20. Xie, H.-G. and F.W. Frueh, *Pharmacogenomics steps toward personalized medicine*. Personalized Medicine, 2005. **2**(4): p. 325-337.
21. Meyer, U.A., *Pharmacogenetics - five decades of therapeutic lessons from genetic diversity*. Nat Rev Genet, 2004. **5**(9): p. 669-76.
22. Issa, A.M., *Personalized medicine and the practice of medicine in the 21st century*. McGill J Med, 2007. **10**(1): p. 53-7.
23. Opdam, F.L., H. Gelderblom, and H.J. Guchelaar, *Phenotyping drug disposition in oncology*. Cancer Treat Rev, 2012. **38**(6): p. 715-25.
24. Fuhr, U., A. Jetter, and J. Kirchheiner, *Appropriate phenotyping procedures for drug metabolizing enzymes and transporters in humans and their simultaneous use in the "cocktail" approach*. Clin Pharmacol Ther, 2007. **81**(2): p. 270-83.
25. Venter, J.C., et al., *The sequence of the human genome*. Science, 2001. **291**(5507): p. 1304-51.
26. Lander, E.S., et al., *Initial sequencing and analysis of the human genome*. Nature, 2001. **409**(6822): p. 860-921.
27. Josephs, D.H., et al., *Clinical pharmacokinetics of tyrosine kinase inhibitors: implications for therapeutic drug monitoring*. Ther Drug Monit, 2013. **35**(5): p. 562-87.
28. Marshall, W.J. and S. Bangert, *Clinical Chemistry*. 2008, Edinburgh, London: Mosby Elsevier.

29. Group, M.-H.S., *Effect of metoprolol CR/XL in chronic heart failure: Metoprolol CR/XL Randomised Intervention Trial in Congestive Heart Failure (MERIT-HF)*. Lancet, 1999. **353**(9169): p. 2001-7.
30. Chen, Z.M., et al., *Early intravenous then oral metoprolol in 45,852 patients with acute myocardial infarction: randomised placebo-controlled trial*. Lancet, 2005. **366**(9497): p. 1622-32.
31. Hansson, L., et al., *Randomised trial of old and new antihypertensive drugs in elderly patients: cardiovascular mortality and morbidity the Swedish Trial in Old Patients with Hypertension-2 study*. Lancet, 1999. **354**(9192): p. 1751-6.
32. McGourty, J.C., et al., *Metoprolol metabolism and debrisoquine oxidation polymorphism--population and family studies*. Br J Clin Pharmacol, 1985. **20**(6): p. 555-66.
33. Otton, S.V., et al., *Use of quinidine inhibition to define the role of the sparteine/debrisoquine cytochrome P450 in metoprolol oxidation by human liver microsomes*. J Pharmacol Exp Ther, 1988. **247**(1): p. 242-7.
34. Frank, D., U. Jaehde, and U. Fuhr, *Evaluation of probe drugs and pharmacokinetic metrics for CYP2D6 phenotyping*. Eur J Clin Pharmacol, 2007. **63**(4): p. 321-33.
35. Tamminga, W.J., et al., *An optimized methodology for combined phenotyping and genotyping on CYP2D6 and CYP2C19*. Eur J Clin Pharmacol, 2001. **57**(2): p. 143-6.
36. Birkett, D.J., et al., *In vitro approaches can predict human drug metabolism*. Trends Pharmacol Sci, 1993. **14**(8): p. 292-4.
37. Eichelbaum, M., et al., *The influence of enzyme induction on polymorphic sparteine oxidation*. Br J Clin Pharmacol, 1986. **22**(1): p. 49-53.
38. Gerets, H.H., et al., *Characterization of primary human hepatocytes, HepG2 cells, and HepaRG cells at the mRNA level and CYP activity in response to inducers and their predictivity for the detection of human hepatotoxins*. Cell Biol Toxicol, 2012. **28**(2): p. 69-87.
39. Glaeser, H., et al., *Influence of rifampicin on the expression and function of human intestinal cytochrome P450 enzymes*. Br J Clin Pharmacol, 2005. **59**(2): p. 199-206.
40. Madan, A., et al., *Effects of prototypical microsomal enzyme inducers on cytochrome P450 expression in cultured human hepatocytes*. Drug Metab Dispos, 2003. **31**(4): p. 421-31.
41. Rae, J.M., et al., *Rifampin is a selective, pleiotropic inducer of drug metabolism genes in human hepatocytes: studies with cDNA and oligonucleotide expression arrays*. J Pharmacol Exp Ther, 2001. **299**(3): p. 849-57.
42. Wenk, M., L. Todesco, and S. Krahenbuhl, *Effect of St John's wort on the activities of CYP1A2, CYP3A4, CYP2D6, N-acetyltransferase 2, and xanthine*

- oxidase in healthy males and females*. Br J Clin Pharmacol, 2004. **57**(4): p. 495-9.
43. Keates, R.H. and K.A. McGowan, *Clinical trial of flurbiprofen to maintain pupillary dilation during cataract surgery*. Ann Ophthalmol, 1984. **16**(10): p. 919-21.
 44. Compendium. *Froben® Fachinformation des Arzneimittel-Kompendium der Schweiz*. 2015 [cited 2016 12.02.2016]; Available from: <http://compendium.ch/mpro/mnr/9886/pdf/de - page1>.
 45. Bosilkovska, M., et al., *Geneva cocktail for cytochrome p450 and P-glycoprotein activity assessment using dried blood spots*. Clin Pharmacol Ther, 2014. **96**(3): p. 349-59.
 46. de Wit, D., et al., *Individualized dosing of tyrosine kinase inhibitors: are we there yet?* Drug Discov Today, 2015. **20**(1): p. 18-36.
 47. Bangsberg, D.R., *Less than 95% adherence to nonnucleoside reverse-transcriptase inhibitor therapy can lead to viral suppression*. Clin Infect Dis, 2006. **43**(7): p. 939-41.
 48. Burkhart, P.V. and E. Sabate, *Adherence to long-term therapies: evidence for action*. J Nurs Scholarsh, 2003. **35**(3): p. 207.
 49. Schneider, J., et al., *Better physician-patient relationships are associated with higher reported adherence to antiretroviral therapy in patients with HIV infection*. J Gen Intern Med, 2004. **19**(11): p. 1096-103.
 50. Meesters, R.J., et al., *Incurred sample reanalysis comparison of dried blood spots and plasma samples on the measurement of lopinavir in clinical samples*. Bioanalysis, 2012. **4**(3): p. 237-40.
 51. Paterson, D.L., et al., *Adherence to protease inhibitor therapy and outcomes in patients with HIV infection*. Ann Intern Med, 2000. **133**(1): p. 21-30.
 52. Erb S, L.E., Elzi L, Hatz C, Klimkait T, Manuel Haschke, Berger B, Duthaler U, Langewitz W, Tanner M, Battegay M, , *Adherence assessment in HIV-infected patients treated with combination antiretroviral therapy (cART) in rural Tanzania*. (manuscript in preparation), 2016.
 53. Edelbroek, P.M., J. van der Heijden, and L.M. Stolk, *Dried blood spot methods in therapeutic drug monitoring: methods, assays, and pitfalls*. Ther Drug Monit, 2009. **31**(3): p. 327-36.
 54. Smit, P.W., et al., *An overview of the clinical use of filter paper in the diagnosis of tropical diseases*. Am J Trop Med Hyg, 2014. **90**(2): p. 195-210.
 55. Koal, T., et al., *Quantification of antiretroviral drugs in dried blood spot samples by means of liquid chromatography/tandem mass spectrometry*. Rapid Commun Mass Spectrom, 2005. **19**(21): p. 2995-3001.
 56. ter Heine, R., et al., *Quantification of protease inhibitors and non-nucleoside reverse transcriptase inhibitors in dried blood spots by liquid chromatography-*

triple quadrupole mass spectrometry. J Chromatogr B Analyt Technol Biomed Life Sci, 2008. **867**(2): p. 205-12.

57. Ter Heine, R., et al., *Clinical evaluation of the determination of plasma concentrations of darunavir, etravirine, raltegravir and ritonavir in dried blood spot samples*. Bioanalysis, 2011. **3**(10): p. 1093-7.
58. Meesters, R.J., et al., *Ultrafast and high-throughput mass spectrometric assay for therapeutic drug monitoring of antiretroviral drugs in pediatric HIV-1 infection applying dried blood spots*. Anal Bioanal Chem, 2010. **398**(1): p. 319-28.
59. Kromdijk, W., et al., *Use of dried blood spots for the determination of plasma concentrations of nevirapine and efavirenz*. J Antimicrob Chemother, 2012. **67**(5): p. 1211-6.
60. Abu-Rabie, P. and N. Spooner, *Direct quantitative bioanalysis of drugs in dried blood spot samples using a thin-layer chromatography mass spectrometer interface*. Anal Chem, 2009. **81**(24): p. 10275-84.
61. Aggarwal, S., *Targeted cancer therapies*. Nat Rev Drug Discov, 2010. **9**(6): p. 427-428.
62. The National Cancer Institute. *Targeted Cancer Therapies Fact Sheet*. 2014 25.04.2014 03.09.2016]; Available from: <http://www.cancer.gov/about-cancer/treatment/types/targeted-therapies/targeted-therapies-fact-sheet>.
63. Centerwatch. *FDA Approved Drugs for Oncology*. 2016; Available from: <https://http://www.centerwatch.com/drug-information/fda-approved-drugs/therapeutic-area/12/oncology>.
64. FDA. *Hematology/Oncology (Cancer) Approvals & Safety Notifications*. 2016 11.03.2016 Available from: <http://www.fda.gov/Drugs/InformationOnDrugs/ApprovedDrugs/ucm279174.htm>.
65. Swaisland, H.C., et al., *Exploring the relationship between expression of cytochrome P450 enzymes and gefitinib pharmacokinetics*. Clin Pharmacokinet, 2006. **45**(6): p. 633-44.
66. de Wit, D., et al., *Midazolam as a phenotyping probe to predict sunitinib exposure in patients with cancer*. Cancer Chemother Pharmacol, 2014. **73**(1): p. 87-96.
67. Li, J., et al., *CYP3A phenotyping approach to predict systemic exposure to EGFR tyrosine kinase inhibitors*. J Natl Cancer Inst, 2006. **98**(23): p. 1714-23.
68. Galpin, A.J. and W.E. Evans, *Therapeutic drug monitoring in cancer management*. Clin Chem, 1993. **39**(11 Pt 2): p. 2419-30.
69. Klumpen, H.J., et al., *Moving towards dose individualization of tyrosine kinase inhibitors*. Cancer Treat Rev, 2011. **37**(4): p. 251-60.
70. Fukudo, M., et al., *Population pharmacokinetics/pharmacodynamics of erlotinib and pharmacogenomic analysis of plasma and cerebrospinal fluid*

- drug concentrations in Japanese patients with non-small cell lung cancer. Clin Pharmacokinet*, 2013. **52**(7): p. 593-609.
71. Petit-Jean, E., et al., *Erlotinib: another candidate for the therapeutic drug monitoring of targeted therapy of cancer? A pharmacokinetic and pharmacodynamic systematic review of literature. Ther Drug Monit*, 2015. **37**(1): p. 2-21.
 72. Kralj, E., et al., *Simultaneous measurement of imatinib, nilotinib and dasatinib in dried blood spot by ultra high performance liquid chromatography tandem mass spectrometry. J Chromatogr B Analyt Technol Biomed Life Sci*, 2012. **903**: p. 150-6.
 73. de Wit, D., et al., *Dried blood spot analysis for therapeutic drug monitoring of pazopanib. J Clin Pharmacol*, 2015. **55**(12): p. 1344-50.
 74. Meesters, R., et al., *Impact of internal standard addition on dried blood spot analysis in bioanalytical method development. Bioanalysis*, 2011. **3**(20): p. 2357-64.
 75. Bond, W.W., et al., *Survival of hepatitis B virus after drying and storage for one week. Lancet*, 1981. **1**(8219): p. 550-1.
 76. Evengard, B., et al., *Effect of heat on extracted HIV viral infectivity and antibody activity using the filter paper technique of blood sampling. Aids*, 1989. **3**(9): p. 591-5.
 77. Centers for Disease Control and Prevention. *Shipping Guidelines for Dried-Blood Spot Specimens*. 1995 09.03.2015; Available from: http://www.cdc.gov/labstandards/pdf/nsqap/Bloodspot_Transportation_Guidelines.pdf.
 78. Johannessen, A., *Dried blood spots in HIV monitoring: applications in resource-limited settings. Bioanalysis*, 2010. **2**(11): p. 1893-908.
 79. Li, W. and F.L. Tse, *Dried blood spot sampling in combination with LC-MS/MS for quantitative analysis of small molecules. Biomed Chromatogr*, 2010. **24**(1): p. 49-65.
 80. Malm, M., et al., *Determination of lamivudine, zidovudine, and nevirapine in capillary blood sampled on filter paper by LC. J Chromatogr Sci*, 2009. **47**(10): p. 855-62.
 81. Sherman, G.G., et al., *Dried blood spots improve access to HIV diagnosis and care for infants in low-resource settings. J Acquir Immune Defic Syndr*, 2005. **38**(5): p. 615-7.
 82. WHO. *United Republic of Tanzania: WHO statistical profile. 2015* 11.02.2016]; Available from: <http://www.who.int/gho/countries/tza.pdf?ua=1>.
 83. AIDSinfo. *Panel on Antiretroviral Guidelines for Adults and Adolescents. Guidelines for the use of antiretroviral agents in HIV-1-infected adults and adolescents. 2015*; Available from: <https://aidsinfo.nih.gov/contentfiles/lvguidelines/adultandadolescentgl.pdf>.

84. World Bank. *Antiretroviral therapy coverage (% of people living with HIV)*. 2015 14.03.2016]; Available from: <http://data.worldbank.org/indicator/SH.HIV.ARTC.ZS>.

